POLITECNICO DI TORINO

Master of Science in Mechanical Engineering

Master Thesis

Numerical investigation of gradient 3D auxetic metalattice realized via additive manufacturing

Supervisor:
prof. Aurelio Somà

Candidate:
Gianluca Piccagli
matricola: 242243

Company supervisor
Advanced Composites Collaboration for Innovation and Science
prof. Fabrizio Scarpa

ANNO ACCADEMICO 2017 - 2018

Pensa al mare, alle onde,
alle stelle, al cielo,
al prato verde…

Ringraziamenti

Non basteranno queste poche righe ad esprimere la mia gratitudine verso coloro che mi hanno accompagnato in questi lunghi, seppur indimenticabili, cinque anni. Ad ogni modo, vorrei ringraziare in primis i professori Aurelio Somà e Fabrizio Scarpa per avermi dato la possibilità di vivere un'esperienza unica e formativa che mi ha fatto conoscere il mondo da una prospettiva diversa. Inoltre, a loro va la mia riconoscenza per avermi sostenuto e guidato benevolmente con la loro conoscenza in questi ultimi sette mesi. Inoltre, un ringraziamento speciale lo devo ai miei amici, ma soprattutto, ai miei genitori che mi hanno aiutato ad arrivare fino in fondo a questo soddisfacente traguardo.

Abstract

In this work, a particular lattice is designed and parametrically analysed so as to quantify the influences on its mechanical properties of different geometrical variables which characterize it. On the one hand, the nature of the project is exploratory and aims at identifying an optimal lightweight structure which could replace the classic honeycomb used by Rolls-Royce in their acoustic liners. Considered Rolls-Royce involvement in the study, the investigation has an industrial perspective and thus, the final proposed lattice must satisfy some shape and functional requirements.
On the other hand, the thesis seeks to find a procedure for introducing these lattices inside a bigger assembly of elements without generating a file which is too computationally complex and which requires disproportionate simulation-times. Thus, using the "Substructuring" ANSYS function, an interesting modeling approach is put forward.
Furthermore, the project consists of several parts. The first step is the geometry definition of the structure as an auxetic and bending-dominated one. The second one, deals with FEM modeling approaches and simulative analyses implementation, whereas in the third part obtained results are shown and a conclusive high energy absorption solution is given.
Lastly, the sample fabrication is analysed and the additive manufacturing technique "Electron Beam Melting" is chosen as the best option having regard to the complexity of the lattice and the material used: 316L stainless steel.

Sommario

In questo lavoro di tesi, una particolare struttura “lattice” è progettata ed analizzata parametricamente allo scopo di quantificare le influenze sulle sue proprietà meccaniche di differenti variabili geometriche che la caratterizzano. Per un verso, la natura del progetto è esplorativa e mira ad identificare una travatura reticolare in grado di sostituire il classico “honeycomb” utilizzato dalla Rolls-Royce nei loro “liners” acustici. Considerando il coinvolgimento dell’azienda Rolls-Royce nello studio, l’indagine presenta una prospettiva industriale e perciò, il “lattice” finale proposto deve soddisfare alcuni vincoli di forma e di funzionalità.
Per altro verso, la tesi aspira a trovare una procedura per introdurre queste strutture all’interno di un più grande insieme di elementi senza generare un “file” che sia troppo complesso da un punto di vista computazionale e che richieda tempi di simulazione eccessivi. Quindi, utilizzando la funzione “Substructuring” di ANSYS, è presentato un interessante approccio alla modellazione.
Inoltre, il progetto consta di più parti. Il primo passo è la definizione della geometria della struttura come un’architettura auxetica e dominata da flessione. Il secondo, tratta gli approcci di modellazione FEM e l’implementazione delle analisi simulative, mentre nella terza parte sono mostrati i risultati ottenuti e una soluzione conclusiva ad alto assorbimento di energia è fornita.
In fine, la produzione del campione è analizzata e la tecnica di fabbricazione additiva “Electron Beam Melting” è scelta come l’opzione migliore vista la complessità della struttura “lattice” ed il materiale utilizzato: acciaio inossidabile 316L.

INDEX

Part I

First part

1.Introduction

After almost six decades of continuous use in aeroengine airframes, the honeycomb is still the main architecture solution in aeroacoustics liners and general sandwich structures. It has several appealing advantages, including design maturity, high specific flatwise and bending stiffness, proven energy absorption capabilities and an easy manufacturing process. However, commercial honeycombs are characterised by relevant disadvantages, and those include high moisture retention, that progressively increases the mass of the liner, a general vibration damping performance that enhances the vibroacoustics impact of the nacelle, with negative effects for the turbofan noise, especially during take-off and landing.

Nowadays, the advent of advanced manufacturing techniques such as "Additive Manufacturing" has provided the possibility to consider new topologies of cellular structures. As a matter of fact, they allow the designer to seek a high level of product customization setting almost no geometric restrains. Moreover, these cutting-edge fabrication processes are a perfect match for metalattices which are structures where material is constituted by unit cells arranged with a specific desired pattern. Currently, most of the publications involved in this topic are focusing on auxetic materials, on bidimensional honeycomb behaviour and, to a lesser extent, on the introduction of gradients along the loading direction of the frame. In fact, a gradient lattice has the advantage of having a gradually varying local distribution of mechanical properties which could provide an unusual, directional and tailorable response under indentation, impact, and vibrating loading. For instance, this morphological solution could be properly harnessed in order to reduce the effects of blade-off phenomena in the nacelle. Furthermore, gradient density lattice under high-strain rates are able to control the plastic energy dissipation more efficiently than the configuration with periodic cells. In addition, a strong localisation of the deformations, which makes possible to generate sacrificial layers under impact for safety purposes.

On the one hand, this project is aimed at combining all these aspects designing a proper new kind of high specific energy absorption lattice to replace the honeycomb used by Rolls-Royce in their acoustic liners. The particular metalattice designed has to satisfy some company requirements so as to be practically applied. In order to analyse the effects of all the main geometric variables of the unit cell, three different parametric analyses are carried out: flatwise compression tests, shear tests and elastic energy absorption tests. It has to be beforehand pointed out that the study is not focused on the material chosen to build the product, which is 316L stainless steel, but only on the optimisation of geometric variables.

On the other hand, this work is intended to provide an appealing FEM modeling approach with which lattices can be simulated in a faster and less computationally expensive way. In fact, these structures can consist of millions of struts which are usually

virtually represented as a whole network of beams joined together. Consequently, for big models and with average computer resources, the FEM classic modeling approach is not doable because of the file heaviness, thus hindering a deeper virtual understanding of the architecture capabilities.
This initial investigation provides only numerical results which have to be proved by experimental tests on a sample meant to be fabricated via "Electron Beam Melting".
In conclusion, the project has been carried out at the University of Bristol, in the "Advanced Composites Collaboration for Innovation and Science" (ACCIS) centre and, as already mentioned, includes Rolls-Royce Group plc as the industrial partner.

2.Literature review

Nowadays, a significant and increasing number of academic works concern mechanical metamaterials and cellular solids. In particular, lattice structures have been brought into focus during the last years because of their tuneable properties and their high strength to weight ratio. From a general point of view, Helou et al. (2018) [1] state: "These structures are an emerging solution to weight, energy and advanced manufacturing time reduction". Thanks to these advantages metalattices have been widely used in marine, automotive and aerospace applications. However, their real introduction into the industrial world was made possible by the redesign and adjustment of already known manufacturing techniques and by the development of completely new production processes such as "Additive Manufacturing".
This section is incipiently going to deal with the whole background ideas from which metamaterials concept originates and, secondarily, it is going to introduce the reader to the state of the art of the main topics related to this work.

2.1. Background concepts

2.1.1. Bioinspiration

Throughout the years, mankind has been evolving and upgrading his own life thanks to a slow but steady improving process. What brought man the world he knows is the unremitting human tendency to observe something and trying to replicate it in a cross-functional range of areas. As a matter of fact, most of the great inventions of all time came from a previous failure in another research field.
Time and again the main source of new ideas is the nature in all of its various shades. In fact, over the years, nature has been modifying its shape in order to achieve the optimal condition. This "optimum" status is to be thought of as the outcome of a topological optimization nature went through over time. From this last statement it is possible to find the original roots of biomimetics and bioinspiraton.
Bührig-Polaczek et al. (2016) [2] state: "biomimetics and bioinspiration are terms that basically reflect the same idea: solving technological problems by analysing, abstracting, adapting and transposing biological principles, that evolved over millions or even billions of years, into the technical world. The mere fact of their existence proves these biological solutions to be an adequate answer to the respective (environmental challenges). Nevertheless, one should bear in mind that biological solutions in most cases do not represent the absolutely optimal solution for given problem as natural systems typically are multifunctional, and thus they are optimised under consideration of several tasks

which, when separated from each other, often would require contradictory individual solutions."
In the last sentences of this statement it is clearly pointed out the need to comprehensively investigate and extract appropriate studying strategies striving for further improvement. It is insofar indispensable to analyse and deeply gain an insight into the property-structure-function relationship of the biological role models in the context of all of their physical and biological constraints.
Outstanding examples of the multifunctionality of nature designed objects are fruit peels, nuts and seed shells. Not only they fulfil the basic requirement of containing the fruit of the seed, but they provide protection from mechanical damage, thermal insulation, buoyancy and many other functions depending on the particular case.
One of the biologically most important tasks lies in the need for high energy absorption obtained with lightweight materials. Likewise, recent advances in the defense, aerospace, automotive, semiconductor and energy industries have triggered a tremendous demand for high-performance materials with lightweight and enhanced mechanical properties.
Thanks to biomimetics field different kind of new structure concepts were created and tested aiming to satisfy the needs of new industrial challenges. Among all, it is possible to mention cellular solids, metamaterials and hierarchical structures. In biology, all of these materials, specially the hierarchical build-up, are responsible for outstanding mechanical properties while using only a limited number of constituent elements. Moreover, it should be highlighted that bioinspiration suggests manufacturing these structures with a bottom-up approach which allows for more geometrical freedom and facilitates the generation of surprisingly complex parts. Besides it is widely known that biological architectures are gradually built from small cells to large organisms.
A recent biomimetics analysis was carried out by Bührig-Polaczek et al. (2016) [2] and it will be herein briefly discussed to clarify how does biomimetics work and to introduce the reader to some of the key aspects of this thesis.
The Pomelo is the largest and heaviest fruit of the genus Citrus (fig. 2.1).

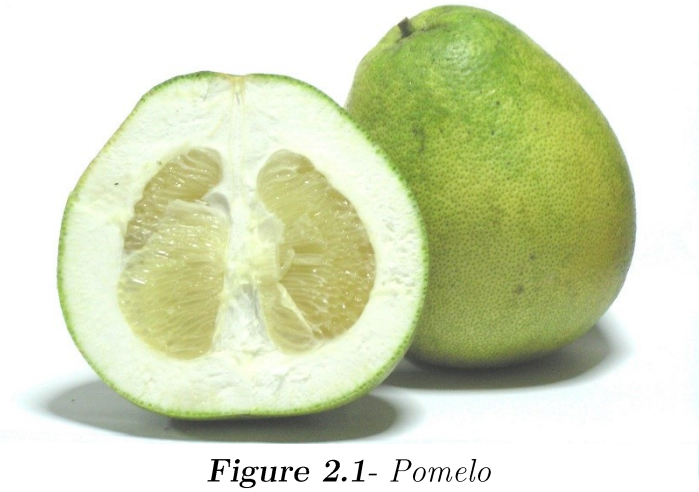

***Figure 2.1**- Pomelo*

Its trees disperse their seeds through a process called endozoochory which is a seed dispersal via ingestion by vertebrate animals: a plant surrounds seeds with an edible and nutritious fruit as a good food for birds and mammals that consume it, digest it and defecate the seeds. However, open contact to the environment speed up decomposition of the pulp and facilitate the mould growth which render the fruit unpalatable for animals. With this in mind, the biological texture of the Pomelo favoured, through natural selection, those structure that were most appropriate for absorbing and dissipating mechanical energy originated from the impact with the ground upon the fruit falls.
Therefore, Pomelo peel shall consist in two parts, flavedo and albedo (fig. 2.2).

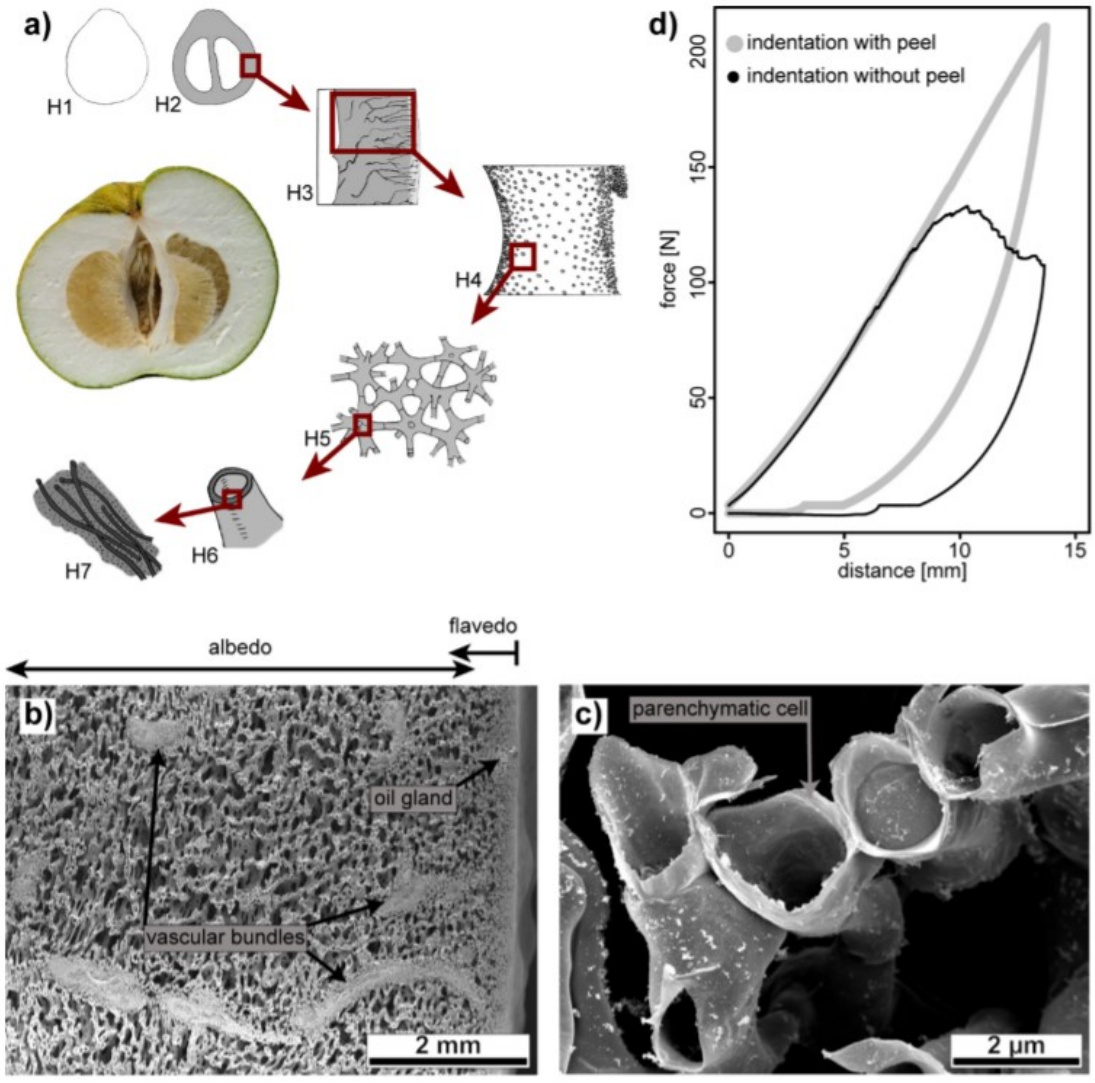

Figure 2.2: *(a) Schematic representation of the hierarchical levels of the Pomelo (H1-H7). (b) SEM image showing the peel. (c) SEM image of prenchymatic albedo cells constituting the struts of the foem-like tissue. (d) Force curve resulting from indenting a Pomelo cut in half with a flat plunger and subsequently indenting the sample at the same location, however, with the peel removed at the location of indentation.*

The former is the outer layer of the peel and it presents a denser texture which spreads radially for a very small thickness. Whereas the latter is the inner subsequent layer which exhibits a more foam-like composition and radially extends for a thicker dimension.
What makes this peel configuration so advantageous for energy dissipation is the gradually changing density of Pomelo anatomical architecture along the radial direction between the flavedo and the albedo and the presence of vascular bundles and parenchymatic cell.
As a matter of fact, the identified structural contributors to the energy absorption are:

- **Density gradient between flavedo and albedo**: open cellular layer that characteristically has excellent energy absorption due to high internal mobility. As investigated by Thielen et al. (2013) [3] the cells in less dense areas (inner ones) are observed to buckle first. To the high compressibility due to large intercellular spaces is mainly attributed the high-energy dissipation capacity during impact. Moreover, gradient is hypothesized to promote uniform collapse.

- **Vascular bundles**: they act as stiffening and supporting elements and help translating local impact stresses into global ones. As a result, they facilitate the energy dissipation.

- **Parenchymatic cell:** the interaction between pressure and load in fluid-filled cell struts causes stiffening before failure.

Having analysed the main features of the Pomelo it is suddenly possible to adapt its architecture to technical solutions introducing hierarchical structures with density gradient configurations in order to achieve better mechanical results with lightweight materials.
In accordance with the cited publication and many others biomimetic works, one of the aims of this thesis is to get to know, with a systematic approach, the behaviour of lattice structures and customizing their properties by introducing geometrical parameter gradients along a direction thus obtaining also a density changing. In this regard, natural materials such as bone and wood have offered great inspiration for cellular solids design.

2.1.2. Introduction to cellular solids

The starting lines of the book *Cellular Solids – Structure and Properties* written by J.Gibson and F.Ashby state [4]: "The word 'cell' derives from the Latin *cella*: a small compartment, an enclosed space. Our interest is in clusters of cells [...], cellular solids. By this we mean an assembly of cells with solid edges or faces, packed together so that they fill space. Such materials are common in nature: wood, cork, sponge and coral are examples."
There are two different kind of cellular solid morphologies, metamaterials and foams (fig.2.3).

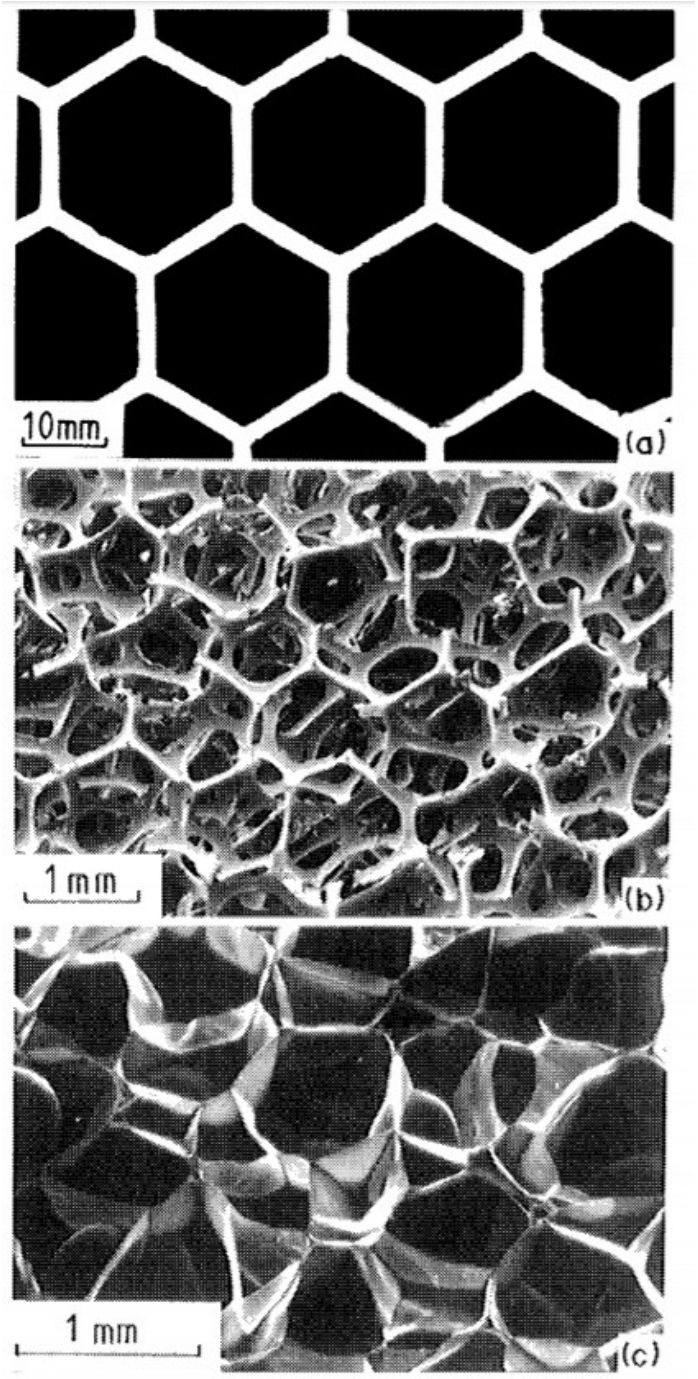

Figure 2.3: *Cellular solids: (a) two-dimensional honeycomb. (b) three-dimensional foam with open cells. (c) three-dimensional foam with closed cells.*

The formers are cutting-edge structures whose properties are mainly determined by their microstructure rather than by the chemical and physical properties of the material constituting them. Their architecture is fully designed in every single part by the engineer so that a specific purpose can be obtained. Honeycombs and three-dimensional lattices belong to this category.
More commonly, it is possible to hear about foams which are three-dimensional cellular material with polyhedral cells. Foams are open-celled or closed-celled respectively if the solid of which the foam is made is contained in the cell edges only (so that the cells connect through open faces) or if the faces are solid too and each cell is seal off from its neighbours. Also foams allow the designer to set out their microstructure but, depending on the manufacturing process used, there is always a threshold after which the microstructure is not controllable anymore.
Notwithstanding the morphological differences, cellular solids most important feature is their relative density, $\tilde{\rho}/\rho_s$. It is the ratio between the cellular structure density and the one of the constitutive material from which the cell walls are made. A solid can be referred as cellular solid if its relative density is less than 0.3.
The mechanical properties of cellular solids depend on several factors such as the size and the shape of cell, physical features of the bulk material, periodicity and connection path between cell struts, geometry and section shape of the single elements, porosity, relative density, presence of geometrical gradients and many others. Moreover, an important factor is the manufacturing process relied on. Thus, it will be given a general introduction to cellular solids behaviour.

2.1.3. Stress-strain behaviour

The compressive stress-strain curve of a cellular solid such as a foam can often be simplified into three regimes, namely, the linear elastic regime, the plateau regime and the densification regime [4]. Figure 2.4 shows the compressive curve. The elastic modulus E of the structure is the trend slope in the first area. This first regime ends at the crush or buckle strain which represents the initiation of the new deformation mechanism. In this second region, there is a plateau whose trend depend on the single unit as discussed by Q.M.Li [5]: it can be a proper plateau if the single cell shows strain-softening characteristics or it can slightly increase if the single unit has strain-hardening characteristics. Nevertheless, in this area further compression causes the cell walls to approach each other and thus forcing the cell to collapse. Material energy absorption is strictly linked with the plateau since it is the area underlying the stress-strain curve. The third regime starts at the onset of densification, when the slope of the curve is not steady anymore and it begins to increase steeply while cell walls come into contact with each other. At this point, an increase of compression leads to complete densification strain with a completely compacted material. Direct evidence of this last saturation of the specimen inner volume is the value of the Young's modulus which closely corresponds to

that of the bulk architecture and the value of the relative density which almost approaches unity.

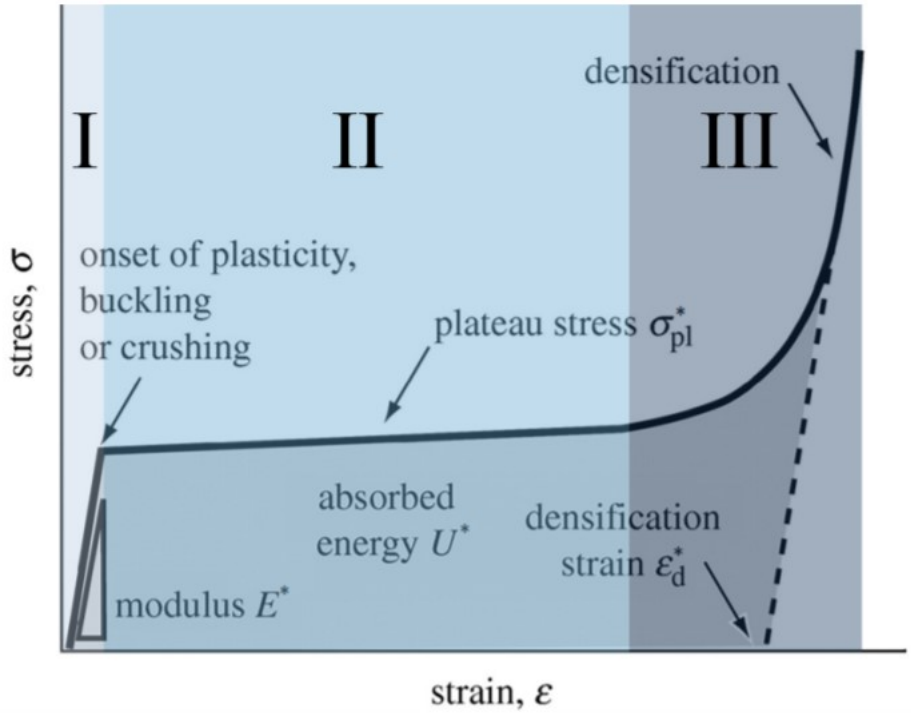

Figure 2.4: *Uniaxial compression of a cellular material: stress-strain curve.*

Cellular solid behaviour, especially for foams, can be distinguished between bending-dominated or stretching-dominated. Open-cell foams are usually characterized by the former behaviour while closed-cell foams are characterized by the latter one. As shown by figure 2.5 these two ways of deformation are completely different and consequently leads to different design implications. Deshpande et al. (2001) state [6]: "The modulus and initial yield strength of a stretching-dominated cellular solid are much greater than those of a bending-dominated cellular material of the same relative density. This makes stretching-dominated cellular solids attractive alternatives to bending-dominated foamed materials for lightweight structural applications. However, unlike bending-dominated foams, in compression the stretching-dominated materials have softening post-yield response due to buckling of the struts. Thus, these materials may be less attractive as energy-absorbers since this application requires a stress-strain response with a long, flat plateau."
In order to explain the bending and stretching dominated behaviours, let's consider the pin-jointed frames shown in figure 2.6 and Ashby's studies [7]. The frame figure 2.6a is mechanism. If loaded, the struts rotate about the joints and the frame collapses: it has neither stiffness nor strength. The frame shown in figure 2.6b is a structure: if loaded the struts are

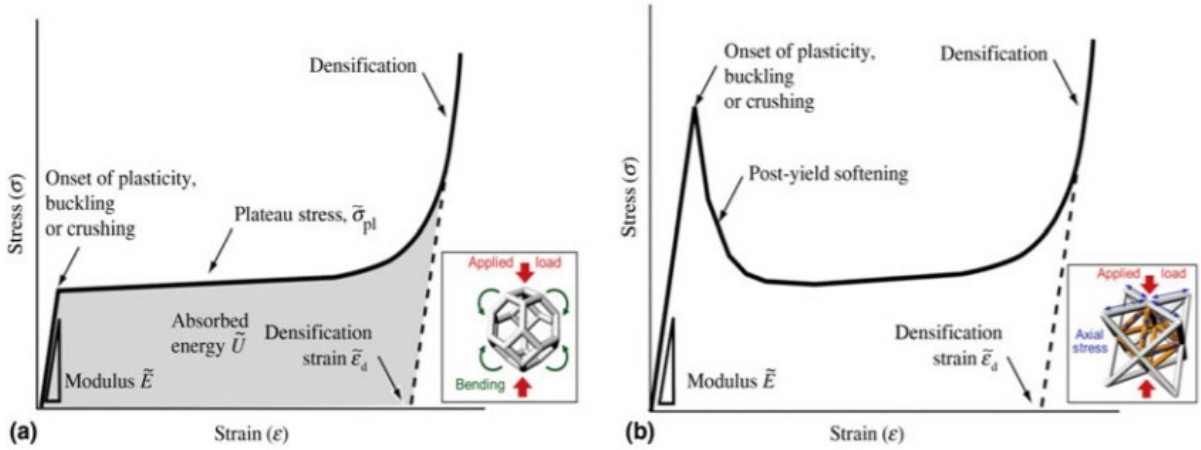

Figure 2.5: *Compressive curves: (a) bending-dominated (b) stretching-dominated.*

characterized by axial or compressive stresses depending on their orientation with respect to the loading direction. Hence, the deformation is stretching-dominated and the frame collapses by stretching failure of the struts. Let's now consider that the joints of both frames are frozen so as to prevent free rotations of the struts. In the case of the first frame, the struts can no longer rotate and the applied load induces bending moments due to the frozen joints, and these cause the struts to bend. However, freezing the joints of the second structure has virtually no effect on the macroscopic stiffness or strength; although the struts bend, the frame is still stretching-dominated and the collapse load is dictated mainly by the axial strength of the struts.

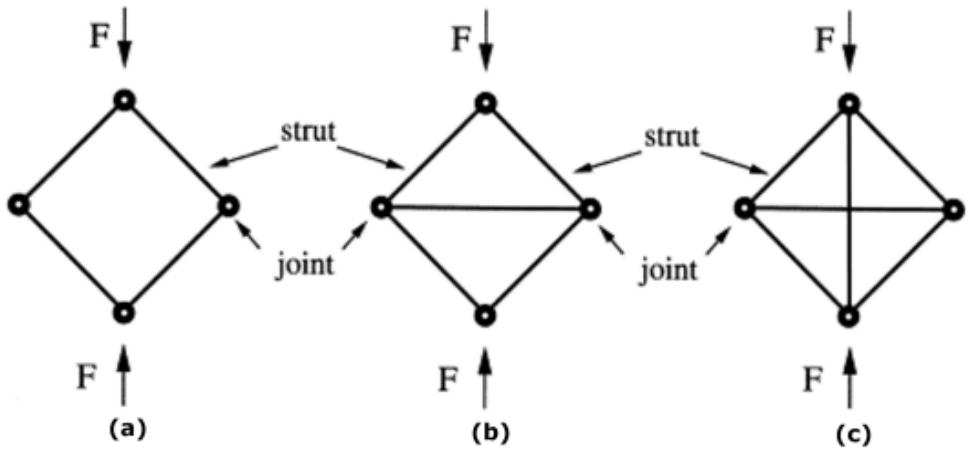

Figure 2.6: *(a) Mechanism. (b) Structure. (c) Hyperstatic.*

Maxwell suggested an algebraic rule defining the condition for a pin-jointed frame of b struts and j frictionless joints to be both statically and kinematically determinate (i.e. to just be rigid). Eq. (2.1) shows the two-dimensional and three-dimensional criteria:

$$\begin{cases} b = 2j - 3 \quad for\ 2D \\ b = 3j - 6 \quad for\ 3D \end{cases} \tag{2.1}$$

These criteria define just necessary conditions for rigidity, but not in general sufficient conditions as they do not account for states of self stress (a self-equilibrated state of strut tensions in the absence of external load) and neither of mechanisms. Maxwell's formulas can be generalised in three dimensions as [7]:

$$M = b - 3j + 6 = s - m \tag{2.2}$$

where s and m are the number of states of self stress and the mechanisms, respectively, which can be determined by finding the rank of the equilibrium matrix that describes the frame in a full structural analysis [8].

If $M < 0$ the frame is a mechanism; it has one or more degrees of freedom. If its joints are locked, as they are in lattice structures, the struts of the frame bend when there is a load; hence it becomes a bending-dominated structure. As stated by Deshpande, these are the most appropriate structure to obtain energy absorption mainly because they are characterized by a significant plateau region due to an increased mobility of the struts.

If instead, $M = 0$, as shown in figure 2.6b, the frame is a structure and when it is loaded, its struts support axial loads, tensile in some, compressive in others, although its joints are not locked (pin-jointed). In this case the deformation is a stretching-dominated and the frame collapses by stretching of the struts. Locking the joints now won't change the structure behaviour.

When $M > 0$, as shown in figure 2.6c, concept of self stress is introduced: if the horizontal strut is shortened, the vertical one is put into tension even when no external loads are applied. The struts are stressed even though the structure carries no external loads ($s = 1$, $m = 0$).

All things considered, stretching-dominated ($M \geq 0$) structures have to be used in robust and lightweight structural application whereas bending-dominated ($M < 0$) ones are to be required for energy absorption application.

In the following pages both behaviours are introduced. Since the aim of the project is to manufacture an optimised metal lattice frame, only the theory related to metals has been taken into account. In practice, Ashby states that elastomeric cellular solids always fail by buckling, metallic foams buckle before they yield when the relative density is less than 0.01 and ceramic solids collapse by strut fracture. All the lattices studied in this thesis have a relative density higher than 0.01, thus only yielding collapse is described.

2.1.4. Bending-dominated structures

Cellular solids are defined by their relative density, for an ideal cell like the one shown in figure 2.7, if $t << L$, it is possible to say that:

$$\frac{\tilde{\rho}}{\rho_s} \propto \left(\frac{t}{L}\right)^2 \tag{2.3}$$

where $\tilde{\rho}$ is the density of the foam, ρ_s is the density of the material used, L is the cell size and t is the thickness of the cell edge.

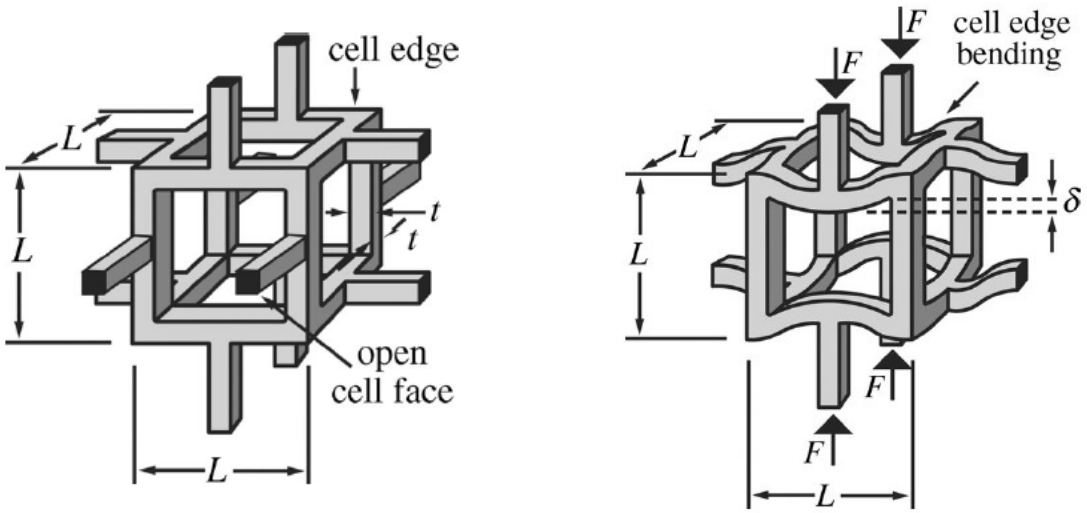

Figure 2.7: *Idealized cell (on the left) and bending-dominated idealized cell (on the right).*

Looking at figure 2.5a we can see that there are three main parameter which have to be determined to fully understand the specimen behaviour:

Elastic modulus $\tilde{E}$;
Plateau stress σ_{pl};
Densification strain ε_d;

These mechanical properties are calculated below, details of which can be found in [4] and in [7]. Having the plateau stress and the densification strain we can have a first idea of the structure energy absorption. This procedure and the following mathematical equations have been derived only for foams, thus they are not used when dealing with lattices.

If the previous cell is loaded as shown in figure 2.7, compressive stress applied exerts a force on the cell edges which makes them bend with a deflection δ:

$$F \propto \sigma L^2 \tag{2.4}$$

$$\delta \propto \frac{FL^3}{E_s I} \tag{2.5}$$

$$I = \frac{t^4}{12} \tag{2.6}$$

where E_s is the modulus of the solid of which the strut is made and I is the geometric moment of inertia of a square. This leads to a strain ε suffered by the cell:

$$\varepsilon = \frac{2\delta}{L} \tag{2.7}$$

Furthermore, assembling all the definitions of stress and strain with bending load provided by linear elastic theory it is possible to define the elastic modulus which characterizes the first regime of the stress-strain compressive curve.

$$\frac{\tilde{E}}{E_s} \propto \left(\frac{\tilde{\rho}}{\rho_s}\right)^2 \tag{2.8}$$

The constant of proportionality is expected to be close to unity because when the relative density equals one the structure real modulus must assume the same value of the material it is made of one.
In order to compute the plateau stress, it is observed that the cell walls yield when the force exerted on them exceeds their fully plastic moment:

$$M_f = \frac{\sigma_{y,s} t^3}{4} \tag{2.9}$$

$$M \propto FL \propto \sigma L^3 \tag{2.10}$$

where $\sigma_{y,s}$ is the yield strength of the solid of which the foam is made of.

With a similar approach it is possible to write:

$$\frac{\widetilde{\sigma_{pl}}}{\sigma_{y,s}} \propto \left(\frac{\tilde{\rho}}{\rho_s}\right)^{3/2} \tag{2.11}$$

The value of the constant of proportionality has been defined both by experiment and by numerical computation equal to 0.3. In figure 2.8 is represented the cell failure due to bending.

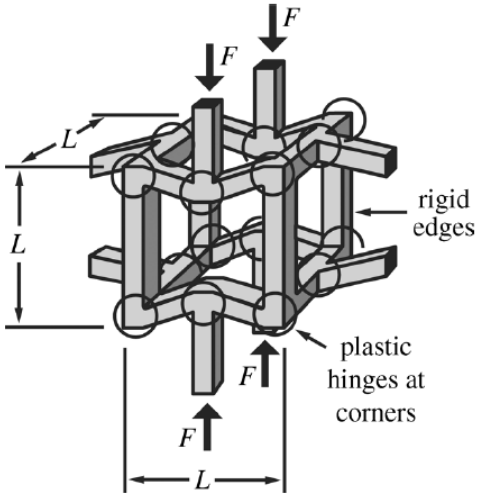

Figure 2.8: *Cell collapsing by the plastic bending of the edges.*

The next step after the collapsing of the cell is the densification of the frame: further bending or buckling are not possible. A strain-induced increase in relative density which is caused by the densification strain:

$$\varepsilon_d = 1 - \left(\frac{\tilde{\rho}}{\rho_s}\right)/\left(\frac{\rho_s}{\rho_s}\right) \tag{2.12}$$

where the dividing term is the relative density at which the frame locks up. It is generally indicated a value for lock up density around 0.6.
Energy absorption is an important feature which makes cellular solid so attractive in engineering applications. Knowing the densification strain, the plateau stress and the volume of the sample, it can be beforehand mathematically estimated as follows:

$$U \approx \widetilde{\sigma_{pl}} \varepsilon_d V \tag{2.13}$$

2.1.5. Stretching-dominated structures

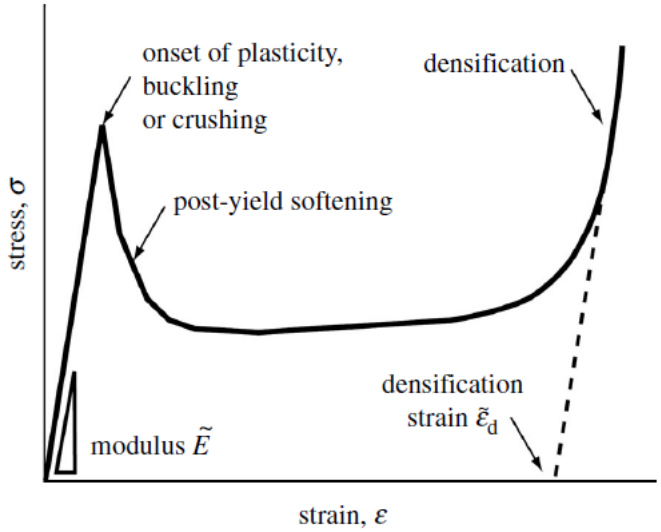

Figure 2.9: *Compressive curve for stretching-dominated frame.*

Consider the tensile loading of the material and its curve shown in figure 2.9. On average, one-third of its struts carry tension when the frame is loaded in simple tension, regardless of the loading direction. It is possible to develop the mathematical formulation following the same approach used for the previous paragraph. Results are shown below:

$$\frac{\tilde{E}}{E_s} \approx \frac{1}{3}\left(\frac{\tilde{\rho}}{\rho_s}\right) \tag{2.14}$$

$$\frac{\widetilde{\sigma_{pl}}}{\sigma_{y,s}} \approx \frac{1}{3}\left(\frac{\tilde{\rho}}{\rho_s}\right) \tag{2.15}$$

2.2. Metamaterials

The mechanical properties of natural materials span a specific, limited range and they are usually related to the physical features of the bulk material. Thus, there are design space limits which cannot be overcome. As years go by, the degree of control over "bottom-up" designed materials processing has greatly progressed and everybody is seeking for materials whose properties could be rationally and wholly designed. Mechanical metamaterials aspire to do that.
The concept of metalattices was first introduced in the field of electromagnetic materials. As written by Kshetrimayum [9] in "*A brief intro to metamaterials*" the russian physicist, Victor Veselago, was the first to proposed metamaterials in 1968 but experimental verification did not occur until recently (1996). In the electromagnetic field these materials are of major interest because they are characterized by negative values of electrical permittivity and magnetic permeability which means that when light enters from vacuum to the metalattices it bends in an unnatural way. Usually light bends toward the normal but for these structures it bends away from the normal as shown in figure 2.10.

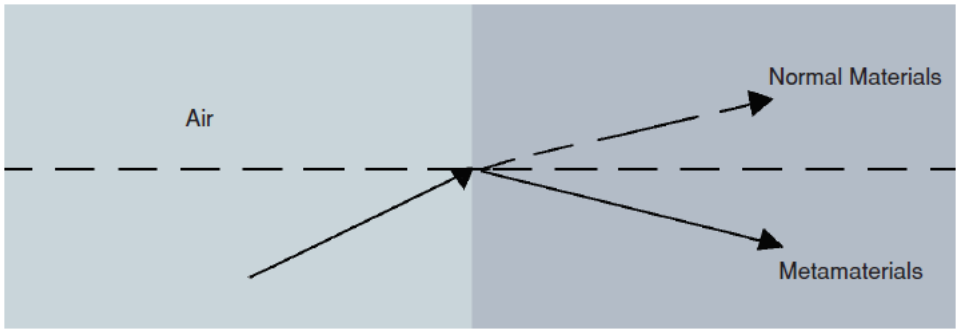

Figure 2.10: *Light bends the "wrong way" when it enters from the vacuum to the metamaterials.*

The metamaterial concept has recently been extended to many other material properties, including materials to achieve novel mechanical behaviours [10]. Various applications include for example, phononic crystals, acoustic metamaterials and auxetic materials. The concept of metamaterials means a frame whose effective properties arise not from the bulk behaviour of the material which composes it, but more from their deliberate inner structuring.
In the spectrum from pure natural materials, that possess intrinsic mechanical properties, to large-scale structures, that are characterized by highly design-specific structural properties, metalattices are in between [11]. When zooming in to look at their micro-scale behaviour, they behave more like structures. However, the overall homogenized

behaviour of metamaterials resembles that of materials. Although concept of mechanical metamaterial is relatively new, particular classes belonging to it were already known since few decades ago such as the auxetic frame.
Traditionally, cellular materials like foams are produced by stochastic processes and thus, their structural parameters are given by a statistical average. Compared to conventional irregular foams, metamaterials design is also more predictable by use of numerical simulations due to the well-ordered frame. However, nowadays there are still some issues related to scalability and manufacturing. As the scale of a unit cell approaches that of the internal structures of the constituent materials, surface phenomena which are negligible at macro-scale may play an important role and actual mechanical characteristics strongly depend on the local interactions between the geometrical structures and the internal structures. On the other hand, the dimension of the struts has minimal threshold which cannot be overcome due to manufacturing constraints and there can be possible degradation in the long-term performance of additive manufactured parts.
Another important feature of these class of materials is the control of the anisotropy of the structure which can modify the stress-strain distribution throughout the specimen. An appropriate example is shown in figure 2.11 below.

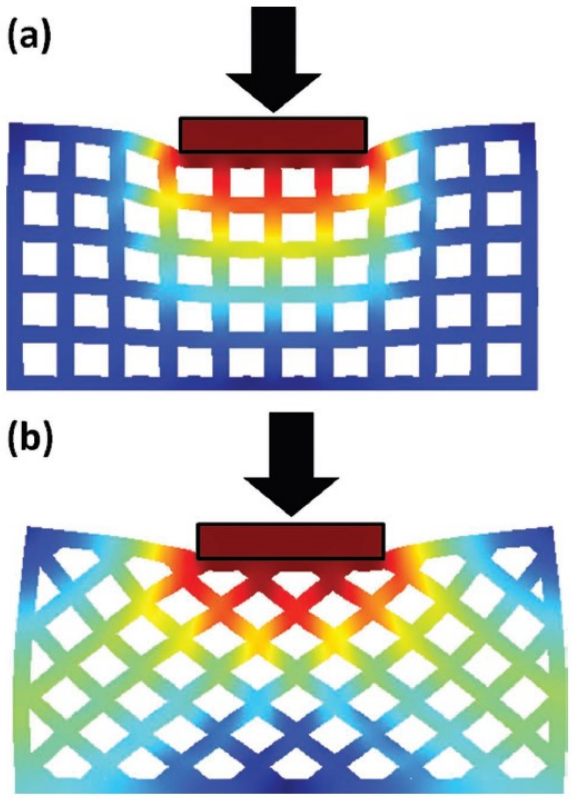

Figure 2.11: *Strain distribution in 2D different frames from the same external displacement.*

All things considered, it is possible to say that metamaterials are the designing answer to the manufacturing freedom introduced to the market by advanced manufacturing processes such as selective laser melting and electron beam melting.

Among all, it is possible to mention the main categories of mechanical metamaterials: extremal materials, negative materials, active/programmable materials, metamaterials based on the ancient Japanese art of paper folding (i.e. Origami).
Extremal materials are defined as structures that are extremely stiff in certain modes of deformation, while extremely compliant in other modes. So, they can be categorized based on their number of compliant modes of deformation: unimode, bimode, trimode etc. Figure 2.12 shows a design of penta-mode material proposed by Milton and Cherkaev.

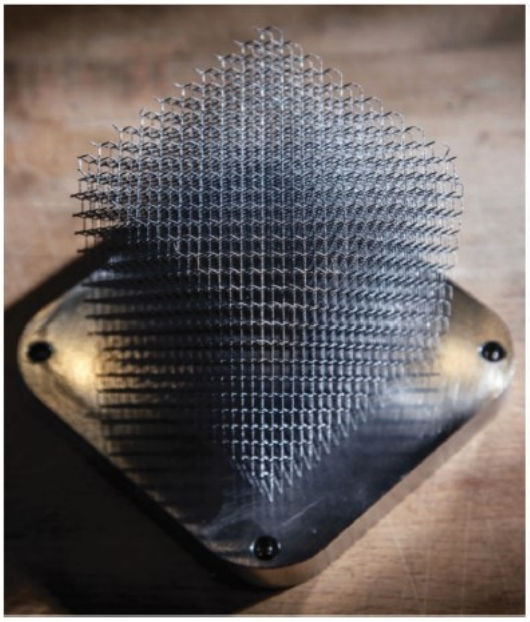

Figure 2.12: *Penta-mode frame*

Negative metamaterials have negative moduli, such as bulk modulus or elastic modulus, basically meaning that a material expands in response to hydrostatic pressure or deforms in a direction opposite to the direction of the applied force.
Active, adaptive and programmable frames allow extreme levels of programmability based on blocks that could perform mathematical operation such as special differentiation in order to activate specific modes of instability when required.
The fourth noteworthy field of research is the paper folding technique. Miura-ori origami is perhaps the most interesting structures and it is shown in figure 2.13. Depending on the shape of the origami frame it has been highlighted that different unusual mechanical properties can be obtained such as negative Poisson's ratios or Young's modulus. Moreover, these structures have shown to demonstrate other significant features such as reconfigurable and reprogrammable behaviours and bi-stability or multi-stability. Nevertheless, even though the technique originated from paper it is now used to fold every type of initially flat material which is possible to handle.

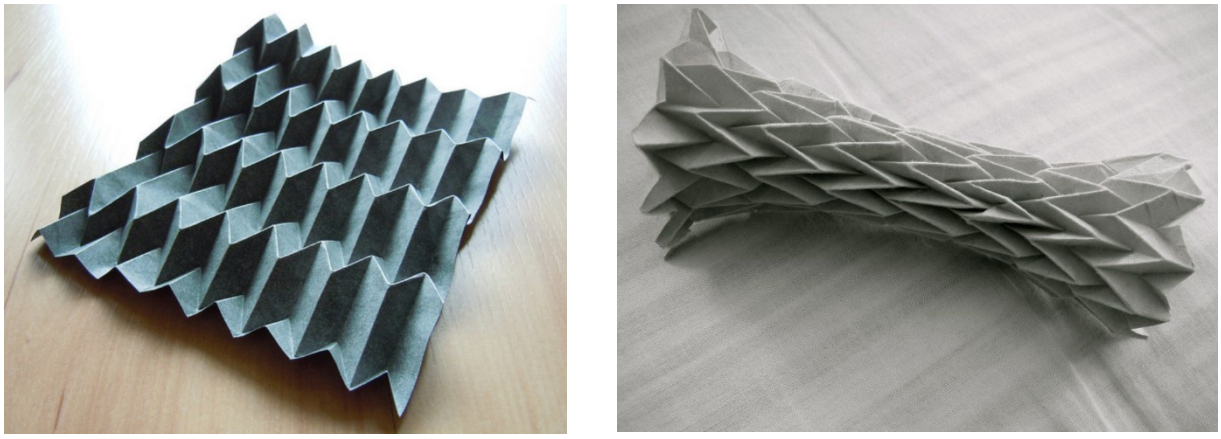

Figure 2.13: *Examples of Origami frames: a Miura-ori shape on the left and a circular origami on the right.*

2.2.1. Lattice structures: applications and benefits

The term lattice structure and cellular material are often used interchangeably in literature because the former is particular category of the latter. As explained in the previous paragraph lattice structure as well as metalattice are open-pored geometrically-ordered frames whose properties are completely defined by a meticulous and tailored design. However, due to the fact that lattice structures appear in varied disciplines such as structural and civil engineering, biological and material sciences and crystallography, there are conflict definitions of what a lattice structure is. Since it is a noteworthy research subject and it is relatively new there is not a real classification of the different structures yet (figure 2.14).

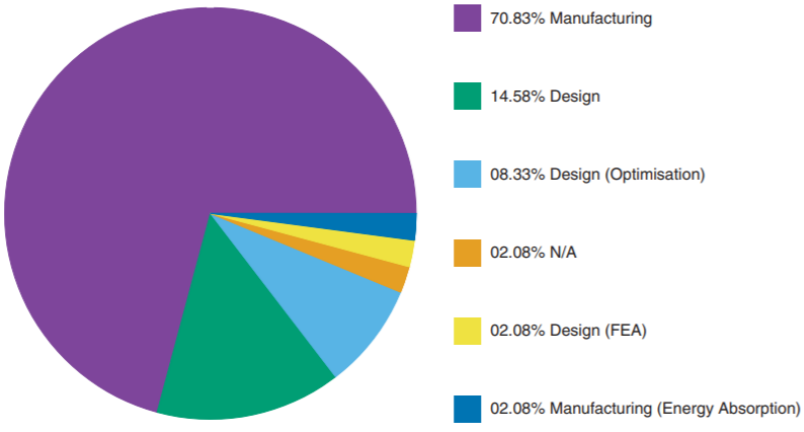

Figure 2.14: *Classification of literature areas that lattice structures are found in.*

For example, according to Ashby [7], lattices are intended to exist in a microscale dimension: usually the unit cell is millimetres or micrometres long. That enables the creation of a proper 'material' with its own mechanical, thermal, acoustic and physical features. On the other hand, Helou [1] states that "lattices are theoretically infinitesimal

in size; however, physical manufacturing has been able to create structures ranging from nanoscale to large scale".
Hitherto, in literature, almost all experimental publications do not conduct a design of experiments in order to properly analyse the effects that differing design variables contribute to the strength of the structure. Due to this, there is a deep lack of design data and statistical analysis to allow the generalisation of cell properties in regards to the inherent strengths and weaknesses of the structure.
For the purposes of this thesis, the definition of a lattice structure proposed by Helou [1] is suggested. "A lattice structure is a space-filling unit cell that is able to be tessellated along any axis with no gaps between cells. The structures are able to be parameterised based on geometry, scale and volume, with either a stochastic, periodic or gradient-dependant topology. They are defined by a reference system that is based on the functional requirements of the end application of the structure."
It is important to underline that the benefits of lattice structures are exploited throughout a variety of industries such as automotive, aerospace, medical and marine industries. In the automotive and aerospace fields applications of these frames have been applied in an attempt to decrease noise conduction, decrease weight and also facilitate the parts recycling. Furthermore, the aerospace industry also aims to increase the performance-to-weight-ratio of parts to obtain better efficiency of vehicles. The energy-absorption properties are also leveraged for protective applications: the lattice can be installed as a sacrificial feature distributing the impact shock across the whole object rather than having just local stresses. From this point of view, auxetic material are perfectly suited.
Even if there is not a clear classification of these structures, some examples are dealt with to give the reader a more practical idea of the typical frames. There are mainly two methods to generate lattice structure: manually generated structure and mathematically generated one. The difference is that the former methodology consists in a design of the frame completely carried out by the designer, whereas the latter methodology defines the frame geometry via algorithms. These concepts will be further discussed in paragraph 2.2.4 ("FEM Modeling"). Figure 2.15 and 2.16 shows some examples of cells and structures.

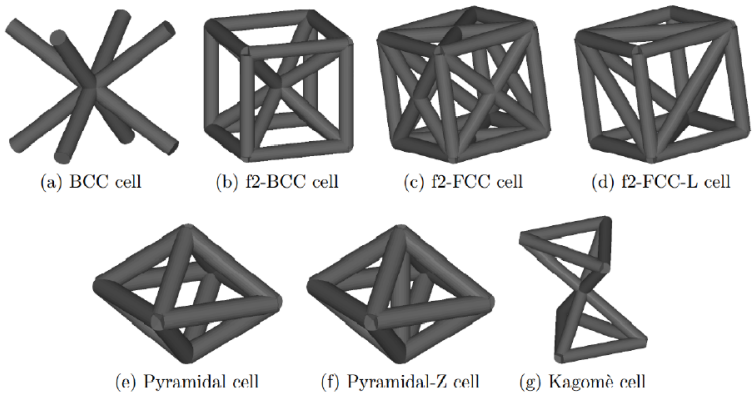

Figure 2.15: *Lattice unit cells.*

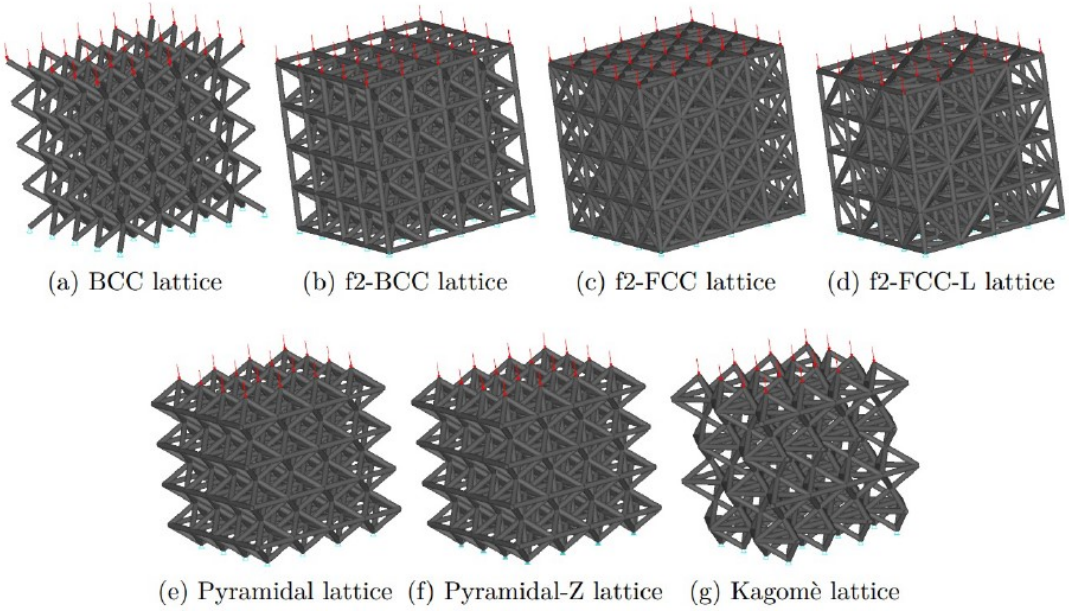

Figure 2.16: *Lattice structures*

2.2.2. Auxetic behaviour

The term auxetic comes from the word "auxetikos" and it means "that which tends to increase". In 1991, Evans et al. [12] were the first ones to use this word to describe those samples which tended to enlarge their cross-section when loaded by an uniaxial tensile stress. Poissons's ratio (ν) is the dimensionless ratio of transverse strain to the longitudinal strain: transverse strain is usually negative for the common materials.

$$\nu = {}^{-\varepsilon_t}/_{\varepsilon_l} \tag{2.16}$$

Counter-intuitively, materials having negative ν or auxetics expand in the unstressed direction under uniaxial stretching.
Auxetic materials are known to exhibit enhanced mechanical characteristics not expected from their conventional counterparts. This particular way of behaving makes the structure collapse inside its own volume rather than outside it and thus, it is appropriate for protection and energy absorption applications. Many other applications can be mentioned such as acoustic vibration filters or microelectromechanical systems (MEMS). The auxetic configuration can be tailored with different types of structures. Among all, it is possible to mention 2D re-entrant honeycombs studied by Gibson, 3D unit cells and models consisting of rigidly rotating parts. Another example of 3D or 2D auxetic frame is the chiral structure: particular models consisting in a number of improper rotation axes which allows the frame to flow into its volume increasing the local density of the sample. Examples of this auxetic frames are shown in figure 2.17.

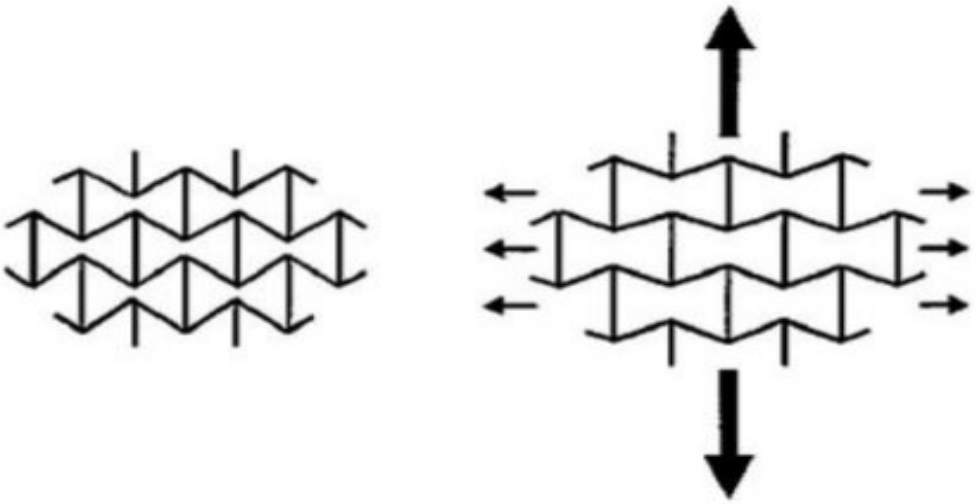

Figure 2.17: *2D re-entrant or butterfly honeycomb frame.*

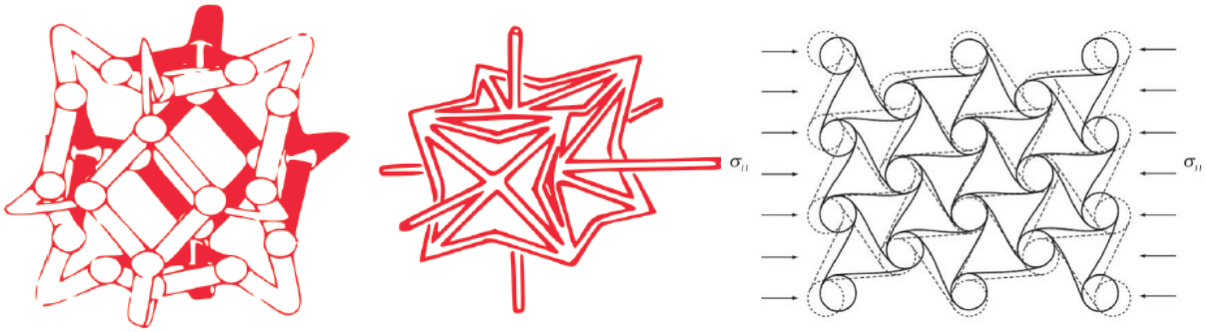

Figure 2.18: *3D re-entrant cell on the left and chiral frame on the right.*

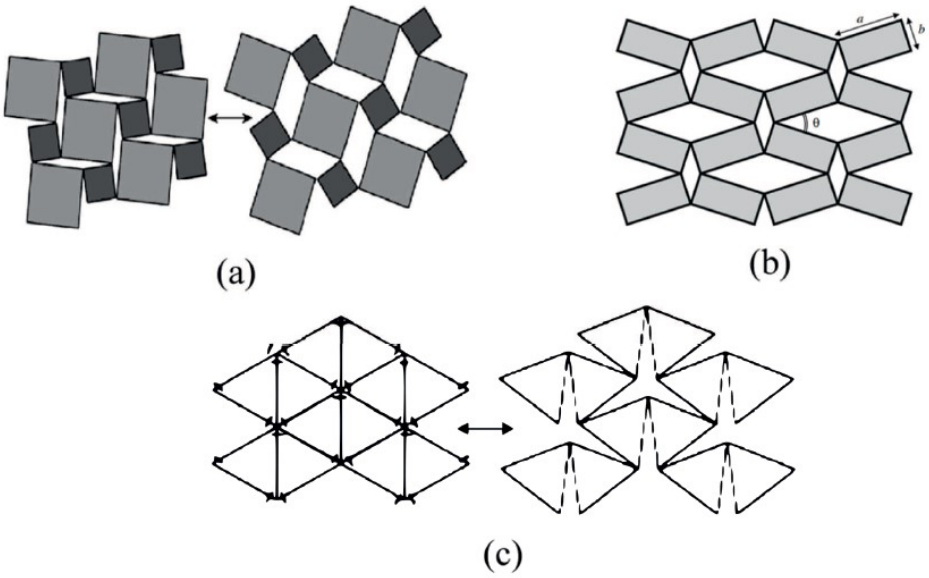

Figure 2.19: *Structures with rotating units: (a) square unit, (b) rectangle unit, (c) triangle unit.*

Throughout the last thirty years, many papers have been written on this subject. Wan et al. [13] dealt with the mathematical background behind the single cell loading and deformation calculating the moments and forces resulting from it and the subsequent stresses and strains. Barchiesi et al. [14] and Lee et al. [10] reviewed the main structures studied hitherto and the main manufacturing methods related to these frames.
However, auxetic structures belong to the extremal metamaterials and just like them they are a relatively new field of research, thus presenting a significative lack of systematic experimental data in the literature.
A particular and rare type of auxetic materials are the dilational materials which have a Poisson's ratio equals to minus one thus the are able to deform homotetically without changing their shape.

2.2.3. Gradient configuration

The advent of new manufacturing technologies like additive manufacturing and Kirigami has deeply pushed the metamaterials designers to explore new uncharted horizonts. One of the new research pathways is the possibility to consider new topologies of cellular structures with gradient characteristics. A gradient lattice is the first step to the realization of the concept of material properties tuneability: it is possible to achieve a gradually varying local distribution of mechanical properties that provides an unusual, directional and tailorable response under indentation, impact and vibration loading. Introducing the gradient into the frame means changing its geometrical or physical parameters along one or more directions of the structure. This changing can be linear or follow some other trend defined beforehand.
Existing gradient lattice configurations have been evaluated as 2D material systems hitherto. Gradient density lattices under high-strain rates are able to control the plastic energy dissipation in a more efficient way that the configuration with periodic cells. The great noteworthy advantages of these way of thinking the structure is the strong localisation of the deformation which can be used as a sacrificial feature under impact in the assembly.
If lattice structures are relatively new, the gradient concept is even newer so only one 3D tetrapot gradient configuration has been designed at the moment. Ground-breaking studies have been published by Lim, Scarpa and Lira. The former pioneered a continuously varying gradient cellular topology based on the variation of the internal cell angle at each cell row. The latters have simulated honeycombs panels made with thickness gradient.
Density gradient is suggested by the bioinspirational example of the fruit Pomelo discussed in the first paragraph, but there is a big number of parameters which can allow the frame to obtain density gradient and other geometrical gradients which will be discussed in the second chapter of this thesis.

Figures 2.20 and 2.21 show respectively in two dimensions the ideas of cell angle gradient and cell edge length gradient. These images belong to Hou et al. [15].

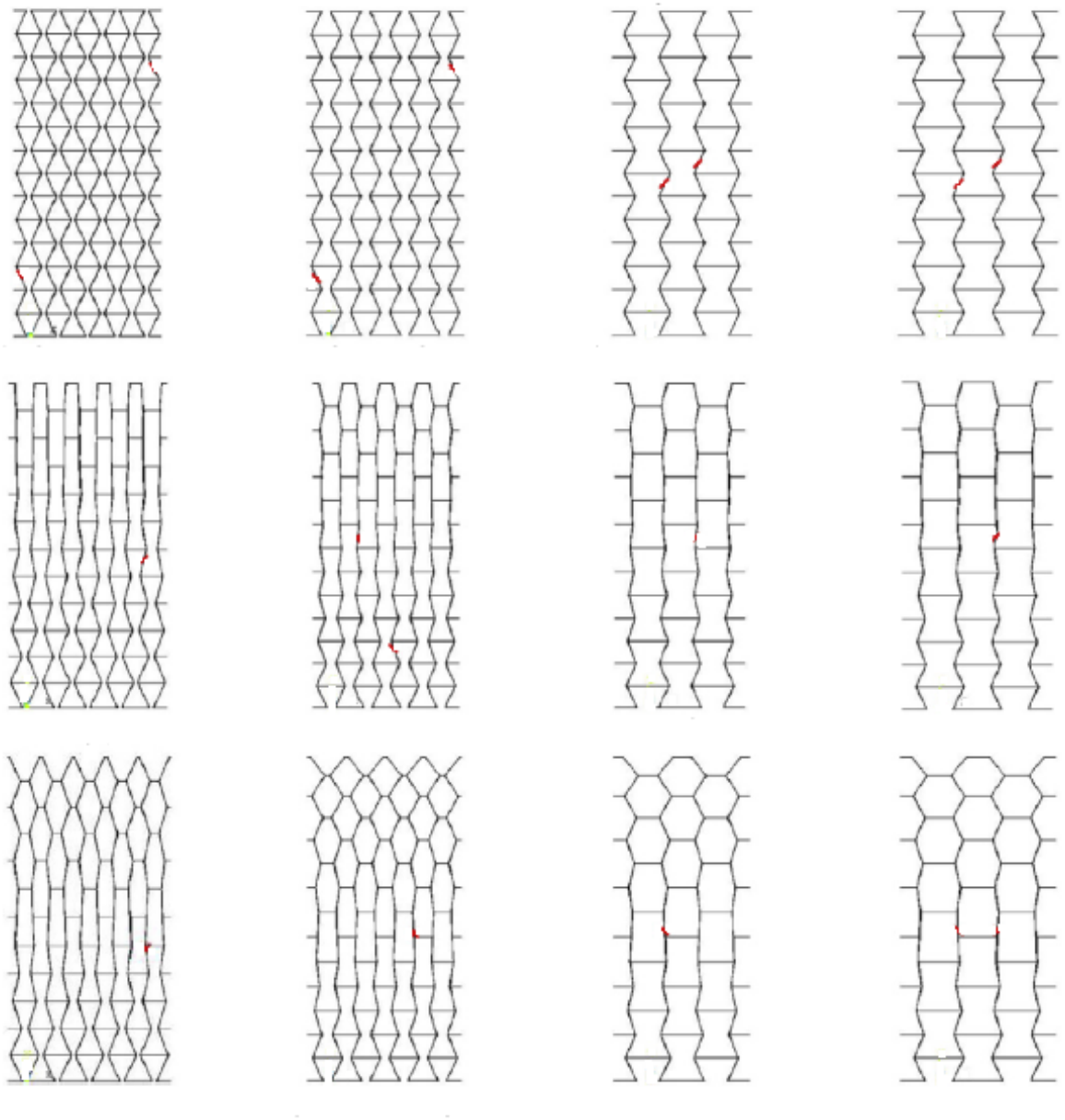

Figure 2.20: *2D cell angle gradient structure.*

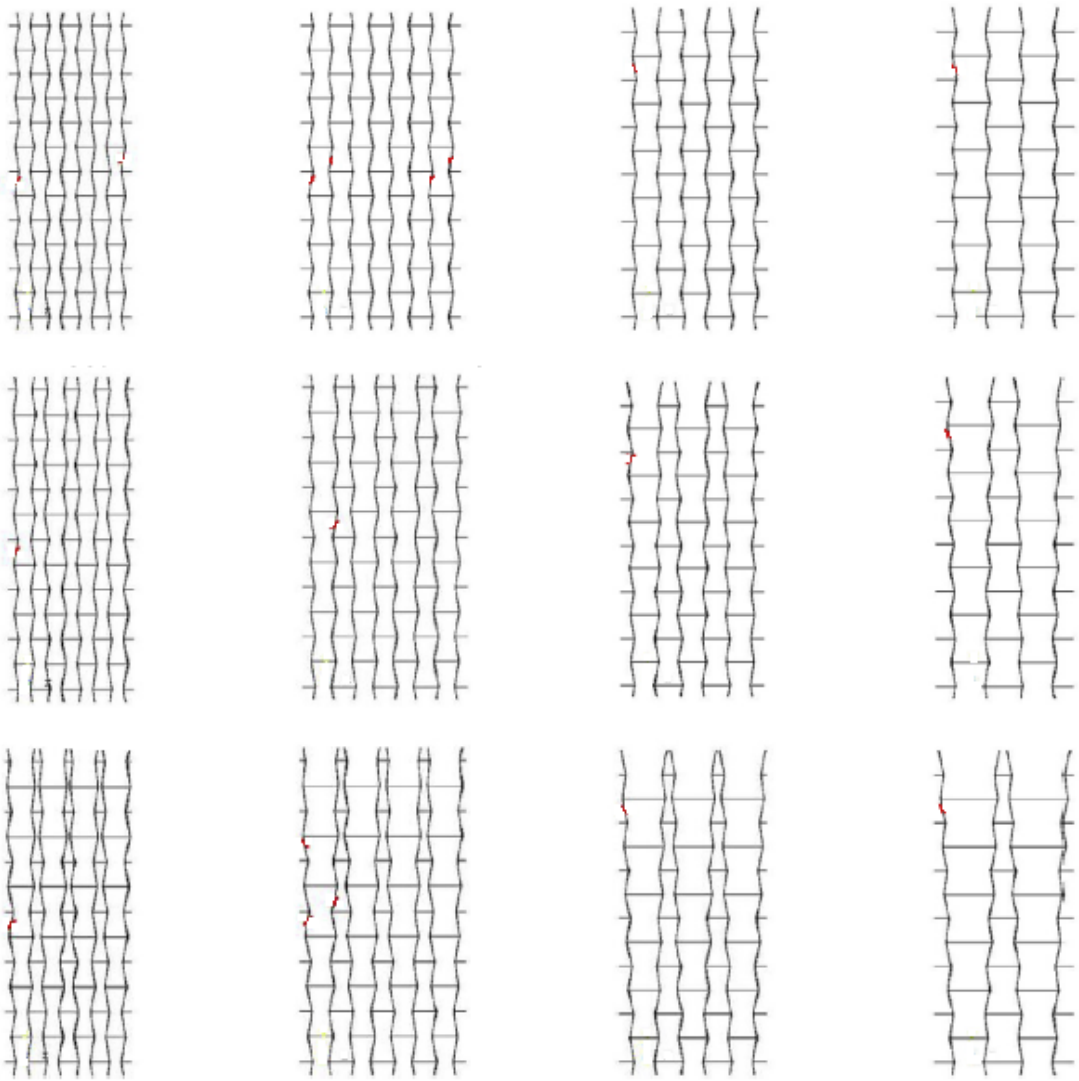

Figure 2.21: *2D cell edge length gradient structure.*

2.2.4. FEM modelling

Finite element method (FEM) is a mathematical technique for setting up and solving systems of partial differentials (or integral) equations. In engineering, the finite element method is used to study systems by dividing it in small elements whose solution is somehow known.
Since metalattices are completely new numerical simulation plays a significant role in the whole analysis. In fact, depending on the particular research aim, it is needed to understand the structures main properties such as the elastic modulus, the compressibility, the Poisson's modulus or energy absorption before beginning the manufacturing part. Obviously, the numerical analysis can be used to mark the path to be followed from a general point of view and experimental measurements are always needed to obtain the specific and more trustworthy values. For example FEM softwares

such as ANSYS or, more frequently, ABAQUS are usually harness to carry out parametric analyses. Figure 2.22 shows a simulation example made with ANSYS.
In literature, there is still no standardised method of modelling and simulating the lattice frame: this is not only due to the novelty of the argument but also to the geometrical complexity and high level of structure customization which is possible to achieve. As a matter of fact, there is a wide variety of unit cells differing from each other in an important way which often forces the designers to make opposite decisions. So, each publication features a different approach.
A common characteristic shared between most studies is the continuum scale approach: lattice strut members are assumed to have uniform mechanical properties and microstructure. Naturally this is not true, because there is a stochastic variation in the microstructure due to the presence of defects derived from the manufacturing process. Lee et al. [16] tried to introduce at least geometric imperfection in their pyramidal truss structure analysis. Mines [17] worked on the plateau stress and collapsing region which lead to the onset strain of densification and pointed out the enormous computational complexity of large lattice frames due to a really high number of elements. As a consequence, it is extremely difficult to run analyses with geometric non linearities and contact elements. Many times in order to grant the computational efficiency, especially in parametric analyses which do not aim to extremely accurate results, it is preferred the beam elements model. Once the structure is fully defined it is advisable to run an analysis with solid elements to obtain more trustworthy values.
It has to be underlined that, especially when simulating microlattices, the continuum scale approach is observed to show limitations. In order to overcome this problem a multiscale modeling approach is suggested: analysing the single cell with appropriate boundary conditions.
Moreover, usually mesh convergence studies are performed beforehand to use the right mesh size in terms of time and computational complexity.
The definition of a finite element analysis procedure identifying boundary conditions specific to lattice structures would be an immensely useful asset so as to be able to compare different publication results. Furthermore, Helou et al. [1] states that there is still no scale effect analysis within the same frame even though the structure behaviour is theoretically expected to depend on it.

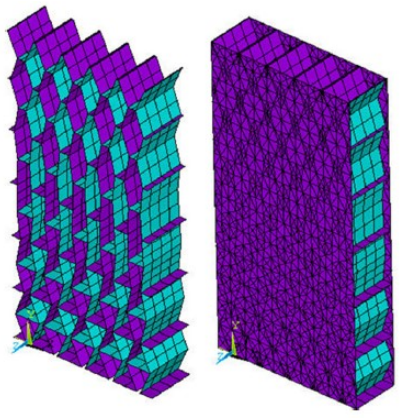

Figure 2.22: *Example of a geometric model in FE analysis of gradient honeycomb sandwich structures [15].*

2.3. Manufacturing processes

There is a wide variety of manufacturing techniques which allow the creation of lattice structures. Although some of them are simply capable of generating reticular frames, others offer the unexpected possibility to fabricate very complex components. It is possible to identify two main categories: traditional methods and advanced manufacturing methods. The formers have the advantage that there is a previous historical knowledge of the process due to the high expertise of technicians who have been working in the field for ages. On the other hand, these processes often have geometrical and structural limitations and drawbacks such as the necessity of creating beforehand the single cell and then assembling all the cells together.
The latters are relatively new and are represented by "Additive Manufacturing" (AM) technologies. The key to how AM works is that parts are made by adding material layer by layer. There are many advantages and some crucial disadvantages when using this process. AM processes are several and many industries all over the world are developing new AM production mechanisms. However, ASTM has defined different classes: "Vat Photopolymerization", "Powder Bed Fusion", "Extrusion-based Systems", "Material Jetting", "Binder Jetting", "Sheet Lamination Processes", "Direct Energy Deposition Processes".
However, for the purpose of this project a metal manufacturing process has to be defined, thus only metal production techniques will be reviewed.

2.3.1. Additive manufacturing

"Additive Manufacturing" is the formalised term for what used to be called "Rapid Prototyping" and what is popularly called "3D Printing". The basic principle of this technology is that a three-dimensional model, initially generated using a "Computer aided design" (CAD) software, can be fabricated directly without the need for process planning. It originated for the polymeric materials production and then it was adapted to ceramics and metals.
This technology is meant to bring a revolutionizing way of thinking the product development through the next years because it allows enormous (but not unlimited) designing freedom, building of lightweight topology-optimised frames, functional assemblies and product customization. Moreover, it has process advantages like the absence of undercuts and times and costs are strictly related to dimensions but not to the geometrical complexity of the part. An example of this last statement is given by figure 2.23 [17].
On the other hand, since it is a new research field there are still few expensive commercial materials printable, working volume are relatively small and building speed are limited.

Therefore, it is still difficult to adapt these fabrication techniques to medium or large production batches.

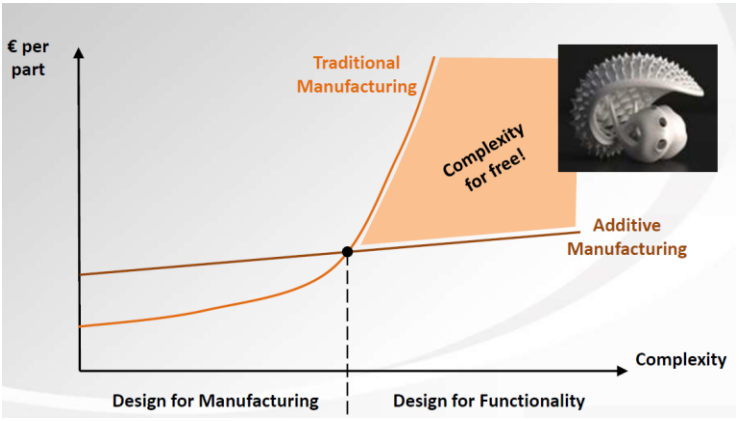

Figure 2.23: *AM advantage.*

2.3.1.1. Selective Laser Melting

The basic concept is the fusion and subsequent re-solidification of thin layers of metal powder which have been spread across the build area using a counter-rotating powder levelling roller. The fusion is obtained by localized heating due to laser beam energy which is focused on the powder following computer-defined paths. The process takes place in an enclosed chamber to prevent oxidation and other type of defects. The powder is maintained at a temperature slightly lower than the powder melting point so as to minimize the required laser energy and to prevent an eventual warping of the structure consequence of a non-uniform thermal expansion and contraction. After the built of each layer the building platform shown in figure 2.24 is lowered. The laser beam is moved and focused using galvanometers. It is important to highlight that this technique is not able to process materials with high reflectivity.

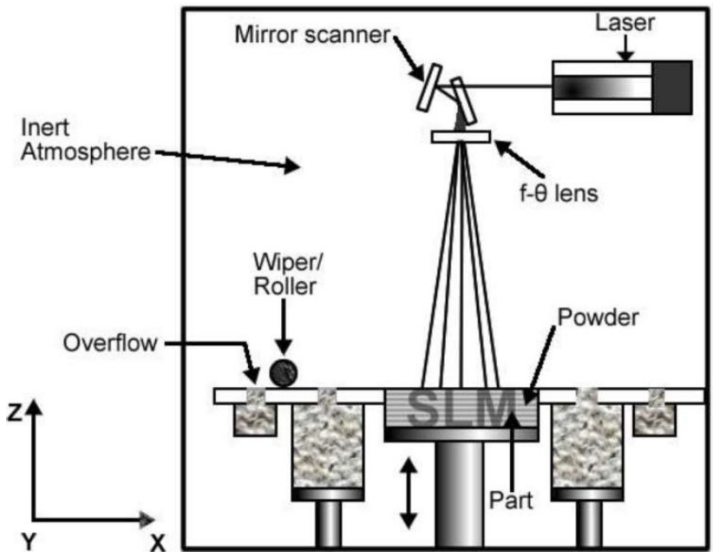

Figure 2.24: *Selective laser melting machine chamber.*

2.3.1.2. Electron Beam Melting

Electron Beam Melting is powder bed fusion process which enables the building of the object by melting the material after it has been deposited. Thus, from this point of view, it is identical to SLM. Unlike SLM, EBM uses a high-energy electron beam as power source and it needs the chamber to be void. Also, this process is able to handle only conductive materials (metals) because powder particles cannot become highly negatively charged. In fact, the repulsive force of neighbouring negatively charged particles can overcome the frictional and gravitational forces holding them in place triggering a rapid powder explosion. Moreover, increasing negative particles in a localised powder spot could repel the incoming negatively charged powder thus creating a more diffuse beam.
Overall, the minimum feature size, layer thickness, resolution and surface finish of an EBM process are typically larger than for SLM one.
Nevertheless, EBM is a much more efficient than SLM because it has a more moderate energy cost and the scan speed is faster.
A schematic illustration of the EBM apparatus is shown in figure 2.25.

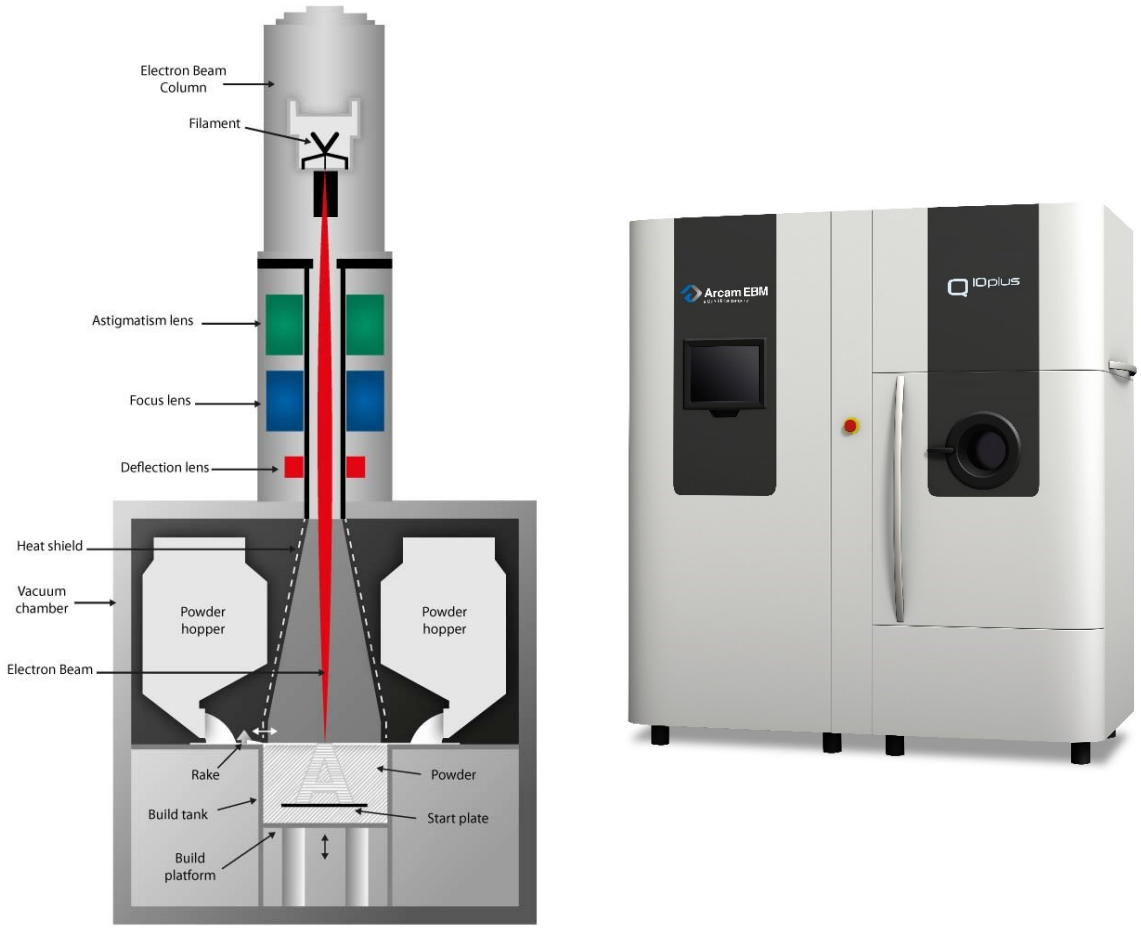

Figure 2.25: *EBM apparatus (ARCAM Q10).*

2.3.1.3. Other additive manufacturing techniques

As said in the introduction of paragraph 2.3, since the aim of the thesis is producing the structure with metal materials only metal manufacturing process are reviewed. Another additive manufacturing method very commonly utilised to produce the lattice frame is Electron Beam Additive Manufacturing (EBAM). Using an electron beam as a thermal source and a metal wire feeder, EBAM is capable of rapid deposition. This technique is fit for building large scale frames because the build volume is almost 6 m in each coordinate system dimension. On the other side, the finishing of the part is not as accurate as SLM.
Moreover, it is a method which can be used also in a low-gravity environment. The building mechanism is shown in figure 2.26.

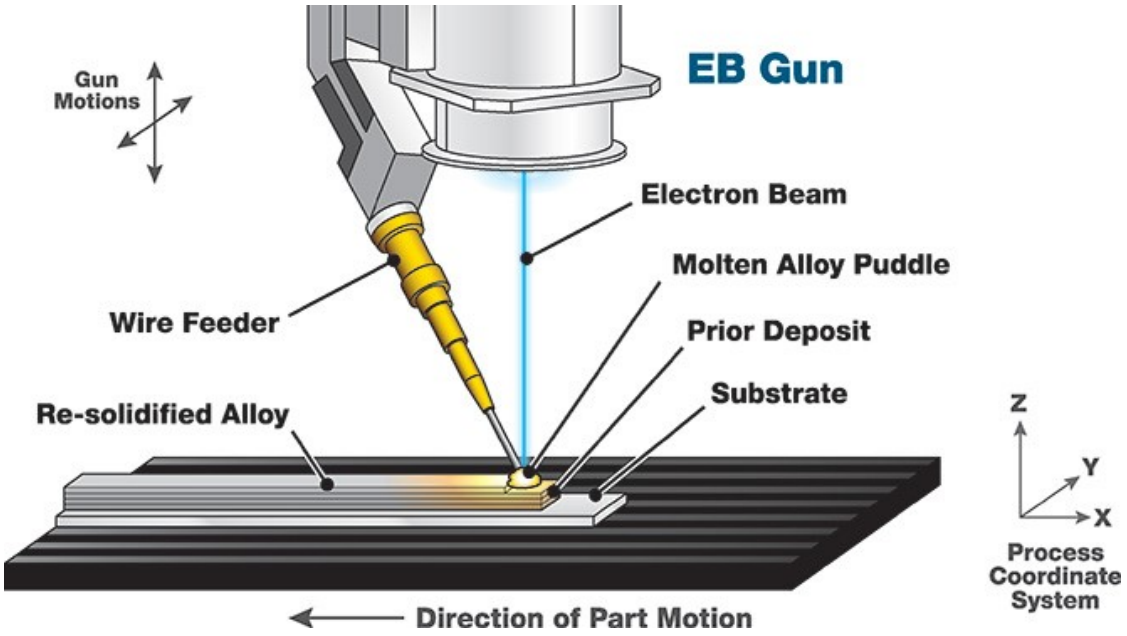

Figure 2.26: *EBAM process.*

2.3.2. Deformation Forming

Deformation forming is a traditional technique which allows the fabrication of periodic-cell structure consisting in only one layer. The shape is given by a simple press forming operation of a 2D pattern with alternate nodes. This 2D mesh is obtained by perforating a metal sheet as shown in figure 2.27. The final step is the bending of the 2D structure at its nodes in order to obtain a specific 3D geometry. It is then possible to bond together the different layers: diffusion bonding, resistance welding, brazing methods or transient liquid phase (TLP). The latter consists in spraying the nodes to be bonded with an alloy

dispersed in a binder which will then be vaporized. The alloy will thus be heated to its melting temperature and left to solidify.
The process causes strain hardening in the deformed parts and so an annealing treating is required.
Generally speaking, this technique shows some limits regarding the processing time, the structural strength, the inefficient use of the materials and last, but not the least, geometrical complexity.

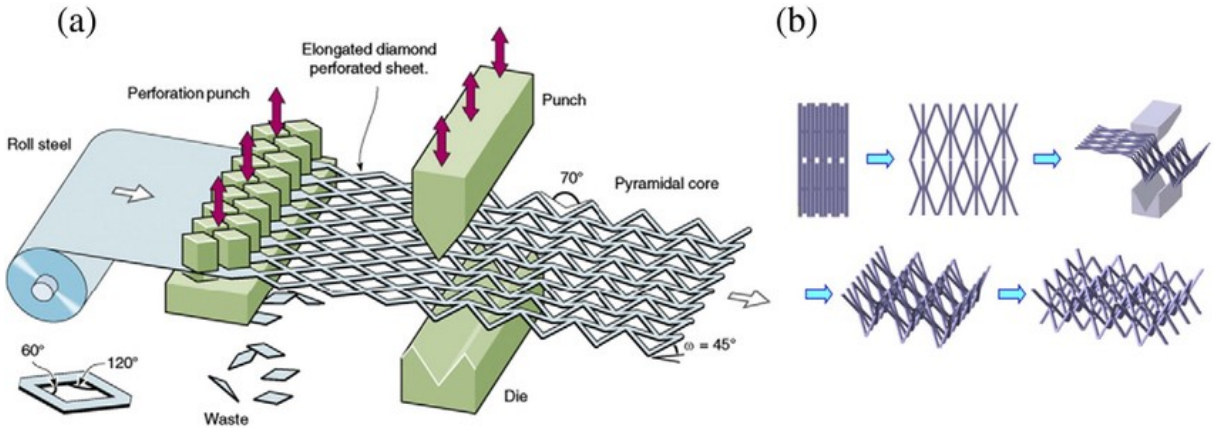

Figure 2.27: *Deformation forming and bonding process.*

2.3.3. Investment casting

Investment casting is definitely one of the most commonly used production techniques when dealing with complex geometry like the one characterizing cellular structures. The process consists in three different steps. The starting phase is the creation of the sample frame with a volatile polymer or wax. Different methods can be used such as injection molding or additive manufacturing. The following step is the coating of the frame with a ceramic slurry. Once the slurry is dried, the polymer or wax material is melted and liquid metal is poured inside the mold. When the metal solidifies, the ceramic shell can be destroyed and the structure can be finished.
This process has theoretically no geometrical complexity limits however practically the more tortuous the frame is the higher are the chances the liquid metal flow solidifies before having reached the extremal spaces. Also, many defects and pores can be found in the object because of the process "iter". In order to make the liquid flow behave in the right way it is mandatory for the metal alloy to show high fluidity.
It has to be underlined that this method is very time-consuming and expensive.
Figure 2.28 represents a sample of Kagome frames realized by investment casting.

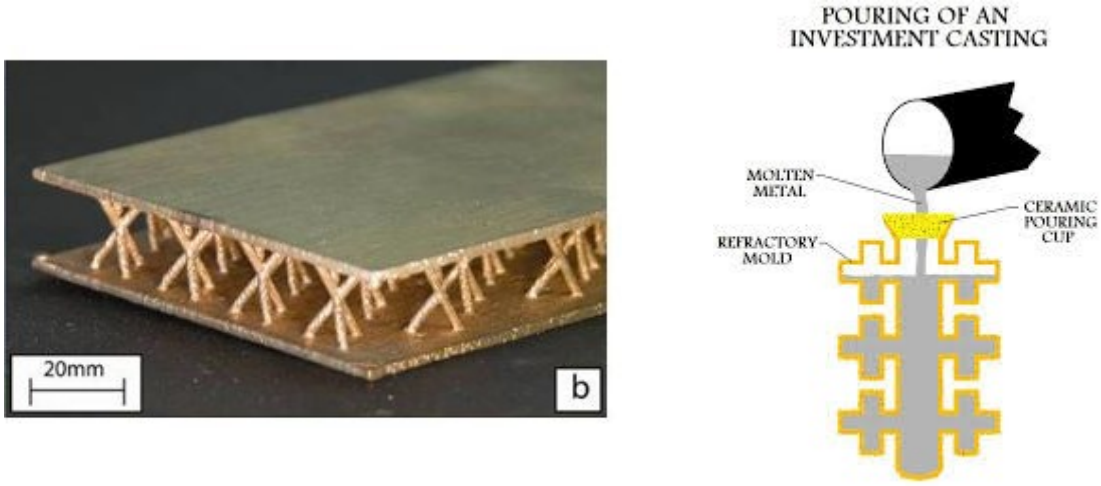

Figure 2.28: *An example of the Kagome frame made with investment casting on the left and the pouring phase on the right.*

2.3.4. Woven and non-woven metal textiles

Woven metal textile process is a simple method of weaving, braiding and sewing of wire drawn from metal alloy to fabricate a woven structure. It is possible to arrange different wire orientations. A wide range of cell aspect ratio and slenderness is accessible. Cellular structures can be made by stacking the fabric and TLP bonding the coupled nodes.
A woven metal frame is shown in the following figure 2.29.

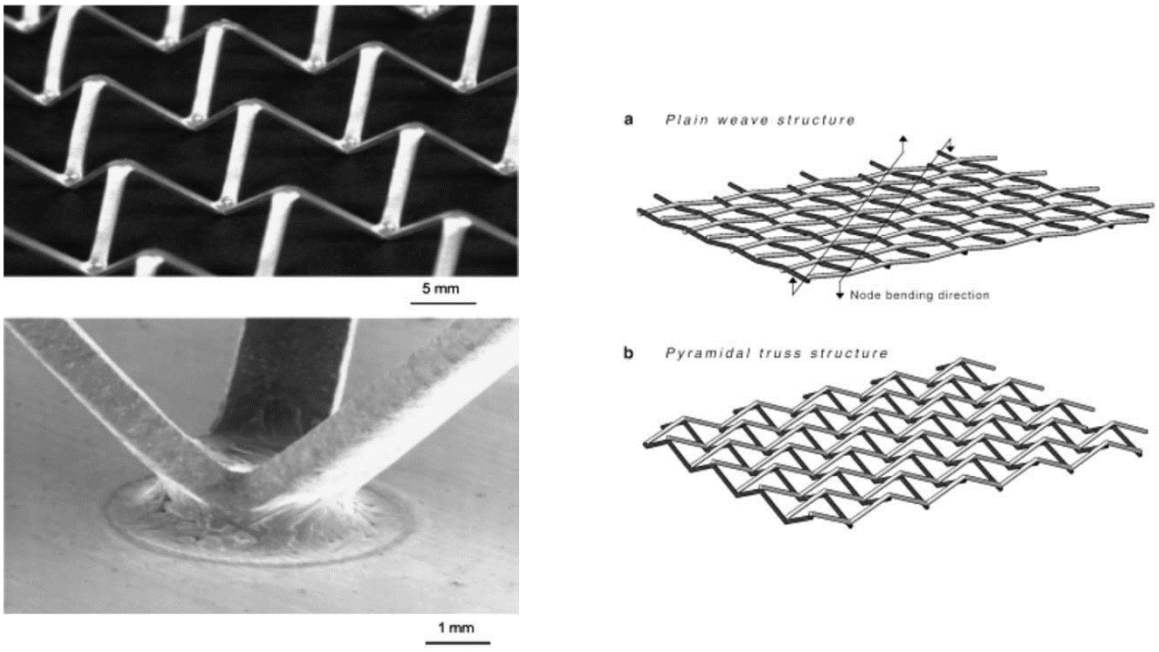

Figure 2.29: *Examples of different woven metal textiles and a representative transient liquid phase bonded node.*

On the other hand, if the frame is made of linear wires or tubes, non-woven textiles processes can be used. These methods using a slotted tool to control wire spacing and orientation, allow the positioning of collinear wires and the alternation of the direction between successive layers. Square and diamond cell structures can be obtained as shown in figure 2.30.

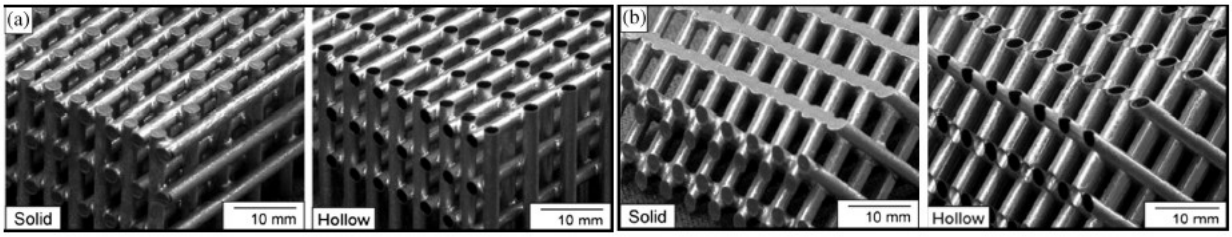

Figure 2.30: *Non-woven metal textiles in square and diamond cell.*

2.4. Project outline and application in Rolls-Royce

From the literature reviewed interesting and steering conclusions can be drawn. 3D lattice structures with gradient configuration and auxetic behaviour are a completely new and forefront concept which has to be wholly studied from either a material and a simulative point of view. As a matter of fact, there is an understandable lack of scientific literature data relating to this type of metalattice and its applications are still to be accurately defined.
If the purpose is to create a frame with a high elastic energy absorption, it is better to design a bending-dominated structure; otherwise, if the aim is to define a very stiff lattice, the stretching-dominated configuration is the way to go.
Bioinspiration can help to identify some aspects which could increase the metamaterial properties: e.g. Pomelo fruit absorbs high deformation energy thanks to its density gradient and its changing geometry along the radial direction.
However, there is still not a standard FEM procedure to analyse these structures and very often the main difficulty lies in the limits of computational resources and in the time efficiency.
Moreover, there are many different ways to manufacture these frames.
The nature of this project is exploratory, with a diagnostic character. The aim of the thesis finds its roots in and industrial challenge: defining an optimised lightweight metamaterial which could be used in different real applications requiring high elastic energy absorption, a functional way of deforming and a sufficient compressive and shear stiffness. This gauntlet was thrown by Rolls-Royce, one of the most important and cutting-edge aerospace companies all over the world.
They wanted the project to give a first solution for this challenge as well as to be an attempt to contribute to a deeper understanding of the factors at play in the behaviour of the structure designed.
Among all, one of the main applications for the defined frame is as an acoustic liner inside the Rolls-Royce engine. In fact, aircraft engines use this component to damp the noise. Liners are applied on the internal wall of the engine nacelle and use the Helmholtz resonance principle for

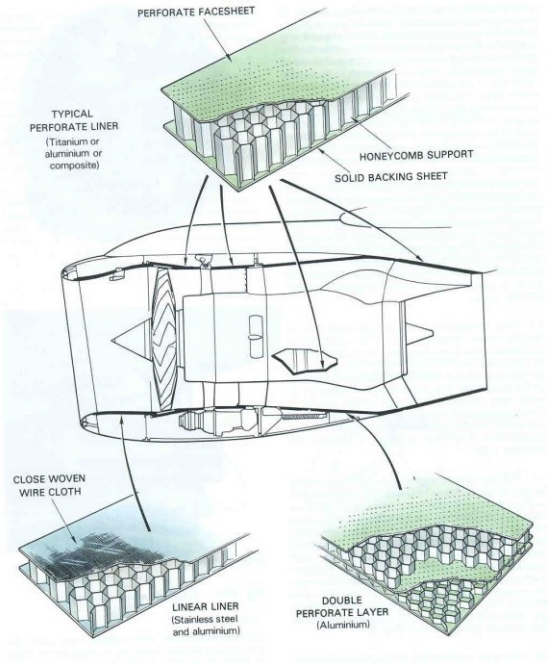

Figure 2.31: *Types of acoustic liners.*

the dissipation of the incident acoustic energy. A Helmholtz resonator increases the amplitude of the vibratory motion of the enclosed air in a chamber by taking energy from sound waves passing in the surrounding space. Thus, the basic liner is made of three different layers: a perforated sheet on the top, honeycomb support in the middle and a backing sheet at the bottom (figure 2.31).
The purpose is changing the honeycomb layer with a 3D lattice which could absorb more specific energy thanks to its auxetic capabilities.
Therefore, the designing and optimisation steps rely on parametric homogenized analyses carried on with FEM simulations both in linear and non-linear fields and underlined specific influences which are taken into account in the final frame design solution. Moreover, once the frame is defined, manufacturing considerations are given to fabricate the samples to be experimentally studied.
On the other hand, the thesis aims at reducing the computational complexities and requirements faced during each simulation, especially with non-linear properties and when the model is an assembly of different parts (e.g. sandwich panels). That is, achieving to define a procedure which could facilitate the direct introduction of this kind of lattice in a model with other parts.
The output of this thesis will ideally serve as a conceptual starting point for more in depth investigations and will need to be followed by the experimental data to validate the parametric analyses.

Part II

Second part

3.Structure definition

In this chapter the definition process of the geometry of the frame will be described beginning with the requirements of the Rolls-Royce group which have to be considered as designing constraints. Starting from these, all the theoretical considerations which brought to the final cell design will be clarified. The structure shape identification is one of the most relevant part of the work because it shows the designing procedure used to obtain certain features and it is a practical example of the "Design for metalattices".

3.1. Single cell definition

As stated in the literature review, hitherto, there have been studies on 2D honeycomb and re-entrant structures, gradient structures and 3D auxetic structures. All the publications point out the natural link between additive manufacturing and lattices and the majority of them analyse the mechanical properties of frames made of cells with a known geometry. This project is meant to go one step forward defining the single cell on its own in order to have particular properties and, once the geometry is almost set, optimising it with a parametric analysis.

3.1.1. Initial considerations

Rolls-Royce is looking for a frame which could replace the actual honeycomb material they are using in their acoustic liners. They want to introduce a lighter alternative and which could possibly still absorb a huge amount of elastic energy during its deformation. Moreover, since the frame is to be used in different applications, in some of them it is required that during its deformation the lattice does not exceed the starting volume in order to ensure the functionality of the item. Nevertheless, there are not strict requirements concerning the elastic modulus and the shear modulus but they both have to be sufficiently high. Thus, the design carried out aims at satisfying all these needs.
After a research in the lightweight structure literature and an initial study phase of the topic, it seemed necessary to reduce the field of investigation just to cellular structures because of their high mechanical properties if compared to their low equivalent density. Moreover, foams and stochastic materials clearly were not an appropriate solution for different reasons: they don't allow to design tuneable properties, there is no possibility of high-level frame customization and they don't show an auxetic behaviour. So, the only category of materials which could fit all the above requirements and provide a customization level as high as the one sought, was found to be the metamaterials one.
Thus, the focal point of the investigation was moved to metalattices and a theoretical design approach has been followed.

As said in the subparagraph 2.1.3 there are two main types of cellular solids: stretching-dominated, with higher specific stiffness, and bending-dominated whose specific energy absorption is more significant. Since the goal of the thesis was to obtain relevant energy absorption with high enough mechanical properties, it was designed a frame which could show a general stretching behaviour and but with bending-dominated deformations on one plane.
That is, the structure was already thought to be applied with a precise orientation in order to be efficient from the energy dissipation point of view. Therefore, the forefront concept was mixing stretching-dominated and bending-dominated properties defining an orthotropic metamaterial having different mechanical features along three mutually-orthogonal directions.
Furthermore, the shape of the single cell in the bending-dominated plane was derived from the classic re-entrant honeycomb cell which exhibits auxetic features thus providing excellent energy absorption and negative Poisson's modulus.
In order to obtain the 3D lightweight cell, the conventional honeycomb walls were replaced with a set of diagonal and horizontal struts as shown in figure 3.1. These elements were positioned in a precise direction so as to increase the stiffness of the structure and to obtain a more homogeneous behaviour of the single unit and of all the assembly. Also, looking ahead it was necessary to orientate the diagonal struts located at the two base sides of the cell in the same direction so that the whole frame building could be ensured without facing overlapping issues between neighbouring cells. In fact, the nature of the structure is periodic and so its generation is meant to be a simple replication of a basic unit. For this same reason, the diagonal strut on one of the two top lateral sides is collinear with the strut located at one of the two bottom opposite sides and the other way around.

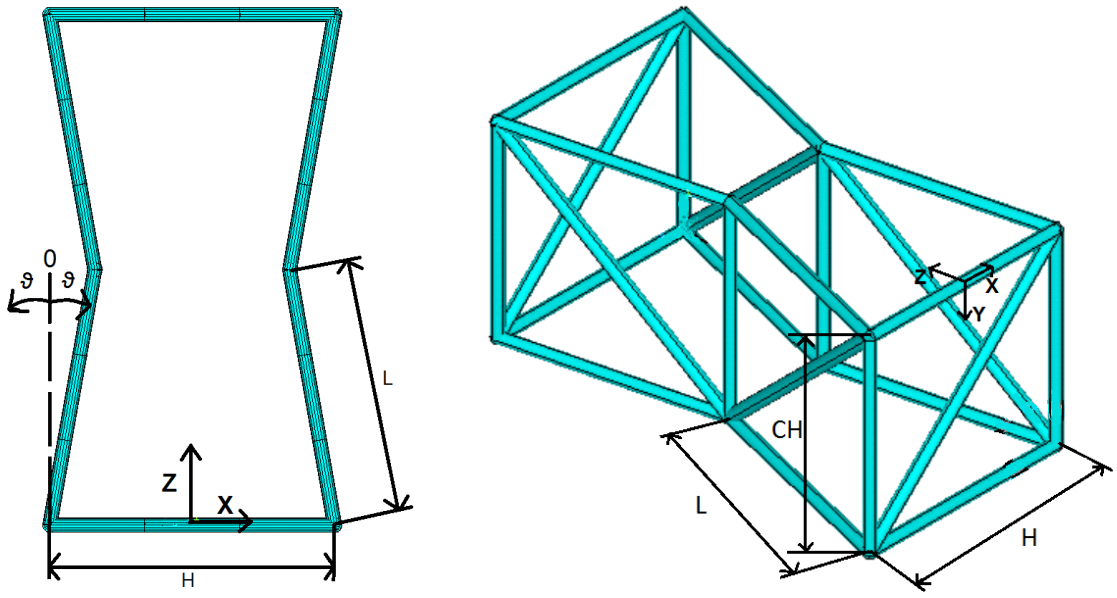

Figure 3.1: *Auxetic 3D lattice unit cell: bending-dominated behaviour on the plane x-z and stretching-dominated behaviour in the other planes.*

The 2D Maxwell's formula can be used to verify the bending behaviour in the x-z plane and 3D one to verify the general behaviour of the 3D lattice. The x-z plane is shown in figure 3.1 and, if only that plane is considered, there are six struts and six joints. As result, formulas (2.1) and (2.2) give a negative M factor (M=-3) thus categorizing the 2D deformation as a bending-dominated one. On the other hand, analysing the x-y plane, five struts and four joints are counted, whereas, analysing the y-z plane, nine struts and six joints are counted. In this case the equation (2.2) gives an M factor equals to zero for both pairs of values, thus identifying the frame as a stretching-dominated.
However, if the whole cell is taken into account, there are twenty-four struts and twelve nodes which lead to negative value of M. Consequently, the general behaviour of the structure is bending-dominated but only the x-z plane is actually mainly characterized by bending. On the contrary, the other two planes are stretching-dominated. Accordingly, from a theoretical point of view, the frame is expected to be stiffer in the y direction and to absorb more deformation energy along the z and x directions.
As a result, the whole lattice is thought to be loaded along the z axis and thus, orientated in that direction inside the acoustic liner.

3.1.2. Cell parameters

Since the thesis has an exploratory nature, the single unit has been parameterized to investigate numerically the different influences which each parameter has on the structure behaviour. So, in this section all the main variables will be introduced and explained referring to the global coordinate system and to the symbols used in figure 3.1. The cell shape is completely described by five key parameters: "H", "α", "ϑ", "CH" and "φ".
"H" is the length of the base side of the cell. That is, the edge which is collinear with the x direction in figure 3.1. This parameter set the dimension of the single cell and consequently of the lattice. Changing its value means observing the "size effect": it is the influence of the dimension of the single cell on the structure behaviour. Furthermore, the variation of "H" can give some information on the effect of the slenderness of the struts used if the dimension of the strut does not depend on it.
"α" is called the aspect ratio of the cell and it is the ratio between "H" and "L". "L" is the length of the lateral edge of the cell as shown in figure 3.1. "α" is a relevant factor because it controls the shape of the cell as well as its size to a lesser extent. If "H" is set, increasing the aspect ratio means reducing the cell height along the z direction by decreasing the lateral edges length.
As far as what concerns the cell shape, another meaningful parameter is "ϑ" which is the angle that measures the inclination of the lateral edges. The angle is evaluated in degree and it is considered zero if the lateral edge is perpendicular to the base side "H".

Furthermore, "ϑ" is positive if it is counter clockwise and vice versa as directly shown in figure 3.1.
The parameter which imparts the three-dimensionality to the cell is the "CH" which stands for cell height. It is the allowance which is measured in the y direction as highlighted in figure 3.1. However, this parameter is less interesting than the others because it doesn't affect the properties in the auxetic plane (x-z) and thus it has an influence only on the elastic modulus in the y direction and on the overall density. Therefore, it has been chosen to ignore its leverage setting its value to ten millimetres for each analysis.
All the factors which have been introduced do not define the type of strut chosen. Since the dimensions characterizing the frame are typically slightly smaller than centimetres, the strut cross-section dimensions must be at least one order smaller than the beam length in order for the lattice not to be a massive one. Consequently, also looking ahead to manufacturing issues, a circular cross-section was designed whose diameter is "φ".

3.1.3. FEM model

The parametric design language provided by ANSYS is basically derived from Fortran. It allows the programmer to generate the geometry and then giving to each part its physical, mechanical and structural properties. Then the structure can be meshed, loaded and constrained as wanted. The last step is the solution process and the definition of the outputs.
All these activities are summarized in three distinct environments:

- Pre-processing
- Solution
- Post-processing

At the beginning of the project, the purpose was to create directly a volume geometry which could have helped to consider the contact between elements. However, with ANSYS there are two many designing obstacles to be overcome and thus, it was decided to define the lattice volume with Solidworks (Computer-aided design software) and Excel. Unfortunately, even though this designing process could have worked (as pointed out in paragraph 3.3), it would have not been possible to carry out a parametric analysis because it would have taken too long. This is why a simpler approach was preferred: defining the whole structure only with lines associated with longitudinal double-nodes element (e.g. beams or links).
As a matter of fact, in order to build the single unit of the frame and facilitate the creation of a periodic lattice in an iterative way the main script relies on a macro called "CELL". A macro is a command file in which it is possible to record a frequently used

sequence of ANSYS commands. Creating a macro enables you to, in effect, create your own custom ANSYS function. This is what was done by defining "CELL": it takes in input all the geometric parameters defined above (apart from the element diameter), the numbers to be assigned to all the twelve keypoints created to generate the single cell, the z location of the first keypoint defined and lastly, the value of the gradient of "H". This last input will be explained in the following paragraph.
What "CELL" does is simply creating a single cell identical to the one shown in figure 3.1 by locating the keypoints in the local coordinate system and by linking them with the appropriate lines. It needs to be underlined that each cell can be located wherever needed thanks to the z location input and that "CELL" works with a local coordinate system which is different from the global one. The script is based on geometric considerations and it is set out the Annex.

3.2. 3D lattice generation

Lattices are periodic structures and so this means that they can be built in a periodic way. That is, by iterating the same commands many times. The 3D frame generation "iter" is the following:

1. First cell;
2. First column;
3. First floor;
4. 3D frame.

The first cell is produced by the "CELL" macro as explained above. Then, the idea is to use the same macro with different inputs in an iterative way to build a single column made of a set number of cells stacked on top of another as shown in figure 3.2.

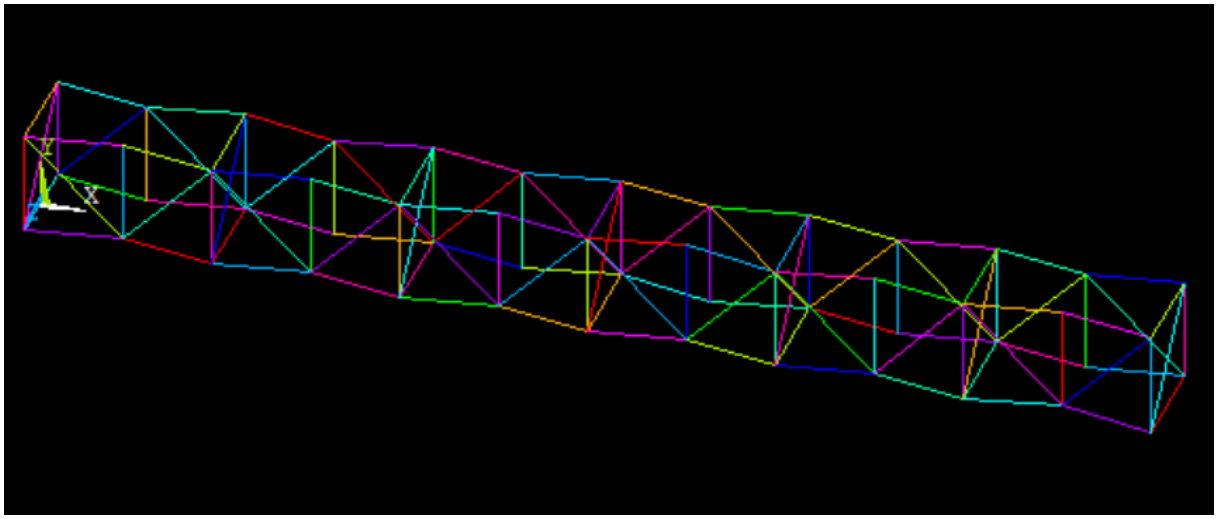

Figure 3.2: *Single column.*

Once, the first column is generated, the "MAIN SCRIPT", which is the file which controls the whole lattice generation, copies it and replicated it as many times as the user wants (figure 3.4). The repetition direction is fixed along the z axis in the local coordinate system (figure 3.2), but it corresponds to the x axis in the global (final) one. The repetition step is automatically defined by the program thanks to an "if" clause which takes into account the presence of the "H" gradient thus modifying the distance between the centre lines ("DBCL") of two consecutive columns as clarified by figure 3.3. The "DBCL" is a parameter which depends on "H", "α" and "ϑ" if the frame doesn't show any base edge length gradient. Otherwise, as shown in the "MAIN SCRIPT" set out in

Annex, it will be calculated in different ways depending on the value of the gradient. However, parameters gradients will be explained in the following paragraph.

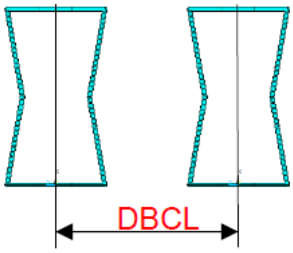

Figure 3.4: *Distance between two consecutive columns*

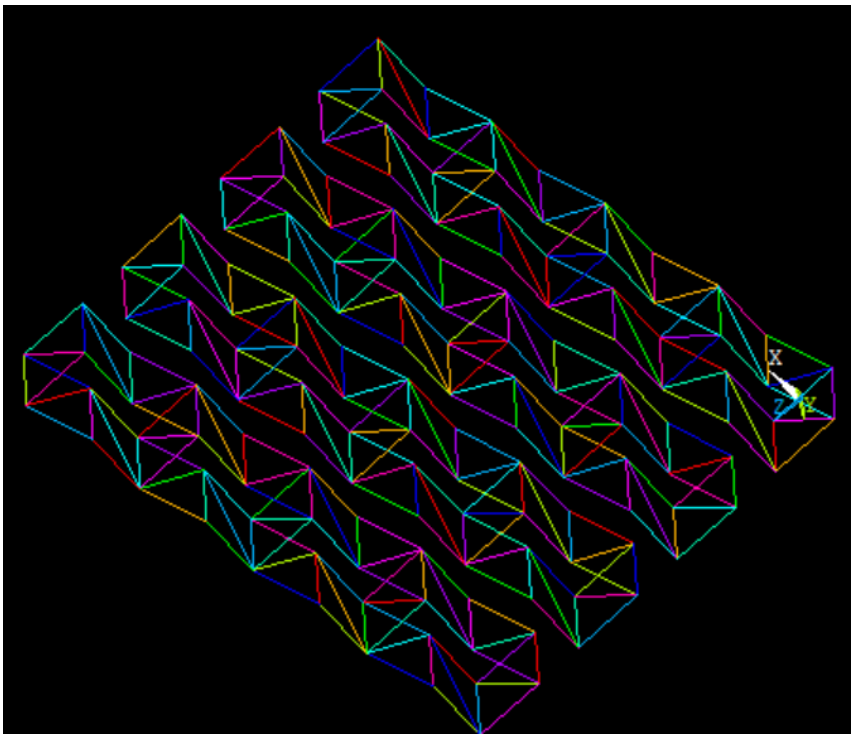

Figure 3.4: *Set of collinear columns.*

To obtain the first floor of the frame it is necessary to bond together the columns. This purpose is achieved by the definition of the macro file "BONDING" whose commands generates a set of programmed lines which link in rationale way the keypoints of the different neighbouring columns. The gist of this script is mainly mathematical because the keypoints must be linked in the proper way so to create an exact periodic structure (figure 3.5). "BONDING" macro is set out in the Annex.
In figure 3.5 the way in which the columns are bonded together can be observed. It is important to underline that consecutives columns show opposite orientation of the diagonal beams of the base face (y-z plane). Therefore, a more isotropic behaviour can be achieved.

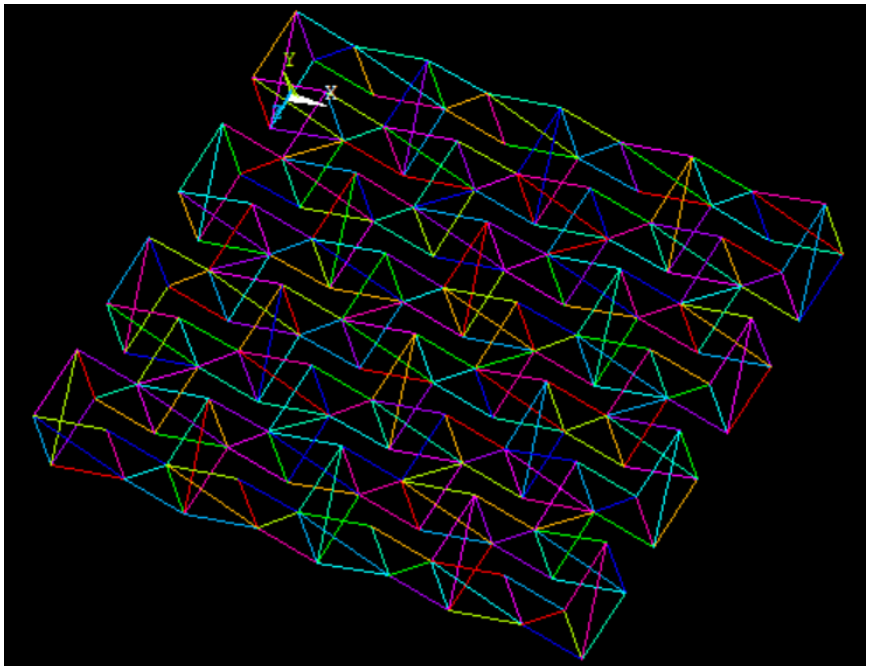

Figure 3.5: *First floor.*

Once the first floor is built, the "MAIN SCRIPT" replicates it along the y axis in the local system as many times as the user prescribes thus creating a 3D lattice. Then the whole frame is rotated in order to make the local and global coordinate system match. The number of columns, rows and floors of the lattice is defined in the "MAIN SCRIPT" via three variables: respectively "NC", "NR" and "NF". Figure 3.6 shows an example of a basic metalattice.

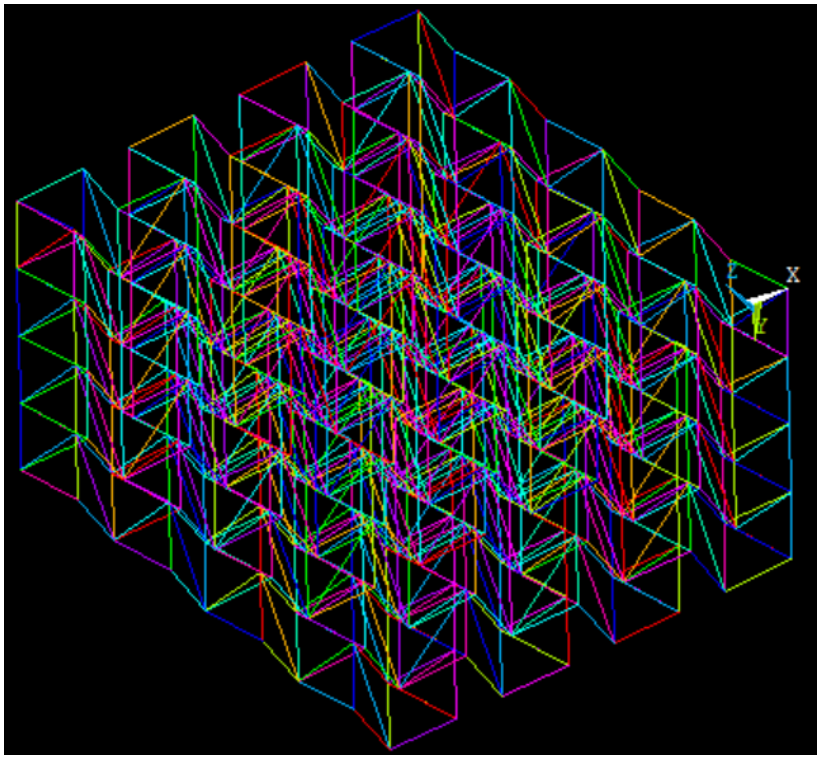

Figure 3.6: *Lattice.*

3.2.1. Gradients

As stated in the previous chapters, the project aims at defining a metalattice with tuneable physical and mechanical properties. This demand is met only with the introduction of special features which can help to customize at a deeper level the lattice: parameters gradients and parameters gradients delay. In this subparagraph the former will be explained.
Hitherto, the scripts used don't allow the lattice to change its unit shape along the z axis because the parameters are constant during all the building process. However, knowing that the metalattice generation is iterative, it is possible to introduce constants to be added at each iteration to the initial parameters values in order to obtain a finite variation of the input given to the macro "CELL" step by step.
This new set of parameters are called "gradients" and are related to the main parameters, apart from the beam diameter. Therefore, there are respectively "DH", "Dα" and "Dϑ". "DH" is the gradient of the base edge of the single cell, "Dα" is the gradient of the aspect ratio and "Dϑ" is the gradient of the angle. By means of these values the morphology of the lattice single unit changes and a modification of the local density of the frame is obtained.
The beam diameter isn't associated with any gradient because from a manufacturing point of view and from a volume designing point of view was thought to be too difficult to obtain. The main issues happen at the joints where there are lot of intersections of beams with different diameters which have to be joined without facing stress concentration problems.
However, from an algorithmic point of view, the idea is implemented by a set of "IF" clauses which change iteration after iteration the value of the input parameter given to "CELL" by adding the value of the gradient inserted by the user every time. This value can be either positive or negative.
It is important to underline that the scripts don't check the geometry of the frame to ensure that it is effectively manufacturable or it has a meaningful shape from a geometrical point of view. Therefore, the user must check by himself that the struts of adjacent columns do not touch each other or that there is no overlapping of beams due to a misleading value of the gradients inserted.
As previously said, the "DH" is crucial factor because depending on its value the lattice is built in different ways and with slightly different shapes. Notwithstanding the idea of building a structure always with the same proportions and whose generation procedure varies continuously from a shape to another, when gradients are considered, some macro adjustments have to be done. As a matter of fact, the distance between two consecutive columns ("DBCL" value in figure 3.4) needs to change depending on the value of the "DH". Otherwise, the base side length could increase more than the space provided between two consecutive columns and there would be an overlapping of cells. So, a set

of “IF” clauses has been written to change the “DBCL” in order to prevent this issue. It is set out hereunder:

```
*IF,DH,EQ,0,THEN                                    !case 1: no H gradient.
DBCL=H1+2*((H1/2)-(H1/ALPHA1)*SIN(-THETA1))
*ELSEIF,DH,GT,0                                     !case 2: positive H gradient.
DBCL=H1+(NR-IQ)*DH+DI*4
*ELSEIF,DH,LT,0                                     !case 3: negative H gradient.
DBCL=H1+DI*4
*ENDIF
```

Unfortunately, the distance between columns changes in a finite way and thus the volume occupied by the lattice varies in an asymmetric manner if the “DH” is positive or negative. This concept will be useful to comprehend some results in the following paragraphs.
It has to be pointed out that from now on the geometric variables at the bottom row (“H”, “α”, “ϑ”) will be called (“H1”, “α1”, “ϑ1”) in order to differentiate the initial value to the values obtained for the other rows adding the gradient constant.
In figure 3.7 three different structure are shown: each structure changes the value of a different parameter through its gradient.

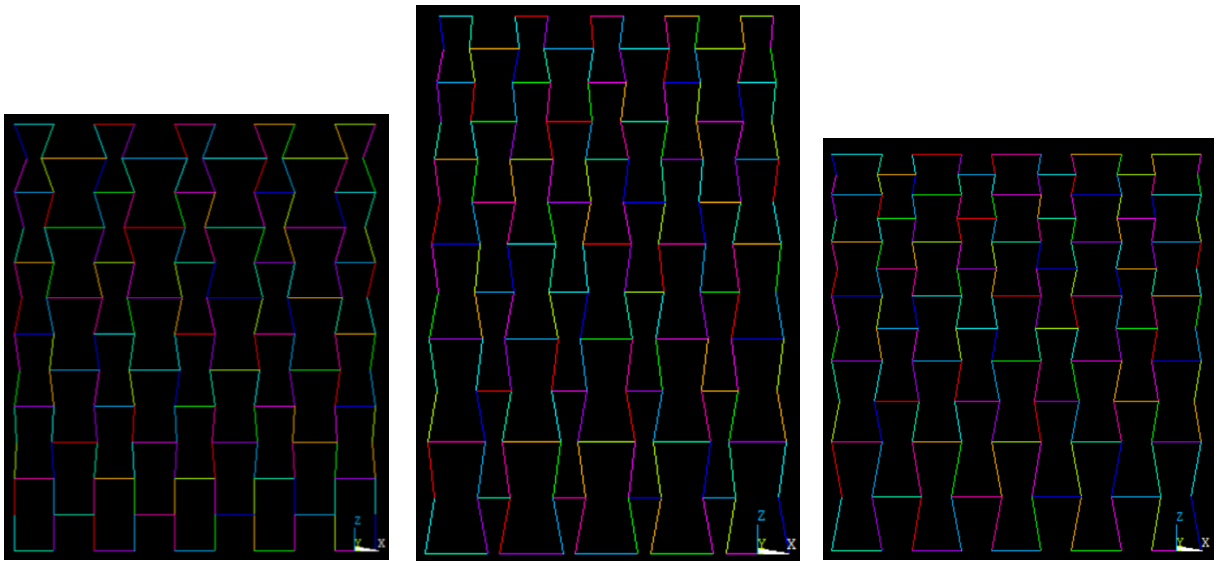

Figure 3.7: *Lattice with “Dϑ” on the left, lattice with “DH” in centre and lattice with “Dα” on the right.*

3.2.2. Gradients delay

From an industrial and designing point of view could also be interesting having the possibility to control the position at which the gradient begins in order to customize the lattice at most. That is introducing in the script other variables which could inhibit the gradients effect by postponing it to the following rows. These variables are called "gradients delays". These special features allow the generation of two completely different structures coexisting within one without any sudden morphology changing which could lead to stress concentration. Furthermore, this means that the designer is given the possibility to adapt the mechanical properties via modifying both frames. For example, the bottom part could be stiffer thanks to a stretching-dominated behaviour and the upper part could be designed with a bending-dominated deformation so as to be softer and more deformable. From this point of view, this concept is very close to Rolls-Royce aims. They would like to reduce the number of layers of the acoustic liner from three to two with a structure which is able to change its behaviour depending on the location analysed.
Unlike the gradient feature, the delay one is not easy to implement because not only a new set of variables is needed but also a completely new set of "IF" clauses which control the building process cell by cell and, depending on the cell position, changes the input to give to the macro "CELL". The algorithm which runs all the logic tests before giving the right inputs to "CELL" is completely included in the previous part of the "MAIN SCRIPT" (set out in the Annex) and the delays parameter for "DH", "Dα" and "Dϑ" are called respectively "DELAY_H", "DELAY_A" and "DELAY_T".
In the image below there is a vivid example of the effect of the three delays.

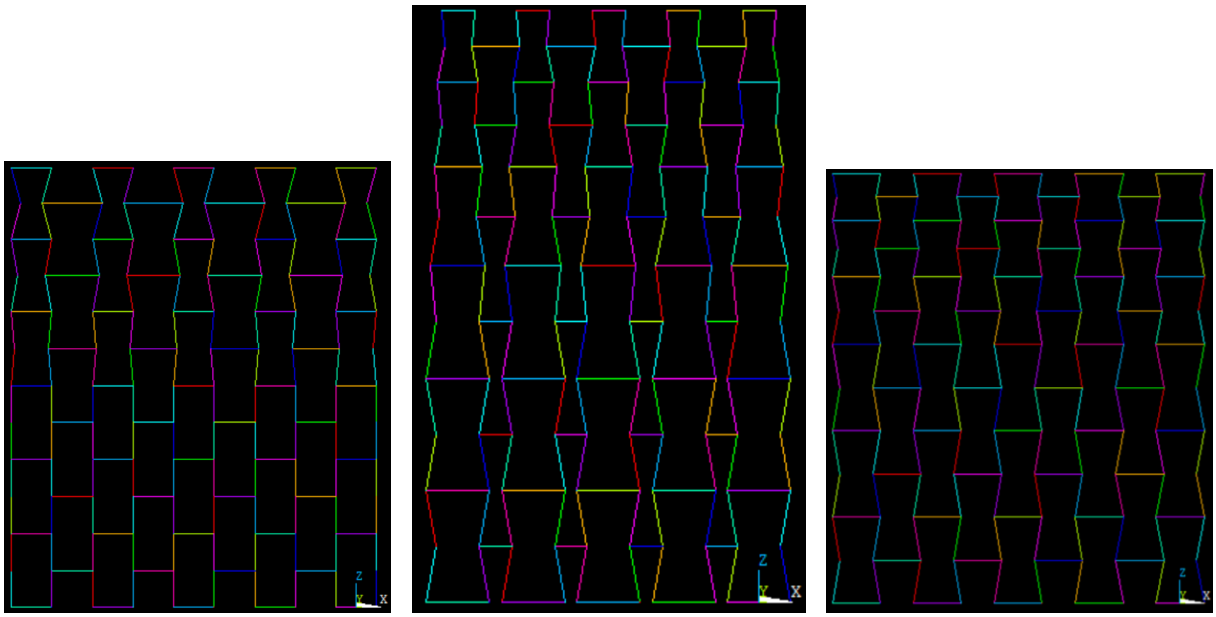

Figure 3.8: *Lattice with "DELAY_T" on the left, lattice with "DELAY_H" in centre and lattice with "DELAY_A" on the right.*

Furthermore, the delays are given in percentage of the number or rows of the lattice: all the frames represented in figure 3.8 have a 40% delay.
In conclusion, it has to be mentioned that is also possible to combine delays and gradients so to have a wider range for the gradients values and a more significant change from a row to the consecutive one. In fact, the gradients ranges depend on the number or rows on which they are applied.

3.2.3. FEM model

In this section an example of a metalattice with all the possible features is given. In figure 3.9 is shown a frame with the following inputs:

H1=10	!base side length of the cells in the initial row [mm]
ALPHA1=1.1	!aspect ratio of the cells in the initial row
THETA1=-5	!angle of the cell in the initial row in degree
CH=10	!cell height in y [mm]
DT=-4	! ϑ gradient
DH=1	!H gradient
DALPHA=0.4	!α gradient
DI=2	!beam diameter
DELAY_H=50	
DELAY_T=50	
DELAY_A=25	
NR=4	!number of rows
NC=4	!number of columns
NF=4	!number of floors

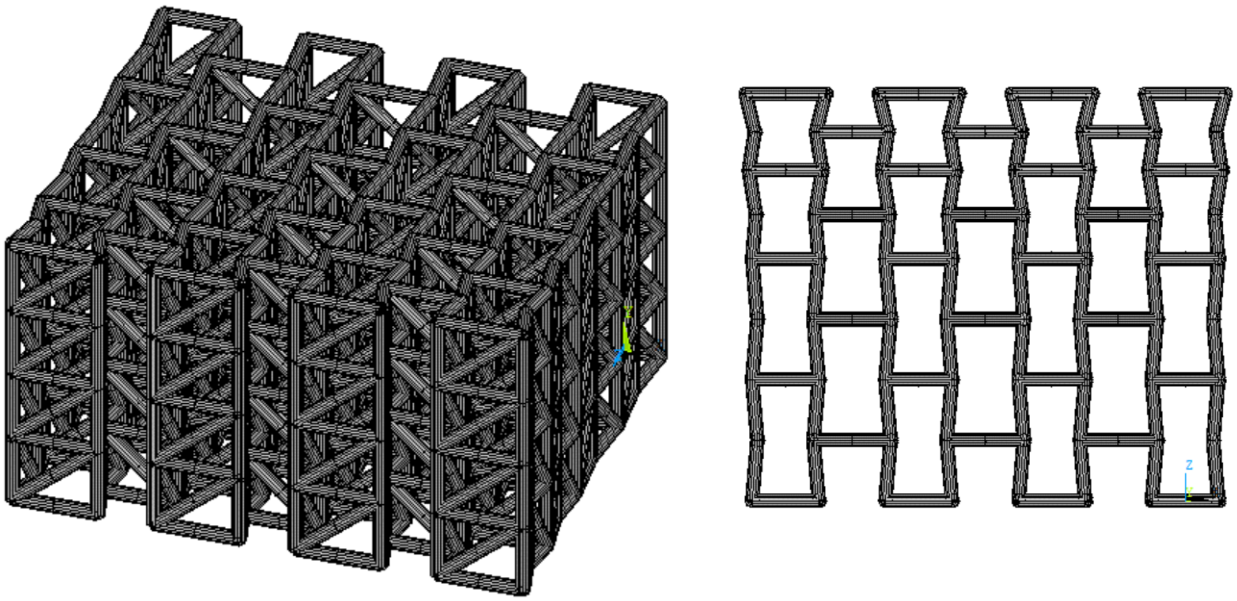

Figure 3.9: *3D volume lattice with the parameters listed in the windows: on the left there is the 3D view and on the right the view of the auxetic plane.*

3.3. 3D volume generation

As already mentioned in the previous paragraphs, the initial idea was to build the lattice directly as a 3D volume geometry instead of modelling it with links or beams (see the next chapter to deepen it). This could have helped to model a more trustful lattice without any infinite stiff joints and with the possibility to insert contact elements between beams and thus achieving a more realistic result. However, to have a look at the effects of each parameter on the mechanical properties of the frame and understand how to design this kind of lattice a simpler approach was preferred.
Once the structure will be designed, a final simulation with a 3D volume frame is supposed to be carried out to get more accurate results before running the experimental part. In order to do so, a procedure has been studied to allow the generation of the CAD file on Solidworks (CAD software) parameterizing it and controlling it with Excel tables. Then the file has to be imported in a CAE software and ABAQUS may be preferred to ANSYS because it can model the contact in an easier and faster way.

3.3.1. Solidworks and Excel

In this subparagraph will be briefly explained how to generate a parametric CAD model: a model which could change its own shape simply varying values in a managing table. The procedure is very simple and the first step is drawing the CAD metalattice shape. What is important is that the allowances have to be matched with parameters (e.g. letters) instead of mere numbers.
Once a sample of the CAD file is fully designed and every dimension is set, the next step is to insert a table linked to the allowances given by clicking on the “INSERT TABLE” option. When the table is created and the two software systems are connected, it is easy to generate in Excel the same features (gradients and delays) described in the previous paragraphs and obtain a fast parametric 3D volume generation of the lattice with the same high level of customization reached by programming on ANSYS.

4.Model benchmarks

In chapter three the focus is on the geometrical characteristics of the lattice model. In this following chapter the emphasis will be given to the modeling issues associated with the lattice simulation by finite elements analysis.
As previously stated, the frame is thought to be simulated as an assembly of two-nodes elements with three-dimensional degree of freedom.
Obviously, it is highly recommended to implement a lattice whose behaviour is, also from a modeling point of view, as realistic as possible in order to obtain an accurate result. In fact, the model response not only depends on its own geometry and on its material properties, but it is also significantly influenced by the element used to mesh the single parts of each struts and on its degrees of freedom. Furthermore, depending on the element used to virtually simulate the components of the lattice, an investigation on the effect of the mesh size could be required.
These analyses are usually common when defining a model because they can help the designer to understand what are the right choices to make when defining the lattice. Plus, it gives an idea of how to prevent the model to be stiffer than reality because of its modeling inaccuracies.
Therefore, in the next paragraphs the "element convergence" and "mesh convergence" studies will be described along with their results which are considered part of the definition of the model. Thus, the studies response is discussed already in this chapter so to provide the necessary information for the following chapters which deal with the implementation of each single analysis.

4.1. Elements convergence

Before dealing with elements convergence it needs to be said that this study is aimed at clarifying the different behaviours the structure shows when meshed with various two-nodes elements. In this way, not only it can be understood which is the best element to simulate the lattice, but also, through a reverse engineering process, it is easy to notice what are the phenomena leading the process of deformation in a precise direction or with a precise structure morphology. This brings us to another noteworthy fact: when simulating this kind of lattice, which is an orthotropic metamaterial showing three mutually-orthogonal axes along which the mechanical properties are completely different, the previous convergence studies have to be done for all the three principal directions. Once the outputs are known for every axis, the appropriate choice must be made in order to satisfy each direction requirements. As a matter of fact, along some of them the element choice is not constrained due to the morphology of the lattice which maybe either more stretching-dominated or bending-dominated when deforming.

On the other hand, this "element convergence" study is meant to graphically quantify when it is actually possible to model the lattice with various elements thus setting a threshold underneath which simpler elements can be used without relevant errors.
In the next subparagraphs a brief introduction to the different ANSYS elements and to their degree of freedom will be given; it will be followed by the description of the analyses and of the results for every case.

4.1.1. Element description

The different elements used to develop this kind of study can be found in the ANSYS technology guide which decribes them in depth [17]. The ones taken into account are three: LINK8, BEAM4 and BEAM188.
They don't differ from each other for the number of nodes but for the degrees of freedom they consider or for the theory from which their mathematical equations are derived.
In this section all the main features will be described strating from the simpler element, LINK8, to the more complex one, BEAM188.
LINK8 is a spar which may be used in a variety of engineering applications. Depending upon the application, the element may be thought of as a truss element, a cable element, a link element, a spring element, etc.
The three-dimensional spar element is a uniaxial tension-compression element with three degrees of freedom at each node: translations in the nodal x, y, and z directions. As in a pin-jointed structure, no bending of the element is considered. The element is defined by two nodes, the cross-sectional area, an initial strain, and the material properties.
The spar element assumes a straight bar, axially loaded at its ends, and of uniform properties from end to end. Also, it has to be underlined that the solution at the nodes is exact because it derives from De Saint Venant theory.
The element x-axis is oriented along the length of the element from node I toward node J. The element LINK8 is represented in figure 4.1.

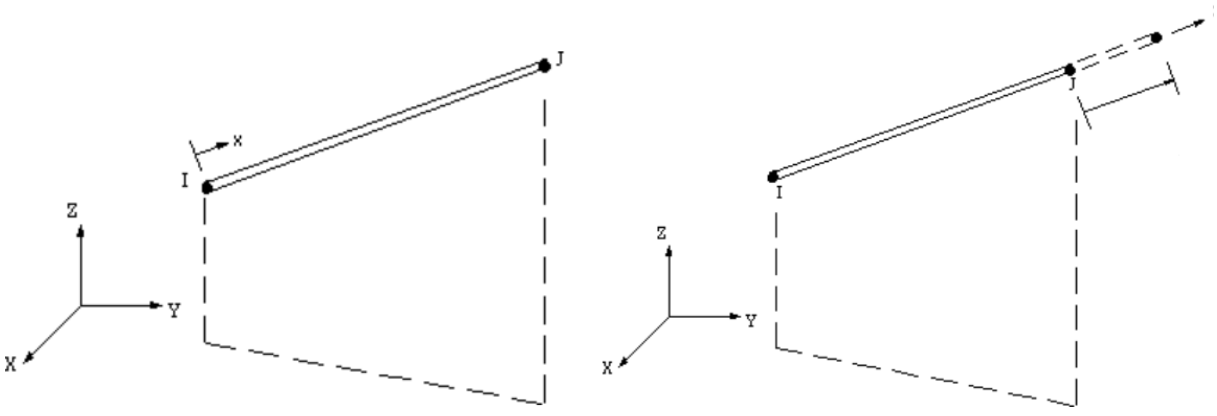

Figure 4.1: *LINK8.*

BEAM4 is a uniaxial element with tension, compression, torsion, and bending capabilities. The element has six degrees of freedom at each node: translations in the nodal x, y, and z directions and rotations about the nodal x, y, and z axes. Stress stiffening and large deflection capabilities are included. A consistent tangent stiffness matrix option is available for use in large deflection analyses.

The geometry, node locations, and coordinate systems for this element are shown in figure 4.2. The element is defined by two or three nodes, the cross-sectional area, two area moments of inertia (IZZ and IYY), two thicknesses (TKY and TKZ), an angle of orientation (θ) about the element x-axis, the torsional moment of inertia (IXX), and the material properties. For user control of the element orientation about the element x-axis, use the θ angle or the third node option. If both are defined, the third node option takes precedence. The third node (K), if used, defines a plane (with I and J) containing the element x and z axes (as shown). If this element is used in a large deflection analysis, it should be noted that the location of the third node (K), or the angle θ, is used only to initially orient the element.

It is important to point out that, depending on the type of analysis, various options can be triggered with the KEYOPTION features and that the solution is exact at the nodes because it derives from De Saint Venant theory thus considering the Euler-Bernoulli beam. It is more suitable for thick beams where the shear deformation is neglectable if compared to the bending one.

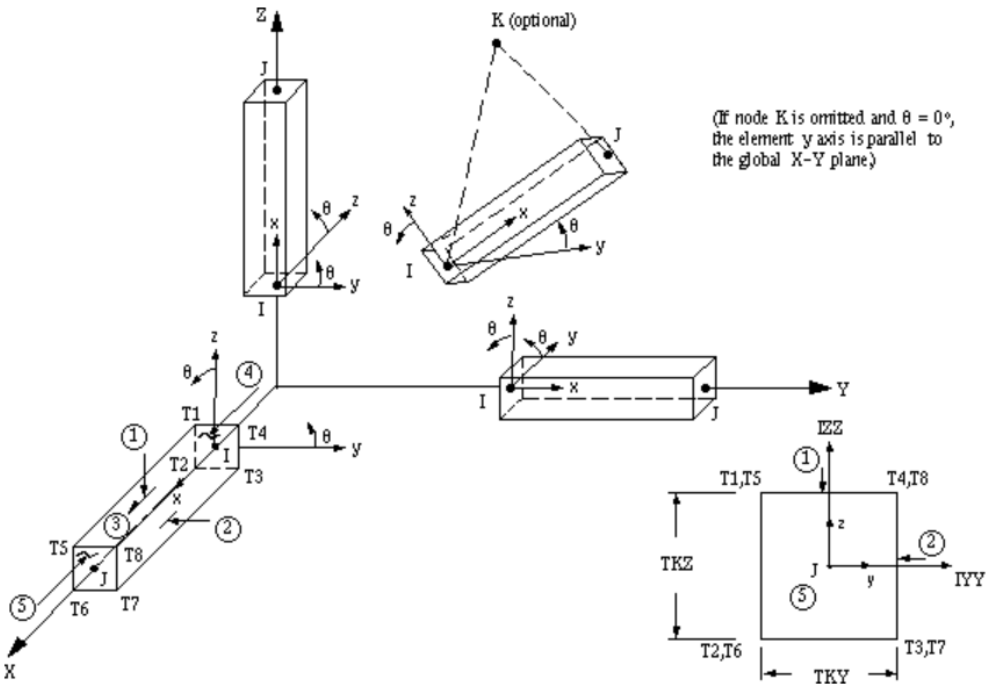

Figure 4.2: *BEAM4.*

BEAM188 is suitable for analysing slender to moderately stubby/thick beam structures. The element is based on Timoshenko beam theory which includes shear-deformation effects, thus allowing the rotation between the cross section of the beam and its "middle line". The element provides options for unrestrained warping and restrained warping of cross-sections. The element is a linear, quadratic, or cubic two-node beam element in 3-D. BEAM188 has six or seven degrees of freedom at each node. These include translations in the x, y, and z directions and rotations about the x, y, and z directions. A seventh degree of freedom (warping magnitude) is optional. This element is well-suited for linear, large rotation, and/or large strain nonlinear applications.

Timoshenko beam theory is a first-order shear-deformation theory: transverse-shear strain is constant through the cross-section (that is, cross-sections remain plane and undistorted after deformation). The element can be used for slender or stout beams. Due to the limitations of first-order shear-deformation theory, slender to moderately thick beams can be analysed. When KEYOPT(3) = 0 (linear, default), BEAM188 is based on linear shape functions. It uses one point of integration along the length; therefore, all element solution quantities are constant along the length. Only constant bending moments can be represented exactly with this option. Mesh refinement is generally required in typical applications.

BEAM188 is defined by nodes I and J in the global coordinate system. Node K is a preferred way to define the orientation of the element. BEAM188 can also be defined without the orientation node K. In this case, the element x-axis is oriented from node I (end 1) toward node J (end 2). If no orientation node is used, the default orientation of the element y-axis is automatically calculated to be parallel to the global X-Y plane. For the case where the element is parallel to the global Z-axis (or within a 0.01 percent slope of it), the element y-axis is oriented parallel to the global Y-axis. Figure 4.3 represents the element.

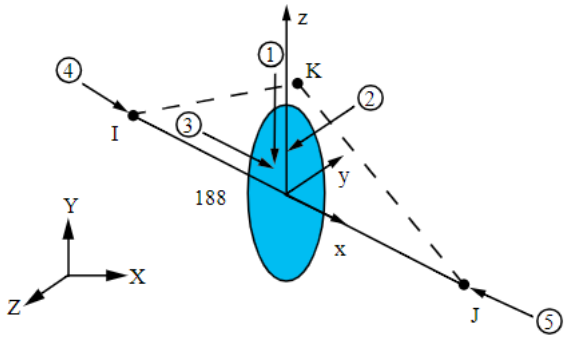

Figure 4.3: *BEAM188.*

The beam element is a one-dimensional line element in space. The cross-section details are provided separately via the SECTYPE and SECDATA commands. Each section is assumed to be an assembly of a predetermined number of nine-node cells (figure 4.3). Each cross-section cell has four integration points and each can be associated with an independent material type. Element output is available at the integration points, as well as values extrapolated to the element and section nodes.

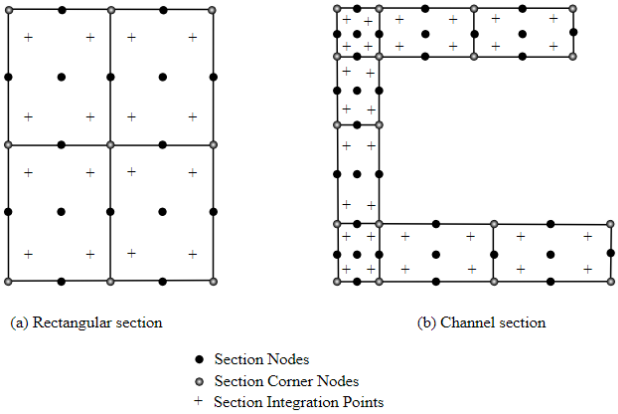

Figure 4.4: *BEAM188 cross-section cells.*

4.1.2. LINK8

The first element to be analysed is the LINK8. The virtual model is set up and the solution environment is entered. However, the software is not able to converge to a solution because the model seems to be insufficiently constrained.
This happens because the link elements don't set the rotation value at both their nodes and so between two consecutive links rotations are not constrained and the structure behaviour results in an overall rigid movement.
To clarify this statement a simple example is provided. Consider the two 3D links models shown in figure 4.5.

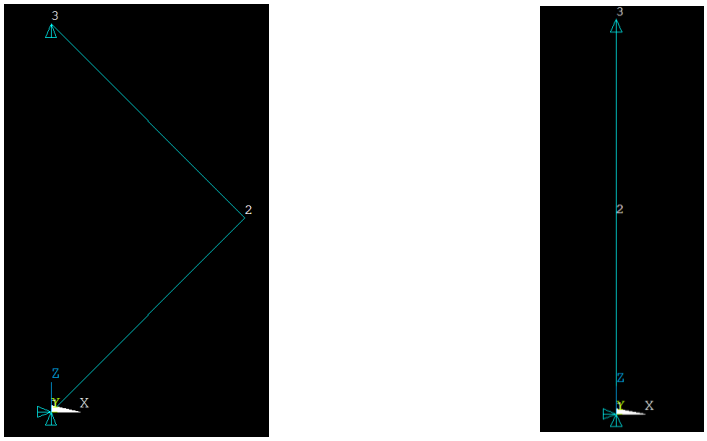

Figure 4.5: *Two-links models.*

They are both given the same set displacement downward at the node number three. The one only difference between them is the orientation of the two link elements but the solution is possible only for the one on the right. This happens because the frame on the right is loaded in compression and thus no rotational conditions are needed. The solution can be computed just knowing the displacements at the nodes. Instead, the model on the left needs rotational constraints at each node which are not given by link elements whose only degrees of freedom are displacements. Thus, the lattice is considered unconstrained and an error message like the one shown in figure 4.6 is displayed by ANSYS.

Figure 4.6: *Error message.*

The only way to manage to simulate the model with links would be introducing at each node of the lattice a torsional spring which constrains the rotations at each node. However, from a modeling point of view this solution is very time-consuming and it goes beyond the aims of this analysis because it cannot be interesting for an industrial application.
In conclusion, it can be stated that these lattices cannot be modeled with links.

4.1.3. BEAM4 vs BEAM188

In the previous paragraph it has been discovered that lattices are almost impossible to be modeled as a network of links, thus mapping out the course toward beams.
However, it is still to be found what kind of beam can be used and if there are some ranges to consider when modelling the frame. In fact, ANSYS offers different type of beams whose analytical backgrounds are dissimilar in some cases.
Depending on the beam slenderness there are two main approaches derived from two theories: the De Saint Venant's theory and the Timoshenko's one. In paragraph 4.1.1 the main differences are deepened.
The proper definition of slenderness is:

$$\lambda \stackrel{\text{def}}{=} {}^{h}/_{\rho} \tag{4.1}$$

$$\rho = \sqrt{{}^{I}/_{A}} \tag{4.2}$$

where ρ is the radius of giration, h is the beam length, I is the geometrical moment of inertia and A is the beam cross section.

For a circle cross-section the λ is equal to $^{4h}/_{D}$, being D the beam diameter and defining the geometrical moment of inertia and the area with the following formulas:

$$I = {}^{\pi D^4}/_{64} \tag{4.3}$$

$$A = {}^{\pi D^2}/_{4} \tag{4.4}$$

However, from a more general point of view, it is possible to define the slenderness just as proportional to the ratio between its length and its diameter.
In the following analyses for slenderness it is meant as a:

$$\lambda = {}^{h}/_{D} \tag{4.5}$$

Therefore, this will be the parameter through which the convergence analyses will be evaluated and the aim is to find out a slenderness threshold beyond which it is possible to use both elements without a relevant error.
As already pointed out, the analyses results are very linked with the direction of loading so because of the shape and, consequently, of the deformation mode.
Moreover, it is to be underlined that the value which will be taken as benchmark for the study is the compressive modulus.
The first axis to be analysed is the z one. The model is the one represented in figure 4.7:

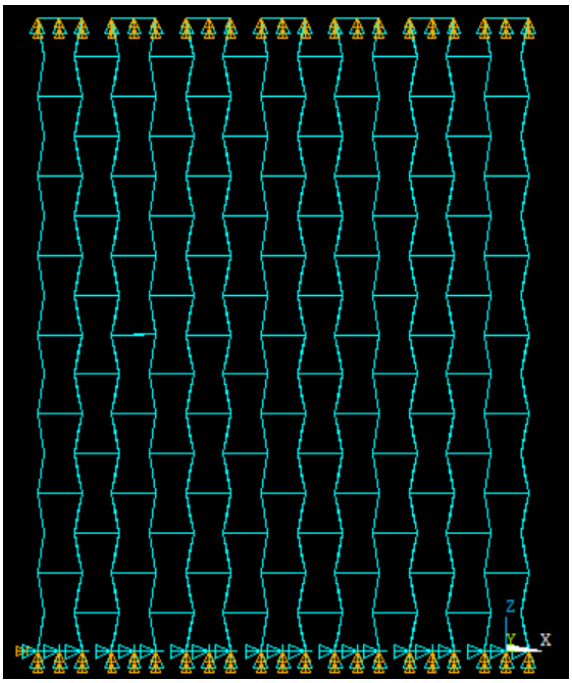

Figure 4.7: *Lattice compressed along the z axis.*

The structure is completely constrained at the bottom nodes and it is loaded with a set displacement (-0.1 mm) at the nodes on the top surface. The non-zero parameters are the following:

- NC=8
- NR=7
- NF=8
- H1=10
- ALPHA1=1.2
- THETA1=-10
- CH=10
- DI=H1/SLENDERNESS

No gradients or delay are considered because in this case the morphology of the frame doesn't matter.
Also, since the whole lattice dimension is controlled by the "H1" value, it has been decided to rely on it for the slenderness calculation. Therefore, the slenderness used is just a benchmark and it is the smallest one in the all structure because the diagonal beams are longer than the side base beam.
This model, like the other two in the x and y directions, has been meshed once with BEAM188 and then with BEAM4 and for both elements the slenderness factor varies from 1 to 6.5. In figure 4.8 the results are displayed.

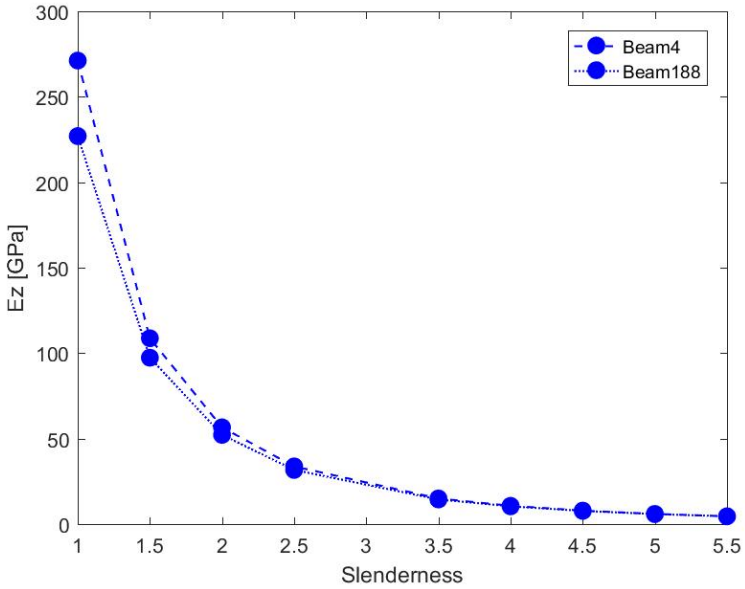

Figure 4.8: *Benchmark in the z-direction.*

What is suddenly clear is the stiffening effect due to the use of BEAM4 elements for small slenderness. This result was expected because of the mathematical hypotheses of De Saint Venant's theory which do not take into account shear deformations because they are neglectable for thin beams and high slenderness. However, for small slenderness shear has to be considered and thus the lattice could be modeled only with BEAM188 which refers to Timoshenko's theory.
In order to obtain a more vivid image of the differences between the two elements, the percentage error which is committed by BEAM4 modelation compared to BEAM188 one has been computed and it is showed in figure 4.9.

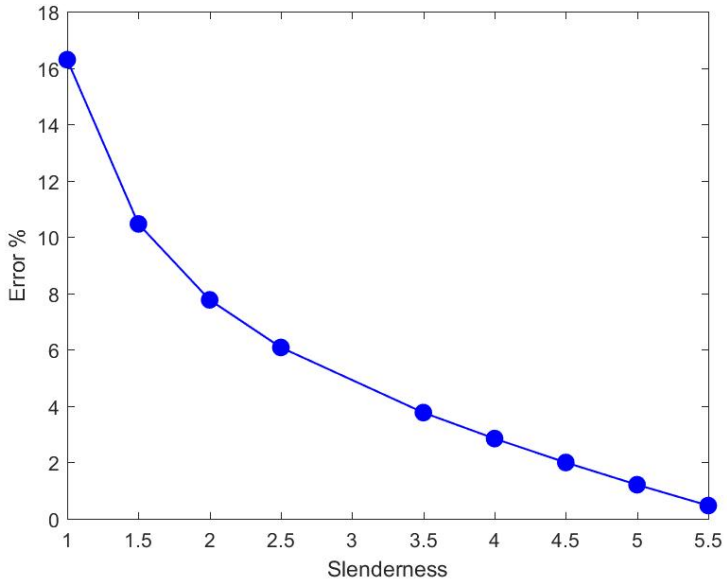

Figure 4.9: *Percentage z-compressive modulus error.*

Looking at figure 4.9 it is possible to state that for a slenderness equal to the unit, BEAM4 tends to present a stiffening error of 17%. Moreover, it is now possible to find a threshold beyond which both elements can be used. As a matter of fact, evidently from a slenderness of 5 the response of both models starts to be very alike with an error percentage definitely lower than 2%.
To be safer, it is proposed λ=5.5 as the point where shear deformations are neglectible when loading the lattice along the z direction and BEAM4 can be used without any mistakes.
The same analyses have been run loading the same model along the x axis as shown in figure 4.10 whereas the study results are set out in figure 4.11 and 4.12.
What can be underlined is the consistency of the trends obtained in the previous graphs referring to the z axis and these ones: there is a stiffening error when using BEAM4 for small slenderness.
However, since the frame is loaded on another plane, the reaction of the lattice is less stiff and thus the influence of BEAM4 elements is even more significant.

Therefore, the threshold is moved ahead and there is no element interchangeability until the slenderness reaches higher values.

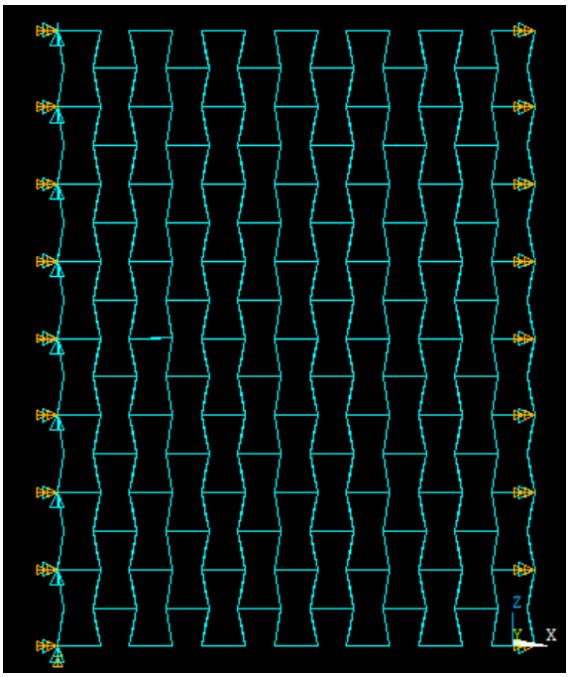

Figure 4.10: *Lattice compressed along the x axis.*

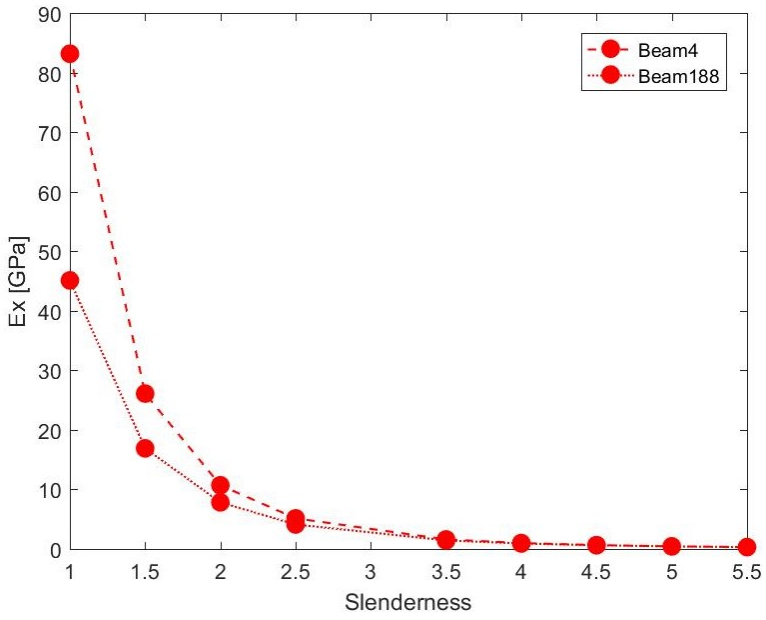

Figure 4.11: *Benchmark in the x-direction.*

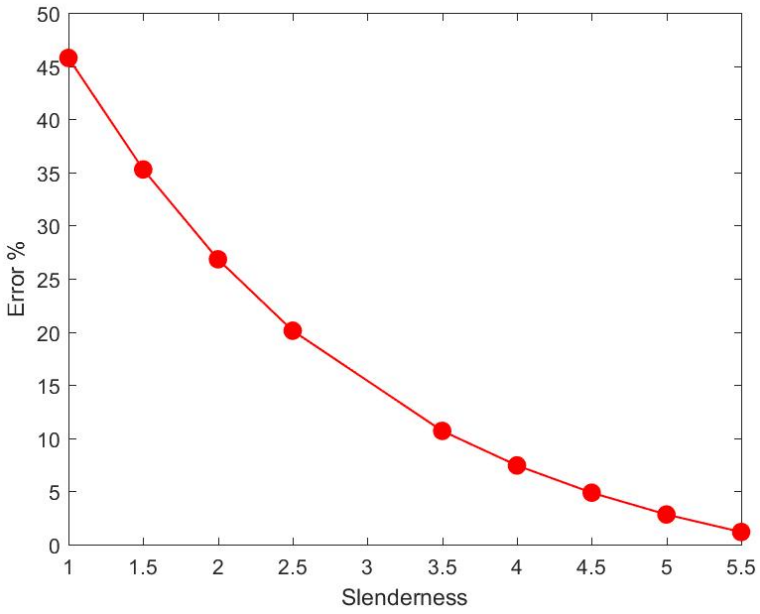

Figure 4.12: *Percentage x-compressive modulus error.*

Looking at figure 4.12, it appears that for a slenderness equal to the unit BEAM4 tends to present a stiffening error of 45% which is much more relevant than the 17% seen in the z-axis.
Furthermore, from a slenderness of 5 the behaviours start to be very alike (error%=3%). Ideally, the percentage error is lower than 1.8% for a slenderness of 5.5. To be safer, it is proposed λ=7 as the point where shear deformations are neglectible and BEAM4 can be used without any mistakes.
The last case to be investigated is the loading along the y direction as shown in figure 4.13.

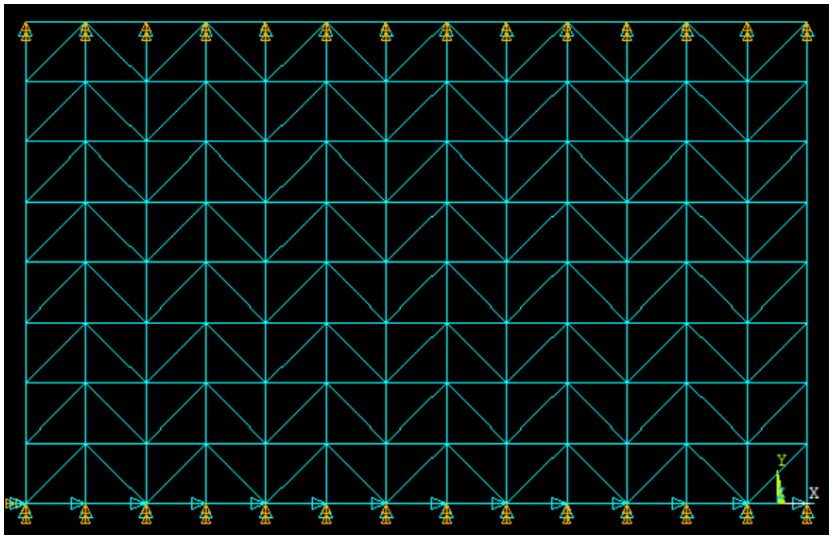

Figure 4.13: *Lattice compressed along the x axis.*

In figures 4.14 and 4.15 results obtained are reported.

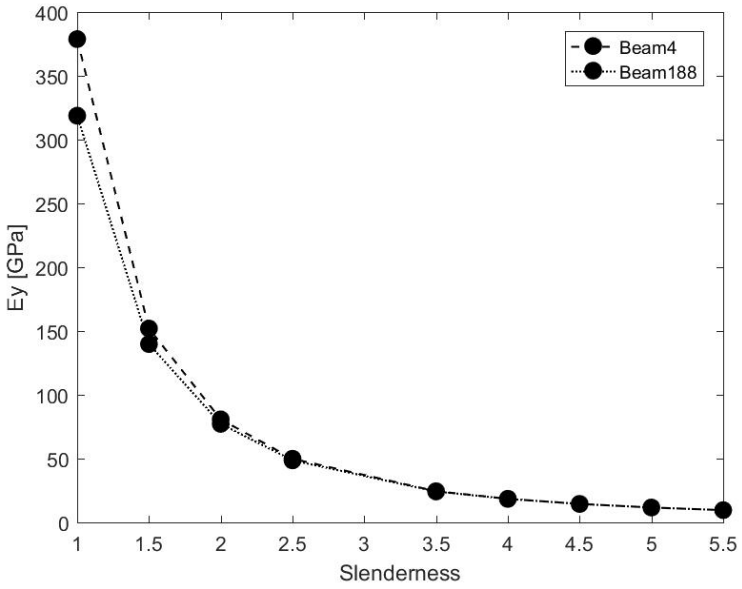

Figure 4.14: *Benchmark in the y-direction.*

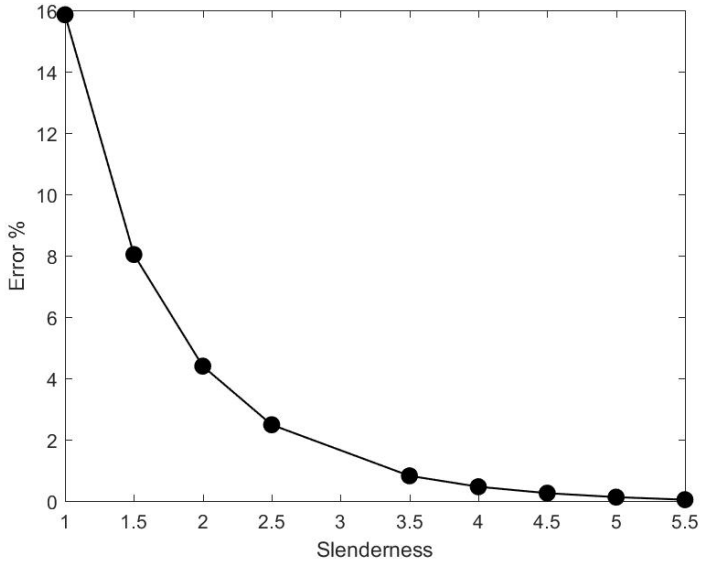

Figure 4.15: *Percentage y-compressive modulus error.*

In this last case, the maximum BEAM4 stiffening error is 16% and from a slenderness of 2.3 the two responses start to be very alike showing a percentage error equal to 3%. However, a safer threshold is set defining λ=3.8 as the point where shear deformations are neglectible and BEAM4 can be used without any mistakes.
In conclusion, summary graphs are reported in figure 4.16 so as to have an immediate idea of the differences between the three cases.

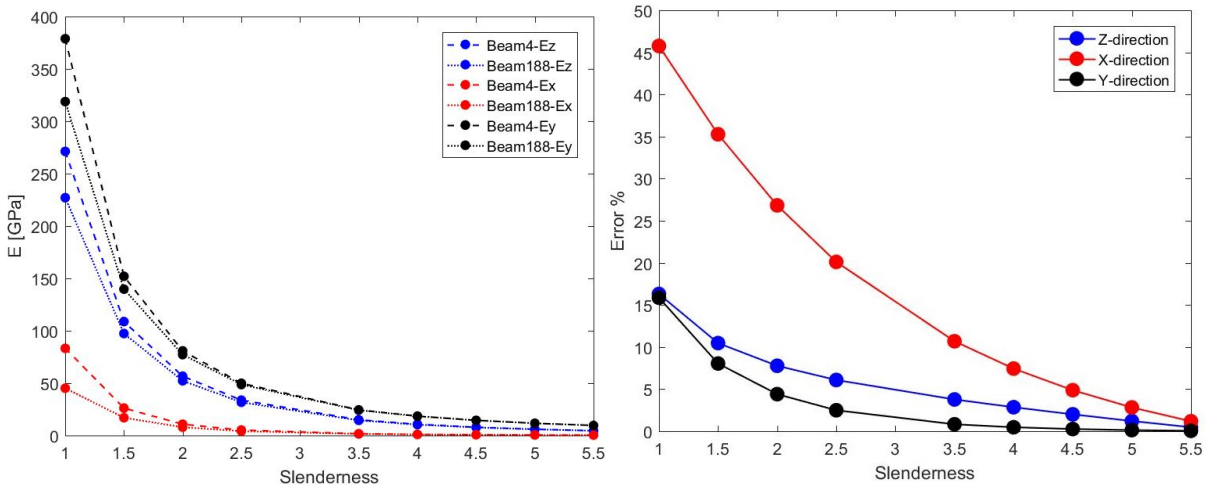

Figure 4.16: *Comparison graphs.*

All things considered, the limiting case is the one loaded along the x axis which has a slenderness threshold equal to 7. This means that the frame when loaded in the x-direction shows much more shear deformation than other cases.
Also, it is noteworthy that the element convergence depends on the behaviour of the structure which can be bending or stretching-dominated: stretching-dominated frames (e.g. Ey) are less sensitive to the shear deformations, thus converging earlier and vice versa.
In conclusion, in the following analyses the element to be used is mainly BEAM188 because, during the parametric analysis, it will be also dealt with slenderness values of 4 or 5.

4.2. BEAM188: mesh convergence

Having chosen the BEAM188 with only two nodes as the element to use to model the lattice, a "mesh convergence" investigation has to be done because this element does not give an exact solution but it computes an approximated one at his nodes. The finite element method is never exact, except for the monodimensional elements whose equations are derived from the De Saint Venant theory, because of the way the set displacements are defined. In fact, finite element analysis is based on a mathematical approach which relies on the principle of virtual work and on the definition of a shape function needed to connect nodal and non-nodal displacements. The approximation lies in the shape function which is used to describe the displacements of the continuous solid. Considering Timoshenko theory, the shape function needs to include one more unknown than the De Saint Venant one because of the shear deformation which is an independent variable. However, with a three nodes BEAM188 the exact solution can be obtained.
Therefore, the way to reduce the approximation is to mesh the object with very small sizes or increase the shape function polynomial order. The latter is ignored even if it is possible since the BEAM188 could be intended as a three-nodes or four-nodes element.
In this paragraph a "mesh convergence" study will be developed in order to find out the maximum mesh size which allows the model to still obtain accurate results without facing any stiffening effects and without generating a useless time-consuming "overmeshed" assembly.
Also, for this analysis the final results depend on the direction along which the lattice is loaded: along the x axis the structure is softer than the z axis whereas along the y axis the frame is the stiffest. Thus, the limiting case for the mesh size is expected to be the one loaded in the x direction.
Before introducing the reader to the analyses, the description of the meshing algorithm is needed to understand what is meant for mesh size. The script meshes the struts dividing them by a user-given length: the command used is "LESIZE" as it is set out in the "MAIN SCRIPT" in the Annex. Since the strut length is rarely a multiple of the mesh given length, the number of divisions per line is often rounded upward by ANSYS. That is, if the beam is ten millimetres and the mesh size is eight millimetres the beam will be divided in two sublines five millimetres length. All things considered, that means that sometimes even if the mesh size parameter is changed the divisions per line are not because the ratio between the beam length and the mesh size rounded upward is still giving the same value. Bearing in mind this statement, understanding some results trends will be simpler.
The investigation process is similar to the one developed for the "element convergence", but this time the changing parameter is the mesh size for all three loading-direction. The benchmark is again the homogenized Young's modulus of the frame.

The model used for all three cases is the same and it is identical to the one used in the previous paragraph. It has to be said the the final Young's modulus results are lower than the ones noticed in the previous graphs because the slenderness considered is fifteen thus softening the frame. However, it doesn't matter because the values of the structure stiffnesses are going to be accurately investigated with the compressive tests described throughout chapter 5. Following subparagraph 4.1.3 order, the first results showed are the ones related to the loading along the z-direction (figure 4.17).

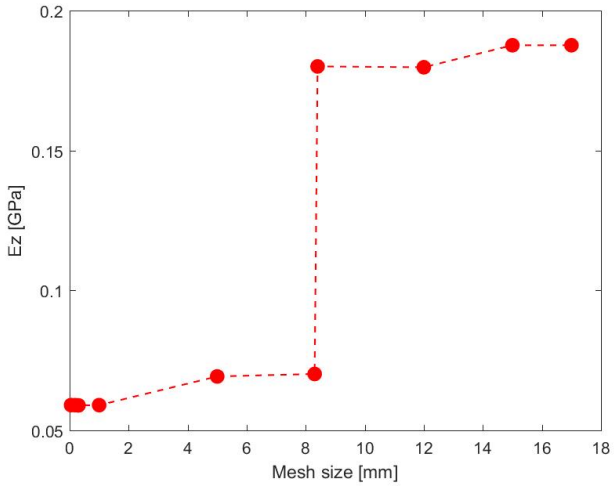

Figure 4.17: *Mesh convergence along the z direction.*

The overall trend is that decreasing the mesh length the solution converges to a softer modulus value. Also, it is noteworthy to mention why there are two parts of the graph with an unexpected steep trend. The most visible one is the huge drop between a mesh size value of 8.2 and 8.4. Figure 4.18 represents the two situations.

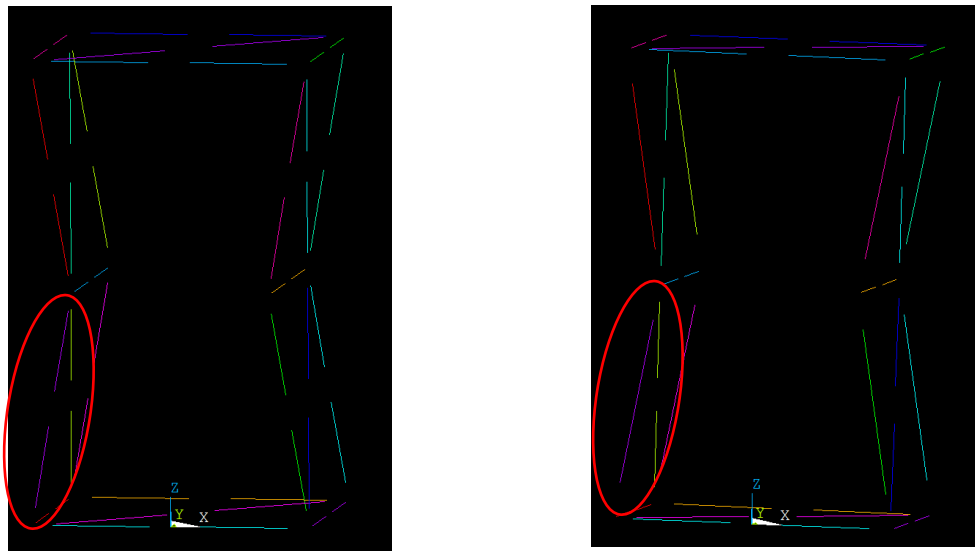

Figure 4.18: *Single cell divisions per line: on the left mesh size equal to 8.2 mm and on the right mesh size equal to 8.4 mm.*

Looking at the lines in the circles in figure 4.18 it is noticeable that in the model with a mesh of 8.2 millimetres the software divides the line in two separate lines whereas for the other mesh length ANSYS doesn't divide it. This happens because the length of that lateral inclined line is 8.3 millimetres and the program deal with it as explained above. Thus, that beam, which is the one giving the majority of the lattice stiffness in the z direction, in the case of a smaller mesh size is much more real and soft than the other case thus resulting in a significant drop of the Young's modulus value.
The same kind of observation can be done when explaining the drop between a mesh size of 13 and 15 mm. This time another the diagonal strut shows the same meshing change as shown in figure 4.19. After the lateral beams, the diagonal ones are the more loaded when the load is along the z axis.

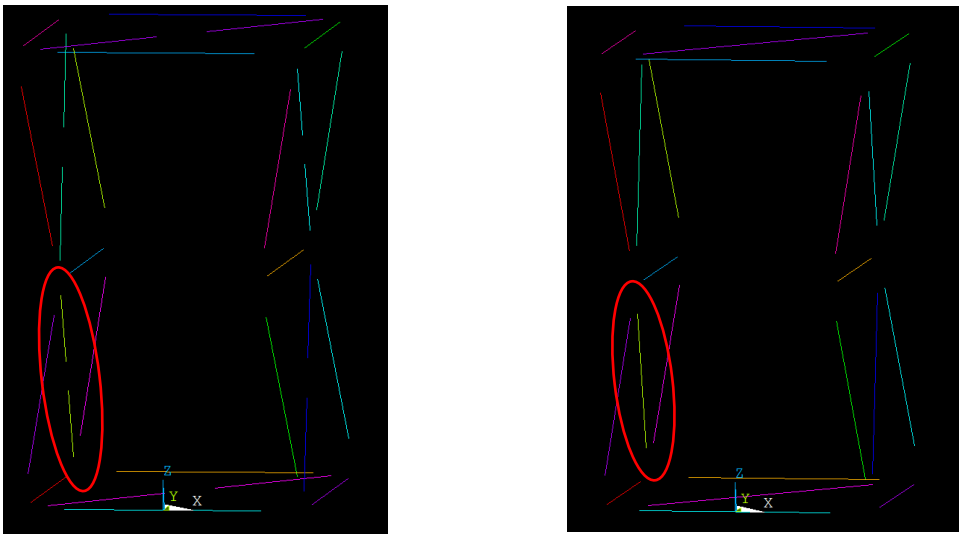

Figure 4.19: *Single cell divisions per line: on the left mesh size equal to 13 mm and on the right mesh size equal to 15 mm.*

However, figure 4.17 is not enough accurate if what is sought is a direct perception of the mesh size to choose for the model to be accurate enough. Thus, a focus on a restricted range is represented in figure 4.20.

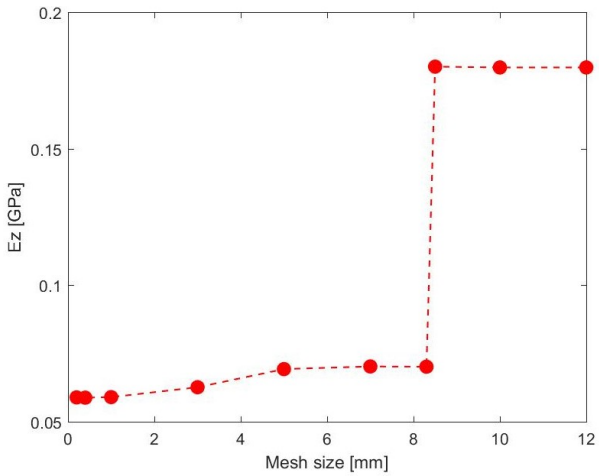

Figure 4.20: *Mesh convergence along the z direction refined.*

Therefore, it can be stated with doing mistakes that a mesh size of two or three millimetres is accurate enough and not too time-consuming as smaller mesh sizes.
The results in the other two directions are similar to this one: figures 4.21 and 4.22 shows respectively the trends for the "mesh convergence" along the x and y loading-directions.

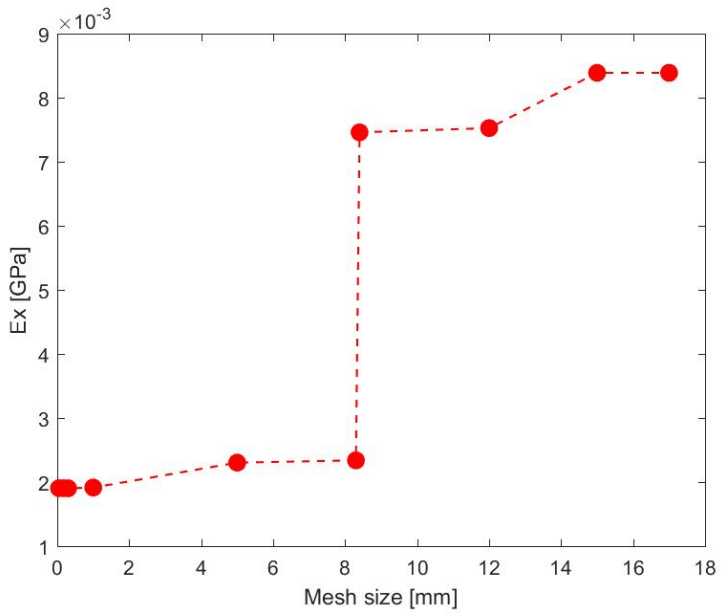

Figure 4.21: *Mesh convergence along the x direction.*

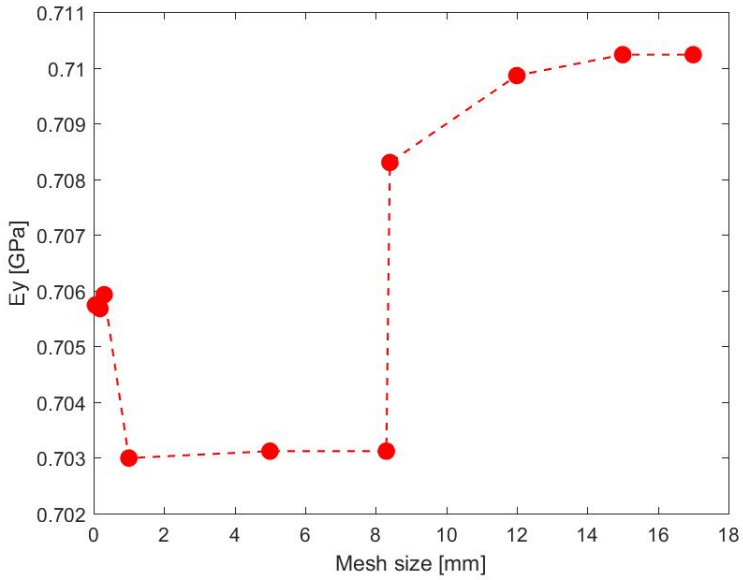

Figure 4.22: *Mesh convergence along the y direction.*

Looking at figure 4.21, the reader can find the same trend found for the analysis along the z direction whereas figure 4.22 shows a slightly different trend because the lattice

behaviour when loaded along the y direction is stretching-dominated. Thus, the stiffness is associated to the compression of each beam collinear with the y axis which almost behaves as a De Saint Venant's link without any significant shear effect. This means that the mesh convergence for this direction of loading is not interesting because the solution is already converged. Figure 4.22 provides a vivid example of what just stated because there is not a clear trend and Young's modulus is practically insensitive to the changing of the mesh size.
To summarize the three analyses, figure 4.23 has been plotted.

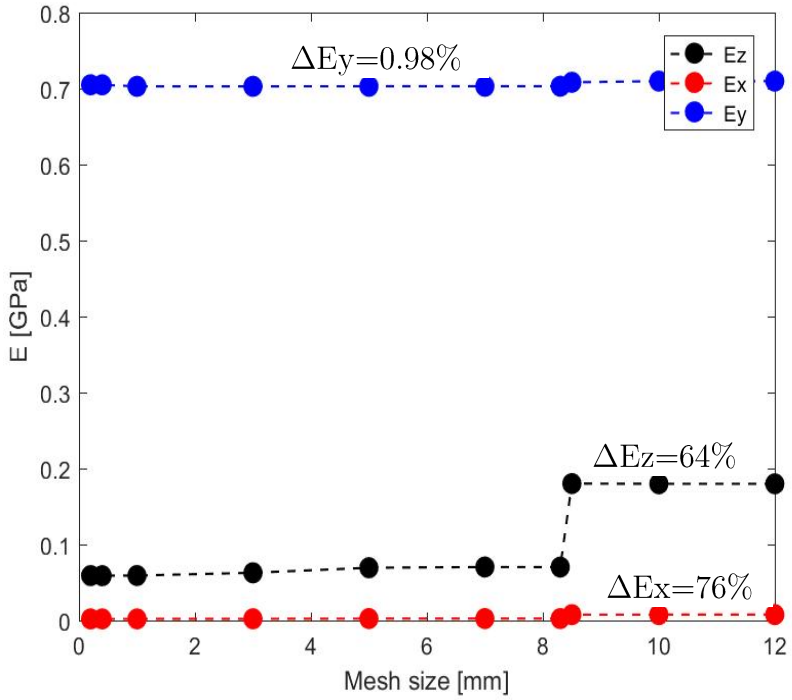

Figure 4.23: *Comparison graph.*

What really have to be underlined are the significative convergences of the analyses along z and x directions which respectively reduce the stiffnesses of the frame by the 64% and by the 76%. In fact, both of them present a bending-dominated behaviour. On the contrary, the y loading case doesn't show any convergence (0.98% stiffness variation). Moreover, this Young's modulus values are consistent with the ones which will be found in the final chapters dealing with the parametric compression tests.
It is pointed out that the above graph, in order to include all the three cases, doesn't show a deep variation for the study along x but actually it is the one which is influenced by the mesh size the most as demonstrated by the percentage reductions mentioned. Thereby, it is again found that the limiting case is the one considering the loading along the x axis providing the validation of the fact that the lattice response derived from this type of loading is the one which is characterized the most by shear deformations.
Insofar, the size mesh to be implemented is about 2 millimetres.

5. Mechanical properties analyses

Knowing the preliminary convergence studies results, the focus has been moved to the third phase of the project: the numerical investigation of the physical and mechanical properties of the new lattice described. Besides, this third step is the core of the project and from its final outputs, decisions will be made so as to define a suitable solution for Rolls-Royce acoustic liners. Three main tests will be run: compression test, shear test and elastic energy absorption test.
When estimating the properties of the structure, a homogenization approach is required to consider the material as a fully dense one. This is the only way to obtain the mechanical properties of this type of lightweight frame. Thus, an approximation is made because the final values have to be thought as equivalent values from a macroscopic point of view.
Moreover, the material chosen for all the analysis is stainless steel 316L because it is available also as powder to be additively manufactured and it is easy to find in the market. Other metal materials can be used so as to extract better responses in terms of strength to density ratio such as Titanium alloys or Nickel superalloys. However, materials properties are not so relevant for the aims of the project because the purpose is to understand the behavioural changes due to geometry variation.
Furthermore, every mechanical characteristic is going to be normalised by the density value of the lattice because the aerospace field first goal is to rely on the product which show the best strength to density ratio. This is due to the enormous costs faced by company related to the mass of the item: even grams are very expensive.
What is to be underlined is that all the models have been loaded and constrained in order to represent the application configuration as much as possible.
In the following paragraph, each analysis is going to be deepen mainly from a physical point of view whereas the results are going to be shown in the third part of the thesis.
For what concerns the programming activities, it has to be reminded that parametric analyses are to be run so new scripts are defined: these are "TXT" files which recalls in an iterative manner the "MAIN SCRIPT" files changing every time the parameter value or the direction of loading. As a matter of fact, there is a single governing parametric file for each test and it runs the studies for all parameters in all direction. About this, it is necessary to anticipate that the elastic energy absorption is only measured for the loading case along the z axis because it is the only case which matters for Rolls-Royce application.
All the simulations change only the value of one factor at a time from a benchmark model which consists of the following reference values:

- θ_1: -10°;
- H_1: 10 mm;
- α_1: 1.1;

- φ: 0.5 mm;
- CH: 10 mm;
- $D\theta/\theta_1$: 0;
- DH/H_1: 0;
- $D\alpha/\alpha_1$: 0;

Also, in this introduction to the single tests it is thought to be useful defining the seven parameters ranges which are going to be evaluated for each test and in each direction. These spectrums have been chosen in order to obtain manufacturable and applicable geometry:

- θ_1: -30 ÷ 10°;
- H_1: 6 ÷ 22 mm;
- α_1: 0.6 ÷ 1.8;
- φ: 0.2 ÷ 2 mm;
- $D\theta/\theta_1$: 0 ÷ 0.3;
- DH/H_1: -0.08 ÷ 0.08;
- $D\alpha/\alpha_1$: 0 ÷ 0.25;

It is important to explain the values of the three gradients ranges. Reading in order, the angle gradient stretches from 0 to 0.3 because both θ and $D\theta$ assume negative values thus all the graphs referring to them will be consistent only if read in opposite direction. DH assumes values which are one order bigger than the one shown but diving by H_1 means diving by ten millimetres thus giving this output.
For what concerns $D\alpha$ studies, for geometric reasons the α_1 is set equal to 0.7 in order to allow a more significative stretch of the $D\alpha$ spectrum of investigation.
Finally, the exact gradients values iteratively assumed by the model are hereunder set out:

- $D\theta$: $[\,0;\,-1;\,-2;\,-3\,]$;
- DH: $[\,-0.8;\,-0.4;\,0;\,0.4;\,0.8\,]$;
- $D\alpha$: $[\,0;\,0.04;\,0.08;\,0.12;\,0.16\,]$;

In the end, the author wants to point out that to set up the analyses settings reference [18] has been considered and that the results obtained are shown and commented in the third part.

5.1. Compression test

The first property investigated is the homogenized Young's modulus. In order to obtain it, the model was loaded with a set downward displacement of the top surface nodes thus simulating a compression. Since the application of the lattice as an acoustic liner requires it to be completely constrained at the bottom and free to move at the lateral surfaces, the model has been implemented with this kind of constraints and loads.
Moreover, to ensure the results of this study another loading case has been simulated introducing on the same model a distributed force at the top surface of the frame in spite of a set displacement. However, the two results are almost identical to each other and the mathematical postprocessing is similar.
Also, in order to avoid scale effect due to a limited number of rows, columns or floors of the lattice, these values have been increased to:

- NR = 9;
- NC = 8;
- NF = 12;

The two compression ways of analysis are shown in figure 5.1: the models belong to the study of the stiffness along the z direction.

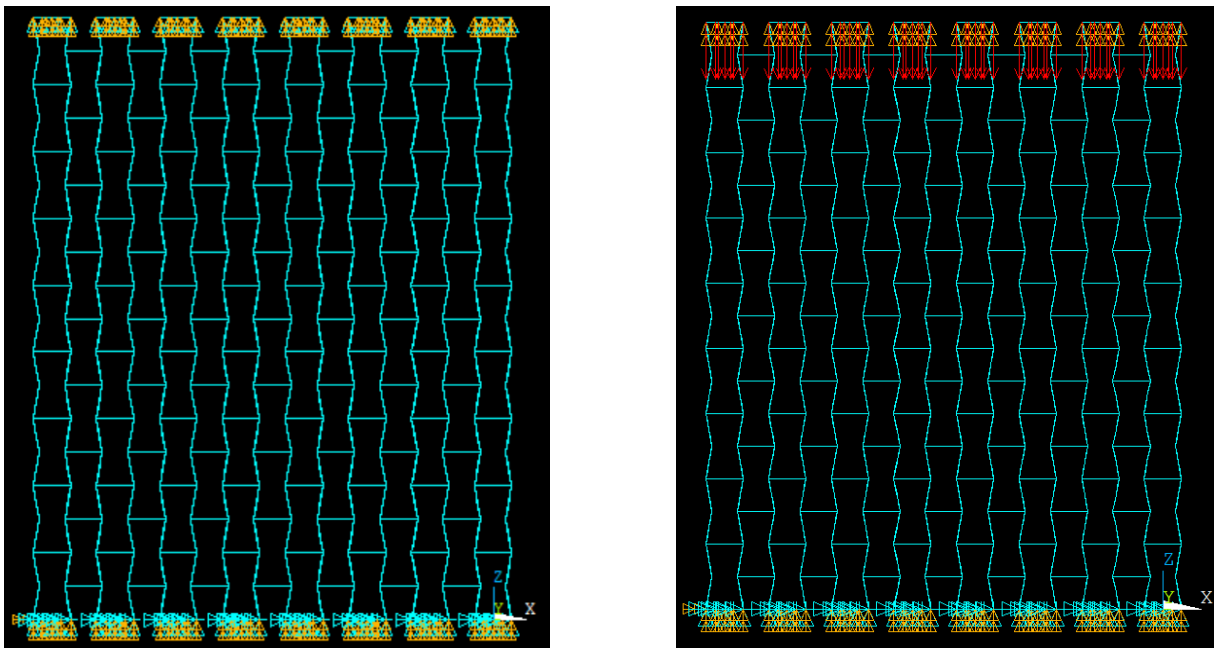

Figure 5.1: *FEM model for set displacement compression analysis along z on the left and set force compression analysis along z on the right.*

5.1.1. Theory

As previously said, the compression test is simulated by a set displacement of 0.1 millimetres of the top nodes of the structure. In this analysis, only the elastic modulus is needed, and this explains the small displacement chosen. The extracted outputs of the investigation are the total reaction force at the top surface of the structure, the mass and the volume of the lattice. The former is calculated as the sum of all the reaction forces at each node of the top surface. The other two data are acquired by the programming function "*GET" of ANSYS APDL in postprocessing environment.
Recalling the well-known elastic constitutive equation:

$$E = {}^{\sigma}/_{\varepsilon} \tag{5.1}$$

And converting the reaction force (R_f) into a proper homogenized stress through equation (5.2) and the displacement (ΔL) into a strain through equation (5.3) the elastic stiffness can be obtained:

$$\sigma = \frac{R_f}{A} \tag{5.2}$$

$$\varepsilon = \frac{\Delta L}{L} \tag{5.3}$$

where "A" is the area of the loaded plane and "L" is the dimension length of the lattice along the axis collinear with the set displacement.
It has to be underlined that the stresses are far from reaching the yielding strength all over the lattice nodes so plasticity is not taken into account.
Once the stiffness is known, it is easy to find the density of the frame diving its mass by its volume and managing to find out the specific stiffness by equation (5.4).

$$\frac{E}{\rho} = \frac{R_f \cdot L}{\Delta L \cdot A \cdot \rho} \tag{5.4}$$

Moreover, all the variables have to be specified for the three loading directions. So, the final equations are:

$$\frac{E_z}{\rho} = \frac{R_{fz} \cdot L_z}{\Delta L_z \cdot L_x \cdot L_y \cdot \rho} \tag{5.5}$$

$$\frac{E_y}{\rho} = \frac{R_{fy} \cdot L_y}{\Delta L_y \cdot L_z \cdot L_x \cdot \rho} \tag{5.6}$$

$$\frac{E_x}{\rho} = \frac{R_{fx} \cdot L_x}{\Delta L_x \cdot L_z \cdot L_y \cdot \rho} \tag{5.7}$$

where equations (5.5), (5.6) and (5.7) determine respectively specific stiffness along z, y and x directions.
The other way of analysing the structure is by loading with forces the top nodes and getting the nodes average displacement of the top surface of the lattice. The final formulas are exactly the same as the ones written above.

5.1.2. FEM models

The script used to run the single compression analysis sets the analysis type to static and doesn't consider non-linear geometry (large deformation) because it is a field not reached yet for the small displacement set. In the Annex an example of the "MAIN SCRIPT (COMPRESSION)" used to analyse the compression along z is given. For the other two cases the procedure is the same, but the locations and directions of constraints and displacements are different.
The model implemented for the analysis along the z axis is shown in figure 5.1 on the left, whereas figures 5.2 and 5.3 show respectively the models defined to extract the homogenized Young's modulus along the y and x directions.

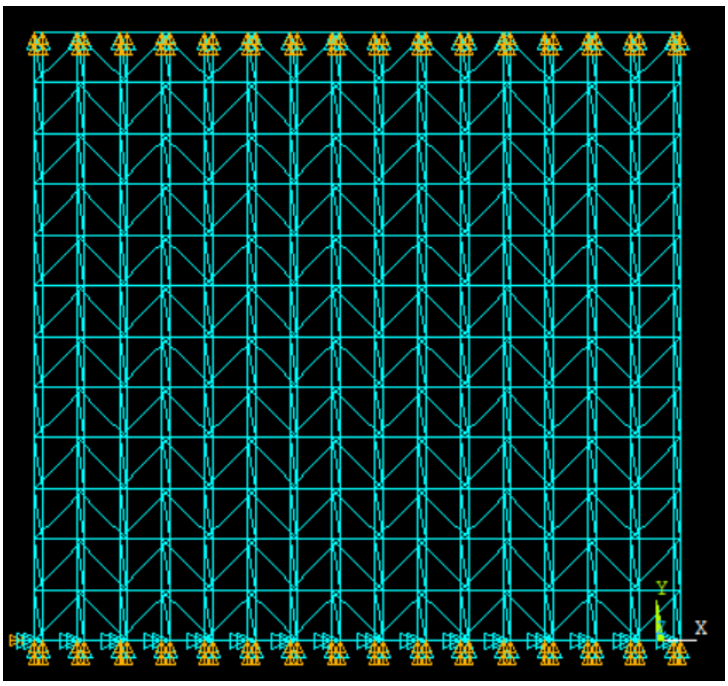

Figure 5.2: *FEM model for set displacement compression analysis along y.*

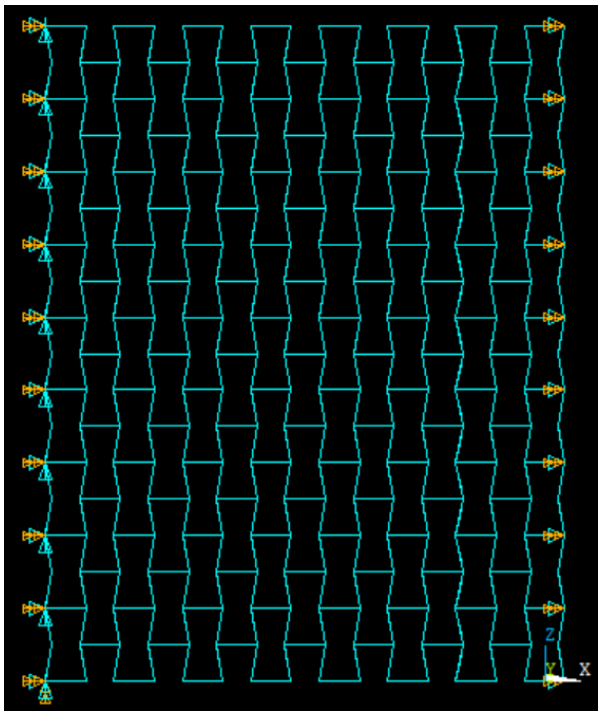

Figure 5.3: *FEM model for set displacement compression analysis along x.*

5.2. Shear test

The second property investigated is the homogenized shear modulus. There is more than one possibility for simulating a shear test. However, only biaxial loading introduces as close as possible a pure shear deformation field, and this is the type of simulation that was implemented. It is shown in figure 5.4 taken from [18].

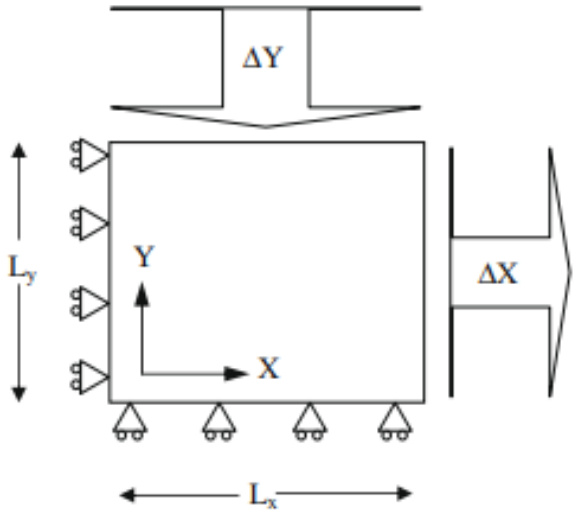

Figure 5.4: *Boundary condition for virtual biaxial shear test.*

As it can be noticed the lattice is constrained with sliders on both lateral edges (which are surfaces considering the three-dimensionality of the structure) and loaded with two opposite displacements along the axes of the plane on which the shear is analysed (e.g. in figure 5.4 the shear on the plane xy). That is, one displacement is negative and the other is positive.
Moreover, the implemented lattice models consist of the identical number of rows, columns and floors of the compression models. As a matter of fact, the same identical structures models are used.
In subparagraph 5.2.2 FEM models are shown for all the three investigation directions.

5.2.1. Theory

The two set displacements necessary for defining the shear modulus are both equal to 0.1 millimetres. Like for the previous analysis, the choice of small displacements is due to the will of avoiding the elastic limits and thus negatively affecting the results.
The outputs of the simulation are the total reaction forces at the two constrained surfaces, the mass and the volume of the lattice. The former is calculated as the sum of

all the reaction forces at each node of the lateral surfaces. The other two data are acquired by the programming function "*GET" of ANSYS APDL in postprocessing environment. The boundary condition for virtual biaxial shear test determine a loading configuration which verify the hypothesis of two-dimensional state of stress (with one principal stress which is zero). Furthermore, the three principal stresses related to the mentioned configuration are exactly the three stresses along x, y and z. Thus, the shear stiffness can be computed with the following equation:

$$G_{12} = \frac{\tau_{12}}{\gamma_{12}} = \frac{\sigma_1 - \sigma_2}{2(\varepsilon_1 - \varepsilon_2)} = \frac{R_{f1}L_1 - R_{f2}L_2}{2L_3(\Delta L_1 L_2 - \Delta L_2 L_1)} \tag{5.8}$$

where the subscript numbers stand for the three different principal directions, "R_f" is the total reaction force, "L" is the dimension of the lattice along a certain direction and "ΔL" is the set displacement along a certain direction. "G" is the shear modulus on the plane determined by the 1 and 2 axes.
Specifying the formula in the three directions to calculate the homogenized shear modulus equations (5.9), (5.10) and (5.11) are obtained.

$$G_{xy} = \frac{\tau_{xy}}{\gamma_{xy}} = \frac{R_{fx}L_x - R_{fy}L_y}{2L_z(\Delta L_x L_y - \Delta L_y L_x)} \tag{5.9}$$

$$G_{xz} = \frac{\tau_{xz}}{\gamma_{xz}} = \frac{R_{fx}L_x - R_{fz}L_z}{2L_y(\Delta L_x L_z - \Delta L_z L_x)} \tag{5.10}$$

$$G_{yz} = \frac{\tau_{yz}}{\gamma_{yz}} = \frac{R_{fy}L_y - R_{fz}L_z}{2L_x(\Delta L_y L_z - \Delta L_z L_y)} \tag{5.11}$$

Figures 5.5 graphically helps to understand better the directions of the shear stiffness:

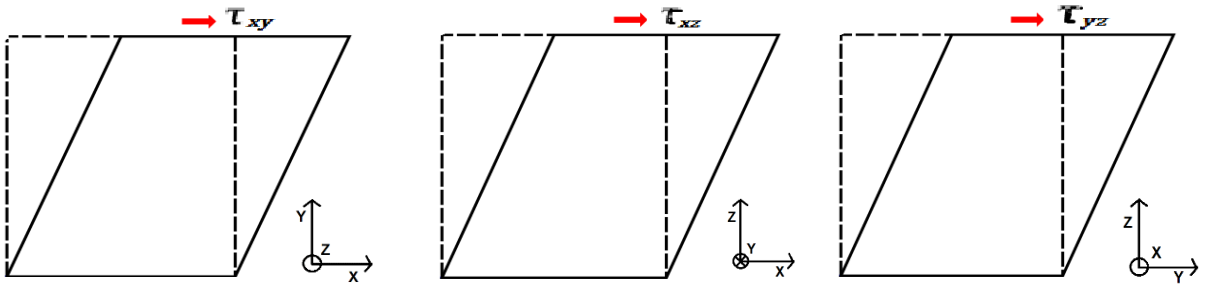

Figure 5.5: *Shear directions for all the three loading cases.*

5.2.2. FEM model

The script used to run the single shear analysis sets the analysis type to static and doesn't consider non-linear geometry (large deformation) because it is a field not reached yet for the small displacement set. In the Annex an example of the "MAIN SCRIPT (SHEAR)" used to analyse the shear stiffness on the plane x-y is given. For the other two cases the procedure is the same, but the locations and directions of constraints and displacements are different as it is shown in figures 5.6, 5.7 and 5.8 which respectively display the models used for the investigation of the shear modulus on the plane x-y, x-z and y-z.
In each model the constraints are orange and the displacements are cyan, and to highlight the displacement direction red arrows has been introduced.

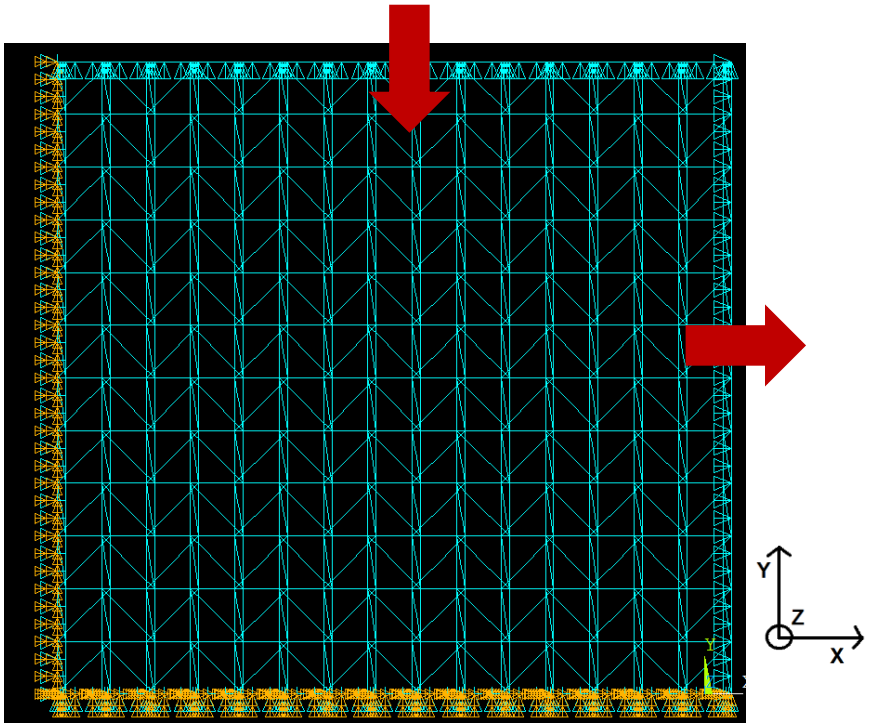

Figure 5.6: *FEM model for shear test on the plane x-y.*

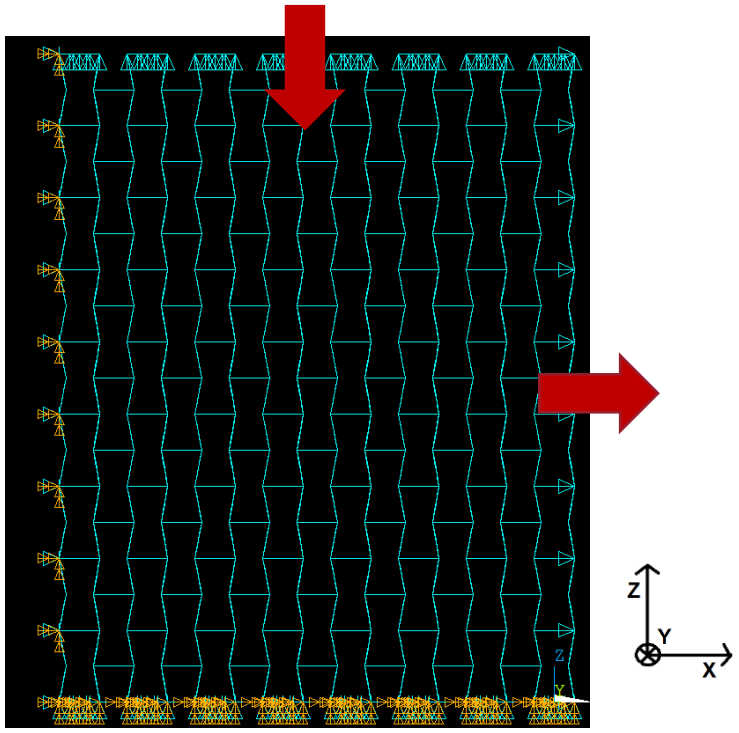

Figure 5.7: *FEM model for shear test on the plane x-z.*

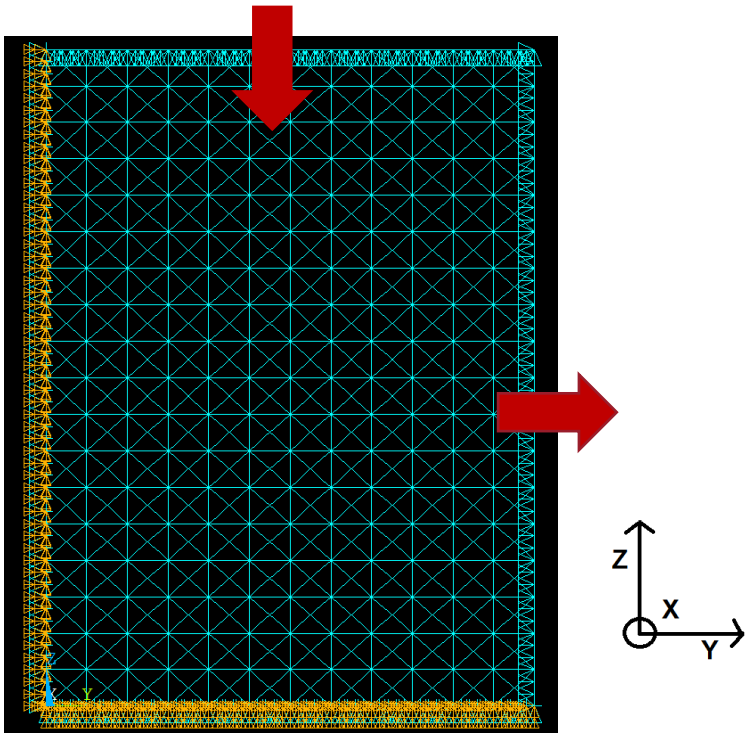

Figure 5.8: *FEM model for shear test on the plane z-y.*

5.3. Elastic energy absorption test

The final feature to investigate is the energy absorption. This is the last set of simulations run but it is absolutely no the least one. On the contrary, considering the application foreseen by Rolls-Royce, this property is the main reason why this kind of auxetic lattice with gradients has been chosen. In fact, this frame, should absorb much more energy than the equivalent honeycomb structure because of the higher mobility the struts are given.
Rolls-Royce is interested in both elastic and plastic energy absorptions. The former is the leading factor during designing conditions where acoustic liner is only meant to absorb the pressure waves energy through the deformation thus damping the acoustic vibrations. In this case, the deformations are very small and the lattice response is in the elastic regime. On the other hand, the company is also interested in knowing the amount of energy dissipated by the structure in the plastic regime because in off-design conditions the liner needs to be the first safety barrier which prevents the collapse of the all aeroengine. So, the liner is supposed to provide large impact energy absorption when crashing and collapsing.
However, the plastic energy absorption analysis couldn't be done without approximation hypothesis and it is still to be measured. In fact, this analysis requires the generation of 3D beam to 3D beam contact elements which is not a completely defined feature in ANSYS 15.0 release and, even if it was, there still would be many programming problems when meshing the lattice. Insofar, contact elements need to be manually associated with the parts which are going to touch each other, but, since lattices consist of an enormous number of struts and it is not known beforehand what regions are going to be in contact, this operation is almost impossible. Therefore, the solution when facing this problem is using 3D volume structures and using an equivalent constitutive law which is obtained via experimental data.
Consequently, only elastic energy absorption has been analysed and it will be referred simply as energy absorption. As already mentioned, the lattice has been designed to show the highest energy absorption when loaded along the z axis. Therefore, the only value which is relevant for the acoustic liner application is the specific energy absorption along the z direction.
Moreover, the models used are slightly different from the previous ones: the number of rows, columns and floors is appropriately reduced so as to minimize the computational complexity of the simulation because new surface contact elements have to be introduced on the top surface of the frame. These more complex elements are needed to reproduce the flatwise compression of the frame consequent to the downward displacement of an upper layer which represents the perforated sheet of the acoustic liner.
The single analysis is identical to the compression test setting the displacement of the upper layer and getting as outputs the total reaction force of the top surface, the mass

and the volume of the frame. However, the study has always a parametric nature likewise the compression test and the shear one. Also, in order to acquire an accurate constitutive equation, ten different simulations with ten increasing set displacements have been run per each parameter. The value of the ten different displacements is different for each structure, insofar they all have different dimensions thus generating dissimilar strains.
In subparagraph 5.3.2 the FEM model is shown.

5.3.1. Theory

The procedure to get the specific energy absorption, which from now on will be called "SEA", relies on two different postprocessing steps: determining the physical relationship between stress and strain and integrating the function obtained over the strain region of interest.
The first phase has the same mathematical background explained for the compression test. This time the Young's modulus is not sought, so only the compression curve is to be displayed and stresses and strains are determined by equations (5.2) e (5.3).
Once, the compressive curve is known, elastic energy absorption can be calculated and it can be divided by the density of the lattice in order to obtain the SEA.
It has to be said that, to get the stress-strain equation it was used a "Matlab" (programming software) function, the "SPLINE", which helps to interpolate the stress-strain values couples obtained by the ten analyses. Then, this function has been integrated over the elastic region.
The elastic region is slightly different for every lattice shape because the strain is influenced by the structure height and the distribution of stresses depends on the morphology of the specific frame. Thus, to have an idea of the real elastic energy absorbed by the specific lattice, for some of the models the integration range has been adapted to their effective elastic region. So, it was checked that for each analysis the yielding strength is not overcome. However, in order to find trustful results all the analysis are close to the yielding point which has been considered the configuration in which only less than the 0.001% of the lattice struts are characterized by a stress which is slightly over the material yielding point. On this subject, it can be said that actually the lattice yielding point may not be the one chosen but a greater value because effectively, that percentage means having one million struts and just ten of them are starting to plasticize. Since the ratio is very small, it should be verified by experimental data if it is actually already relevant. Anyway, 0.001% is used to ensure the rightness of the final results.
In most of the cases the strain range was the one written in equation (5.12) because of their structural and dimension similarities:

$$SEA = \int_0^{0.0025} \sigma(\varepsilon) d\varepsilon \tag{5.12}$$

5.3.2. FEM model

The script used to run the single elastic absorption analysis sets the analysis type to static and consider non-linear geometry (large deformation) because it is a field that may be reached for the last analyses which show bigger set displacements.
The "MAIN SCRIPT (SEA)", which is the file implementing the simulation, is different from the previous ones, because it defines plane elements "SHELL181" on the top surface of the lattice in order to simulate the contact with the upper layer meshed with "SOLID186" elements. More information can be found in [17].
Moreover, the introduction of surface contact is obtained by "TARGE170" and "CONTA174" elements: respectively associated with the bottom surface of the upper layer and with the shell elements on the top surface of the lattice. The contact is implemented as a rigid to deformable one, thus the "TARGE170" are modeled as rigid parts and the "CONTA174" are modeled as deformable bodies.
The final virtual model is the one shown in figure 5.9, and that is the only direction along which the SEA has been investigated.

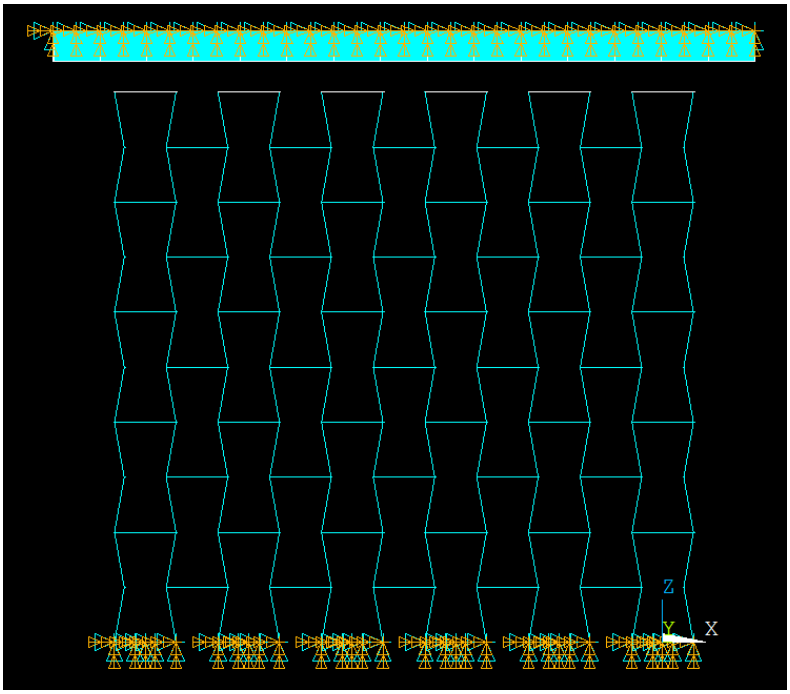

Figure 5.9: *FEM model for SEA along the z axis.*

6.Substructuring

As stated in the thesis's outline, the aim of the project is not only investigating the material properties of type of lattice designed but also giving an appropriate solution to reduce the computational resources and the time required by each analysis. In fact, the idea is to define a method which could provide the industrial companies a faster way to directly introduce and analyse the lattice. All the parametric analysis, especially the elastic energy absorption one, can be very time-consuming, and, both form an academic and an industrial point of view, trying to find a procedure which could minimize the computational complexities faced is daily occurrence.
Considering energy absorption analyses described in chapter 5, a significative problem of time was faced. Taking into account non-linear geometry and surface contact elements, simulations can last up to fifteen minutes for large displacements. This means that obtaining the compressive curve for a certain frame can take almost more than one hour on average. Thus, the whole time needed to run the parametric analysis along all the three axes is approximately five days.
Therefore, this is a vivid example of the necessity to implement a time reducing simulative model.
However, it is important to underline that the concept is not related to a particular kind of structure and it thought to be suitable for all structures.
Also, referring to periodic structures such as lattices the aim is to define a way of introducing them in a previously set volume inside an assembly of parts.
As a matter of fact, these structures are mainly used to fill the free space inside a bigger system of layers: e.g. the acoustic liner is made of two extremal layers among which the lattice is thought to be applied (another example could be sandwich panels).
Taking inspiration from the additive manufacturing concept of slicing an object to reproduce it by adding a layer above another one, all the efforts have been put in finding a way to define a macro unit made of several different other elements, but which could be dealt with as a single element. That is, figuring out a solution which could condensate together the various behaviours of an assembly and faithfully reproducing it relying on a set of master nodes user-defined.
Searching in [19] a relevant ANSYS procedure which could perfectly match these necessities was found: "Substructuring".
In the next chapters it is going to be explained from a mathematical and modeling point of view. Moreover, a general numerical investigation of the advantages and disadvantages of the above-mentioned procedure is made in order to define an initial benchmark. There has not been time to deepen this concept, thus this study is to be considered as a trailblazing step toward an interesting modeling option. In paragraph 6.2 the type of analysis is explained.

6.1. FEM Theory

Substructuring is a procedure that condenses a group of finite elements into one element represented as a matrix. This single matrix element is called a "superelement". It can be used in an analysis just as any other ANSYS element type would. The only difference is that the superelement has to be created beforehand by performing a substructure generation analysis.
The reasons for substructuring are: reducing computer time and allowing solution of very large problems with limited computer resources. Examples of the former are nonlinear analyses and analyses of structures that contain repeated geometrical patterns which is clearly the lattice case. In a nonlinear analysis, the linear portion of the model can be substructured so that the element matrices for that portion need not to be recalculated every equilibrium iteration. In a structure with repeated patterns, a superelement can be generated to represent the pattern and simply make copies of it at different locations, thereby saving a significant amount of computer time.
An example of the second reason is an analysis that is too large for the computer in terms of wavefront size or disk space requirements. In such a situation, you can analyze the model in pieces, where each piece is a superelement small enough to fit on the computer.
A substructure analysis involves three distinct steps:

- Generation Pass;
- Use Pass;
- Expansion Pass;

Figure 6.1 shows the procedure steps:

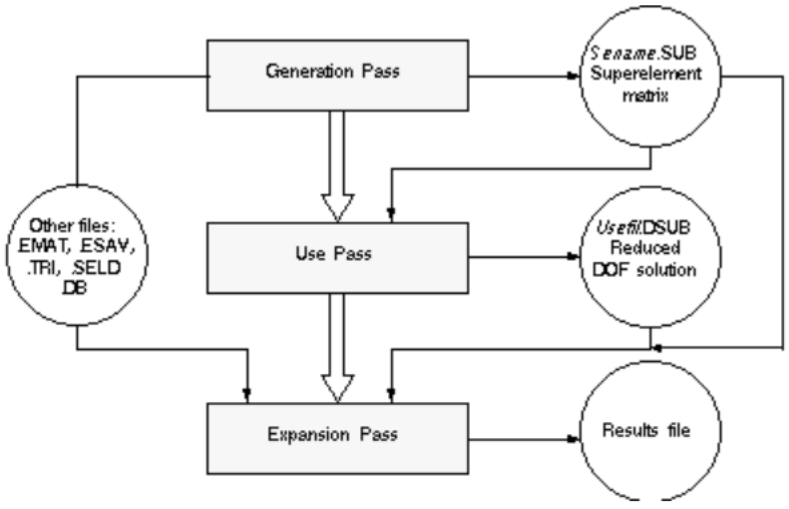

Figure 6.1: *Substructuring steps.*

The generation pass is where a group of "regular" finite elements is condensed into a single superelement represented with a single matrix. The condensation is done by identifying a set of master degrees of freedom, which are mainly used to define the interface between the superelement and other elements. Figure 6.2 shows a plate-like structure that is to be analysed with contact (interface) elements. Since the contact elements require an iterative solution, substructuring the plate portion can result in a significant savings in computer time.

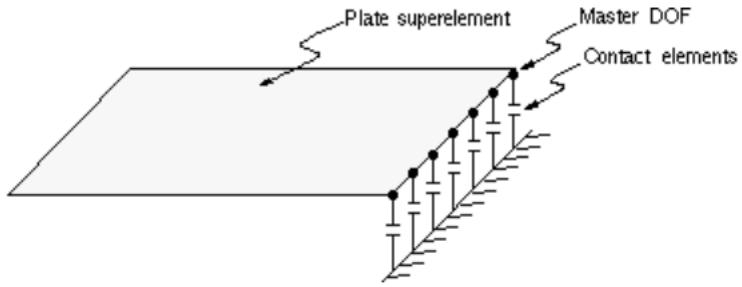

Figure 6.2: *Example of a substructuring application.*

The use pass is where the superelement is used in an analysis by making it part of the model. The entire model may be a superelement or, as in the plate example, the superelement may be connected to other non-superelements (see figure 6.2). The solution from the use pass consists only of the reduced solution for the superelement (that is, the degree of freedom solution only at the master DOF) and complete solution for non-superelements.
The expansion pass is where the reduced solution is started and results are calculated at all degrees of freedom in the superelement. If multiple superelements are used in the use pass, a separate expansion pass will be required for each superelement. Sometimes this third step is unnecessary because the inner lattice results are not sought.

6.2. Substructuring features investigation

A numerical investigation of the advantages and disadvantages of the Substructuring procedure compared to the classic approach has been carried out. Before proceeding with the study description, it needs to be defined what is it meant when saying the classic approach: it is the typical modeling process through which the user has to associate to every single portion of the model its meshing element. On the other hand, the superlement definition allows the generation of a bigger assembly made of multiple portions which are already meshed.
The case study analysed consists of three various ways of modeling the same lattice: using the classical approach, the single-superelement one and the multiple-superelement one. The former has already been outlined, whereas the latters refer respectively to modeling the structure with one bigger superelement or doing it via a smarter but more complex choice, relying on three smaller superelement.
Figures 6.3, 6.4 and 6.5 show the three cases.

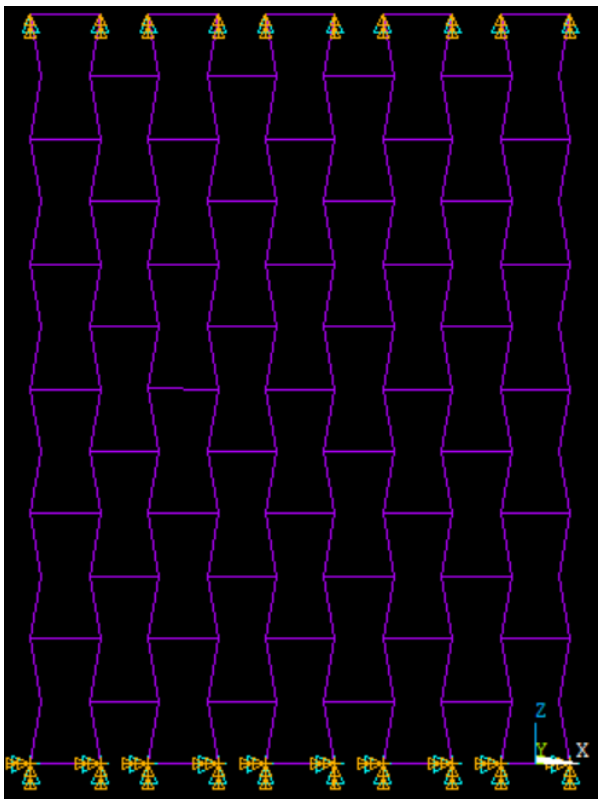

Figure 6.3: *Lattice meshed with the classic modeling approach.*

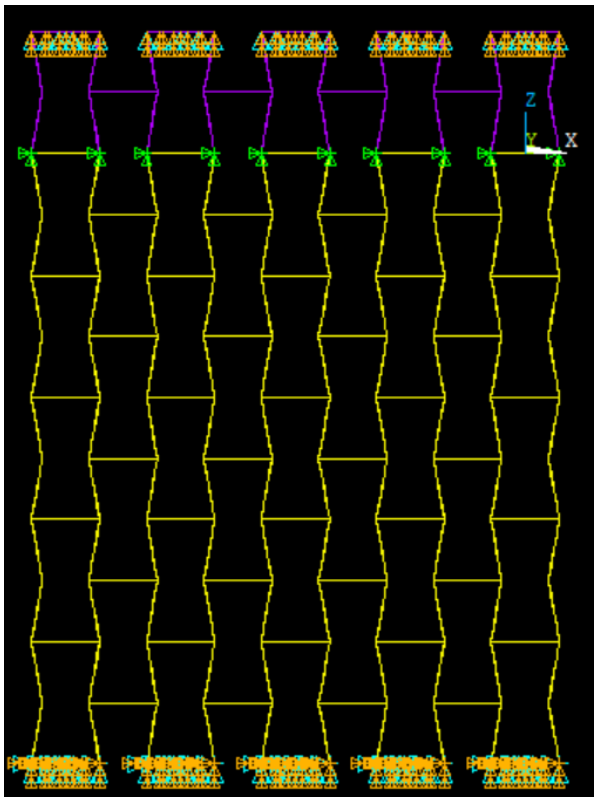

Figure 6.4: *Lattice meshed with the single-superelement modeling approach.*

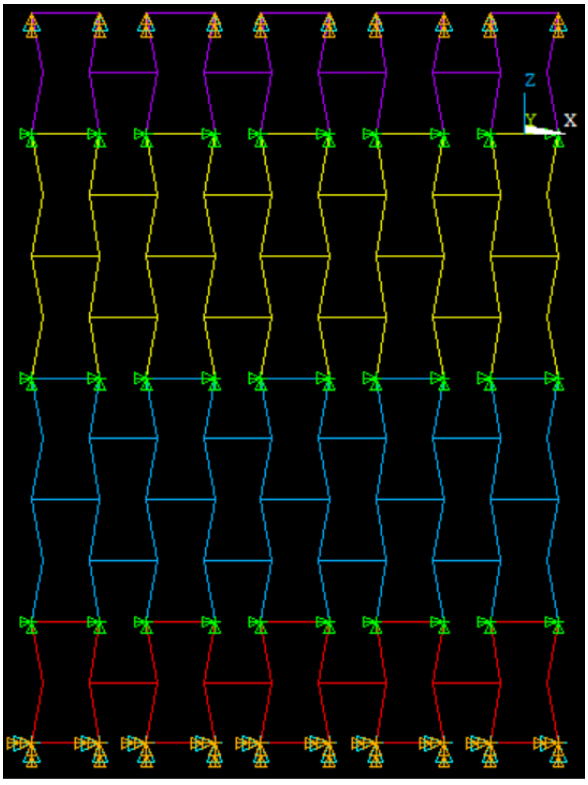

Figure 6.5: *Lattice meshed with the multiple-superelement modeling approach.*

In each figure colour purple represents the portion of lattice meshed directly without introducing it as a superlement with the classic approach. On the contrary, colour yellow represents the first superlement introduced in the assembly, cyan the second and red the third. Thus, in the single-superelement approach cyan and red are not present.
As it is noticeable in both cases which rely on the substructuring procedure, a non-superlement region has been left in order to show that the two modeling approaches are consistent with each other thus allowing increasing the simulative design choices.
The green triangles in every figure are couplings either between two superelements or between a superelement and a non-superelement.
Furthermore, the analysis type is identical to the compression test, but these models have been also investigated with non-linear geometry in order to get an idea of what is convenient when dealing with non-linear analyses.
Results are shown in the third and last part of the thesis.

Part III

Third part

7.Results

Having introduced the background theory and the models characterizing all the analyses carried out, in this chapter the postprocessing of the data and the final results are set out.
The postprocessing has been made with the programming environment “Matlab”.
Furthermore, the most relevant results will be deepened and a final lightweight lattice with high elastic specific energy absorption, high elastic stiffness and high shear stiffness will be proposed considering the designing constraints.
Since the number of graphs obtained is enormous some of the them are displayed in a smaller scale.
It has to be mentioned beforehand that all the results referring to the base side length gradient are fluctuating because of a non-continuous change in the lattice generation which leads to a discontinuous and asymmetric modification of the volume, density and stiffness trend.

7.1. Compression test

It is reminded that the compression tests have been run along all the three directions iteratively changing the value of the seven parameters mentioned in chapter 5.
All the results are displayed by trends which describe the relationship between the specific Young's modulus and the changing parameter.
The first results shown are the ones along the z axis:

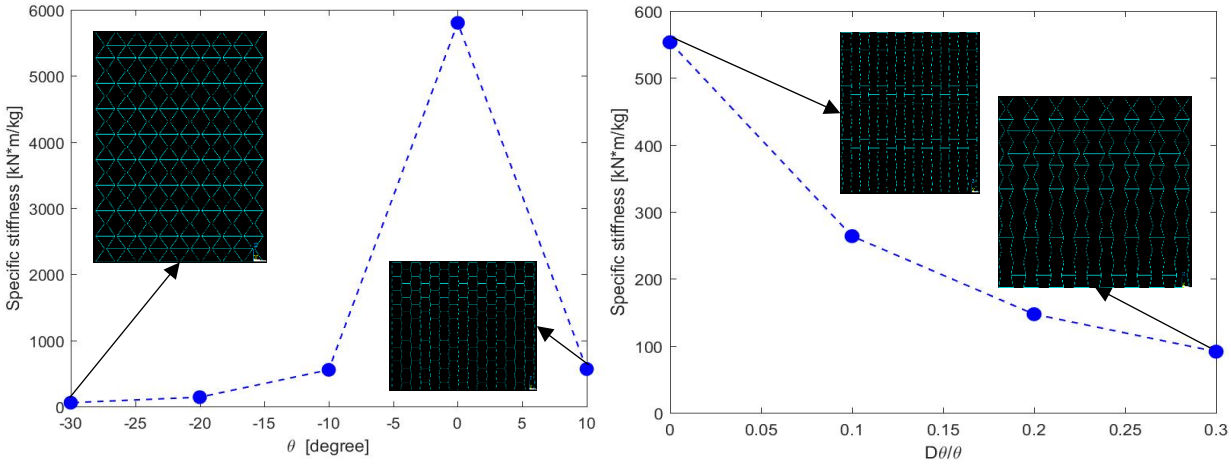

Figure 7.1: *Specific stiffness in function of the angle and of the angle gradient.*

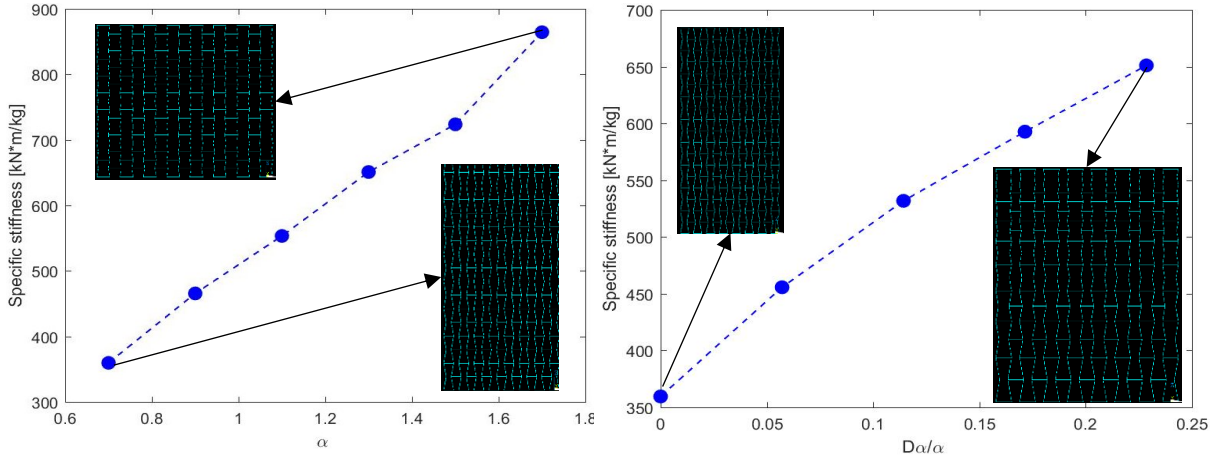

Figure 7.2: *Specific stiffness in function of the aspect ratio and of the aspect ratio gradient.*

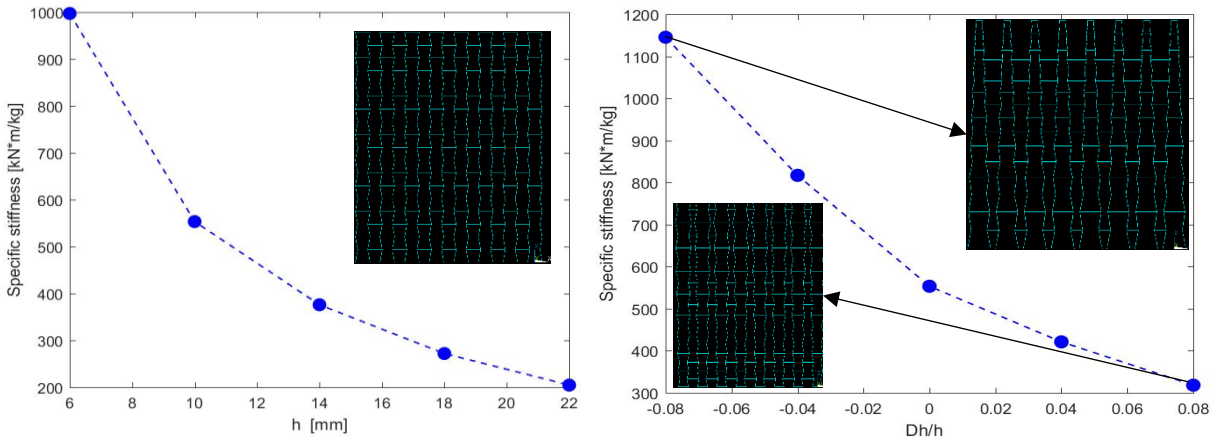

Figure 7.3: *Specific stiffness in function of the base edge and of the base edge gradient.*

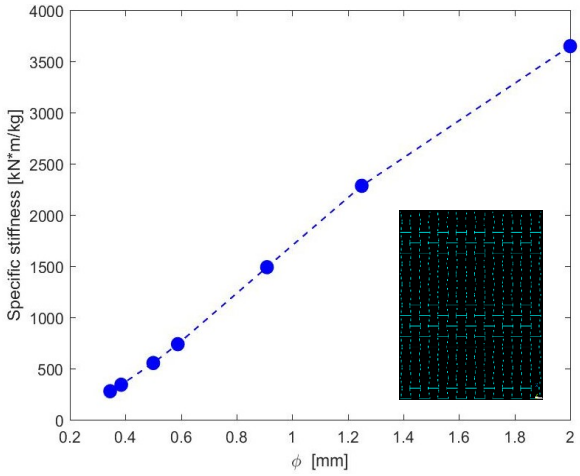

Figure 7.4: *Specific stiffness in function of the beam diameter.*

Every parameter gradient graph is consistent with its parameter graph since the value associated with no gradient in the former is the same found in the latter. Moreover, the trends are changing in the same way.

The effects of the angle and of the diameter are the most relevant thus being the first parameter to be changed. As expected, when the angle is close to zero the lattice behaviour is more stretching-dominated and consequently the frame is stiffer but should absorb less plastic energy. Furthermore, notwithstanding reducing "H" means reducing the density, the overall specific stiffness trend undergoes a vivid decrease. That is, the stiffness is decreasing in a massive way. The specific Young's modulus trend increases steeply as α increases because the lateral inclined beams length is reducing when the aspect ratio is increasing.

For what concerns the specific elastic stiffness values, it must be stated that along the z axis this structure is softer than along the y one. It is also softer than the normal honeycomb. However, this is a consequence of the bending-dominated behaviour designed.

The second results shown are along the y direction:

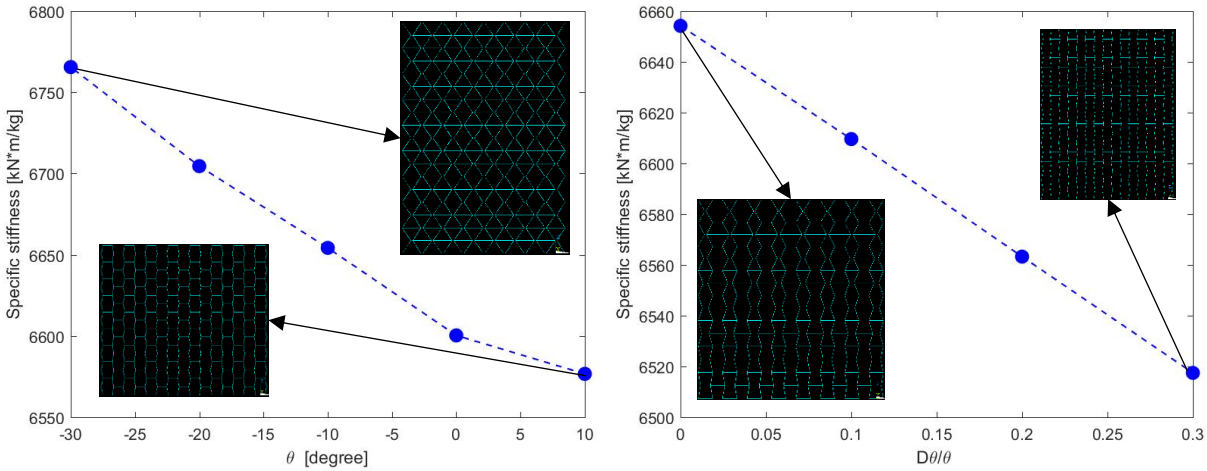

Figure 7.5: *Specific stiffness in function of the angle and of the angle gradient.*

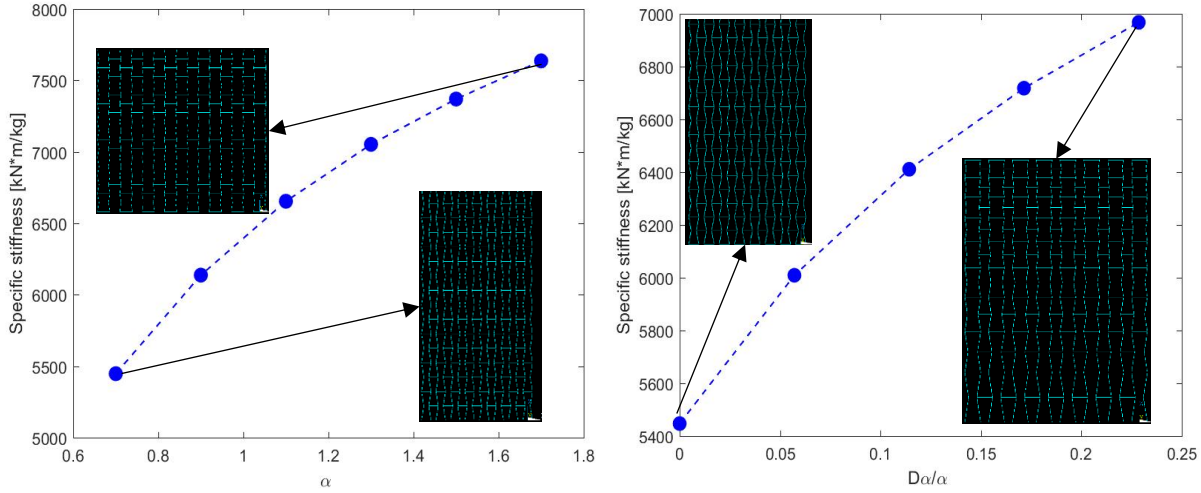

Figure 7.6: *Specific stiffness in function of the aspect ratio and of the aspect ratio gradient.*

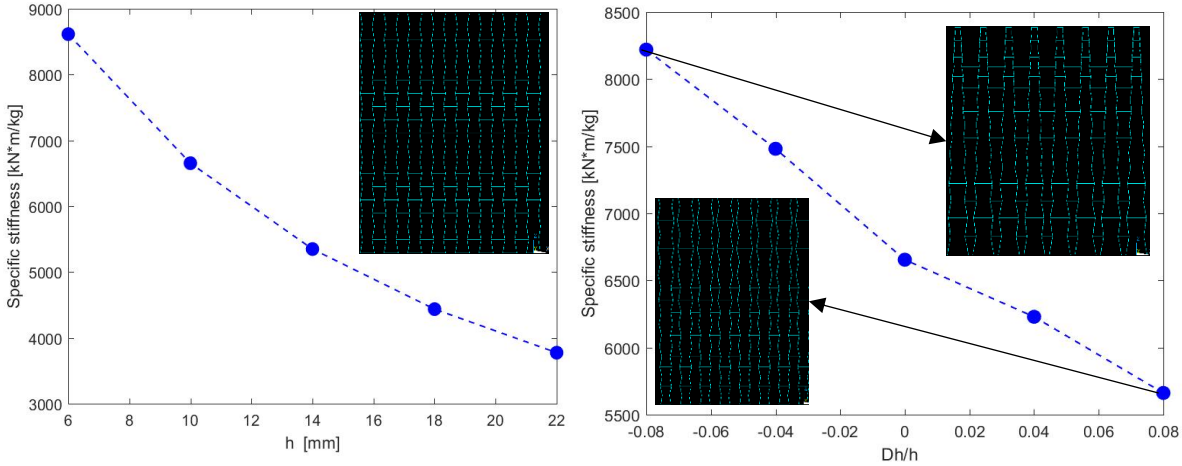

Figure 7.7: *Specific stiffness in function of the base edge and of the base edge gradient.*

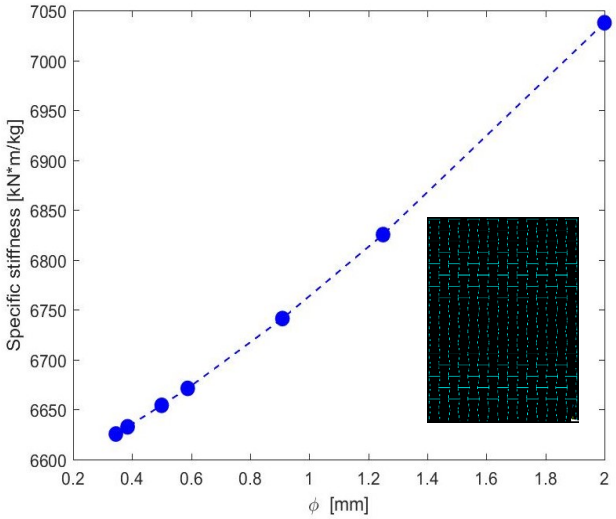

Figure 7.8: *Specific stiffness in function of the beam diameter.*

Every parameter gradient graph is consistent with its parameter graph since the value associated with no gradient in the former is the same found in the latter. Moreover, the trends are changing in the same way.
It is noteworthy to mention that the stiffness along y is less influenced by the chosen parameters than the one along the z direction because all of them are mainly modifying the geometry in the z-x plane.
The effects of the base edge and of the aspect ratio are the most relevant thus being the first parameter to be changed. This is expected because they have a significative impact on the density trend and a low one on the stiffness. Furthermore, notwithstanding reducing "H" means reducing the density, the overall specific stiffness trend undergoes a vivid decrease. That is, the stiffness is decreasing in a more massive way. The specific Young's modulus trend increases slightly as ϑ decreases mainly because the stiffening columns approach each other.
The diameter increase is less effective than in the analyses along z because the stretching stiffness is higher than the bending one. In fact, the well-known equations (7.1) and (7.2) show the displacement obtained respectively with stretching and bending loading:

$$v = \frac{F \cdot h}{E \cdot A} \tag{7.1}$$

$$v = \frac{F \cdot h^3}{3 \cdot E \cdot I} \tag{7.2}$$

If the beam geometry, the material and the load is the same the displacement "v" is always smaller for stretching loading because both the moment of inertia and the area of beams are related to dimensions which are generally one order smaller than the length of the beam "h". Moreover, looking at these formulas it is possible to understand why

the diameter influence is more meaningful for the z Young's than for this one: the moment of inertia goes with the fourth power of the diameter whereas the area only goes with the second power of it. The same logic explains why the specific stiffness when studied in function of the base edge length decreases more in the z axis results.
There is a discrepancy between the specific stiffness in function of the angle and the one in function of the angle gradient: for no gradient the specific Young's modulus value is consistent in both graphs but increasing the gradient the trend in the angle gradient analysis decreases which is the opposite evolution found in the right graph of figure 7.5. This effect is due to the density increase which is more relevant than the pure stiffness one when changing the angle gradient. Within the analyses in function of the angle, this doesn't happen because the most significant change characterizes the compressive modulus itself. Figures 7.9 and 7.10 show this concept.

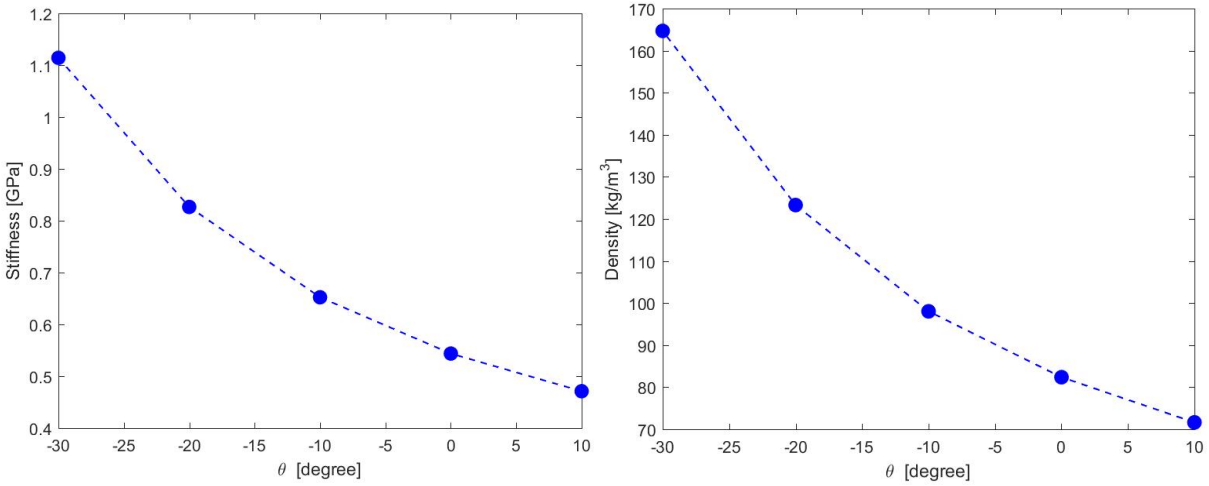

Figure 7.9: *Compressive stiffness and density in function of the angle.*

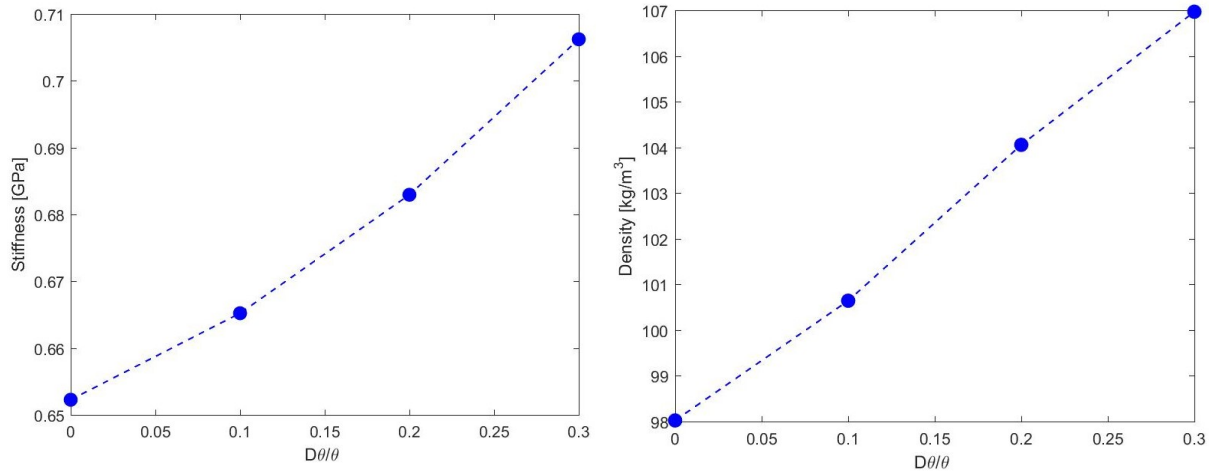

Figure 7.10: *Compressive stiffness and density in function of the angle gradient.*

Thus, there is a 63% density decrease coupled with a 56% stiffness one when varying the angle compared to a 9% density increase coupled with a 7% stiffness one when varying the angle gradient.
For what concerns the specific elastic stiffness values, it must be stated that along the z axis this structure is softer than along the y one. However, if compared to the honeycomb used by Rolls-Royce the stiffness is still slightly lower.
The last results are the ones along the x direction. It has to be said that the analysis in function of the base edge length gradient has no practical sense because the frame consists of inclined lateral surfaces and thus, the deformation when the lattice is compressed cannot be of any use.

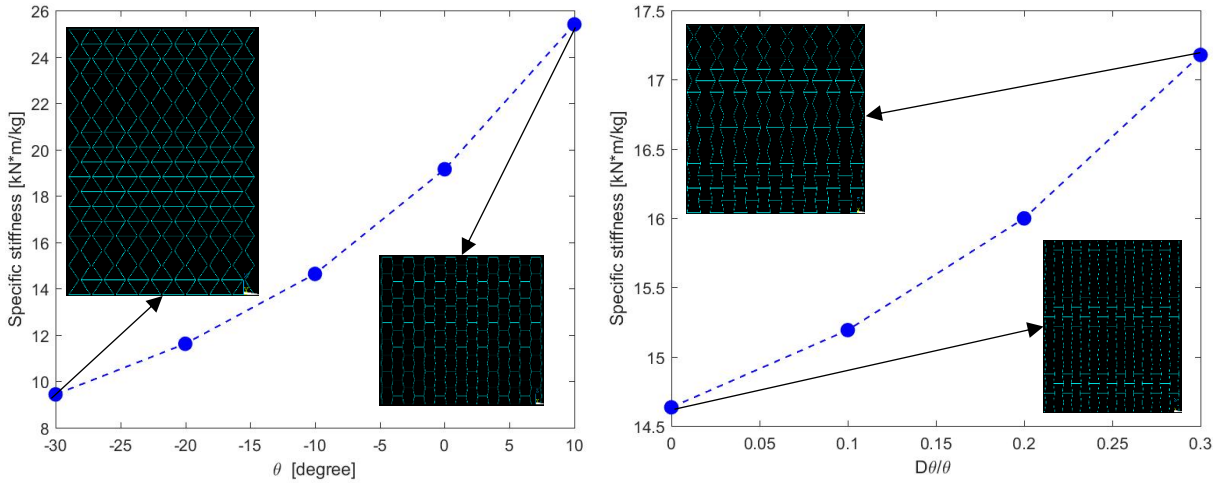

Figure 7.11: *Specific stiffness in function of the angle and of the angle gradient.*

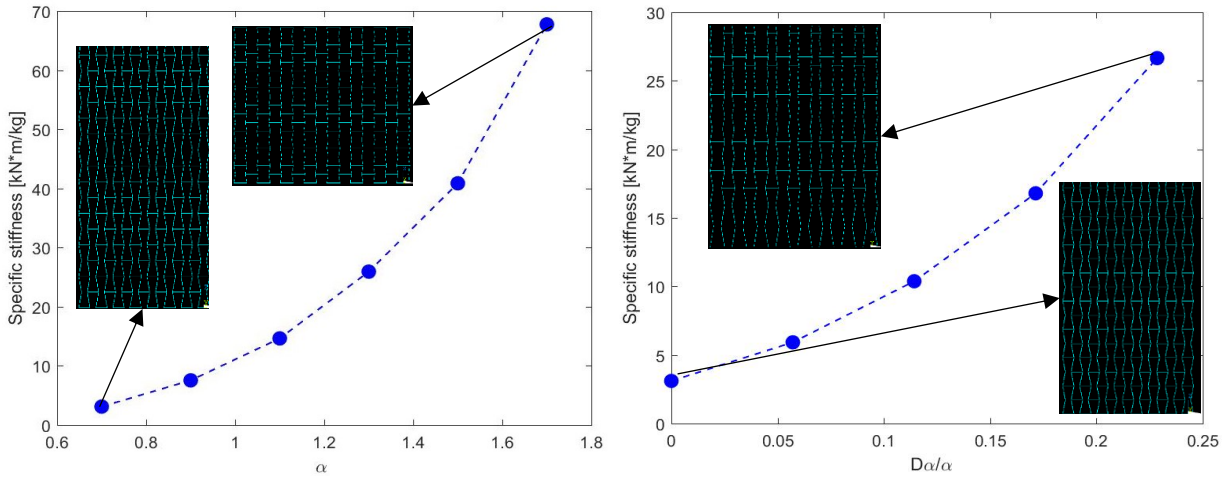

Figure 7.12: *Specific stiffness in function of the aspect ratio and of the aspect ratio gradient.*

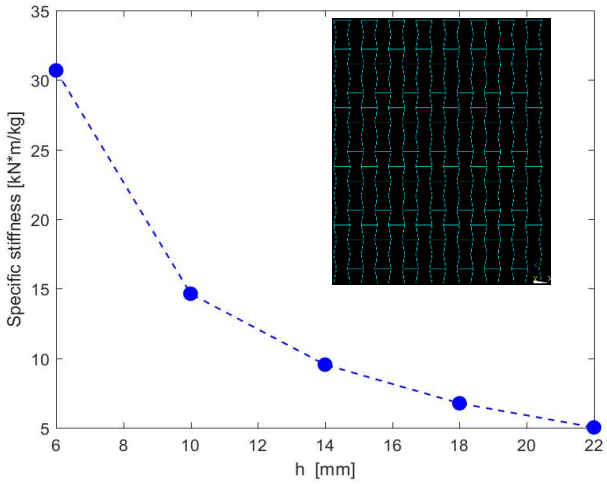

Figure 7.13: *Specific stiffness in function of the base edge length.*

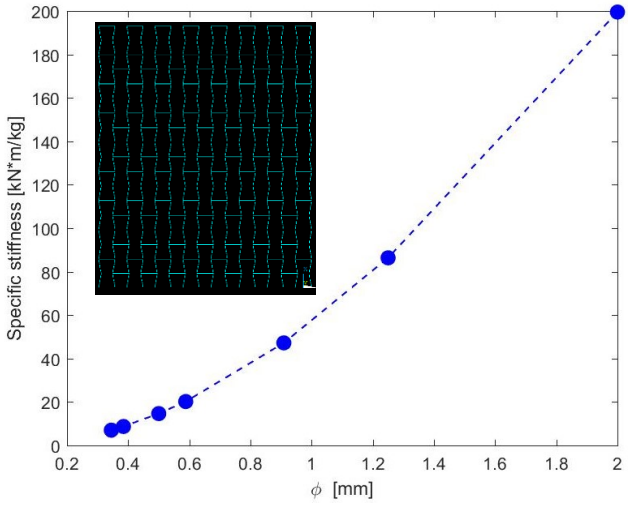

Figure 7.14: *Specific stiffness in function of the beam diameter.*

In contrast to the previous set of graphs showing the results along the y direction, these figures point out a massive influence of all parameters on the specific stiffness along the x axis. Also, it is important to underline that the Young's modulus along the x axis is the lowest one.
The same discrepancy between angles results and angle gradient results found in the previous analysis are faced and can be explained in the same way.
Moreover, the lattice is evidently bending-dominated like the for the z direction and thus the effect of the diameter is very relevant.
The specific stiffness trend in function of the angle is very influenced by the density trend.
In conclusion, in order to compare the trends along the three directions and understand better the influences of the parameters, summary graphs are exposed in the next page. They show on the y axis the ratio between the stiffness and its maximum value for each direction and on the x axis the value of the parameter whose effect is being analysed.

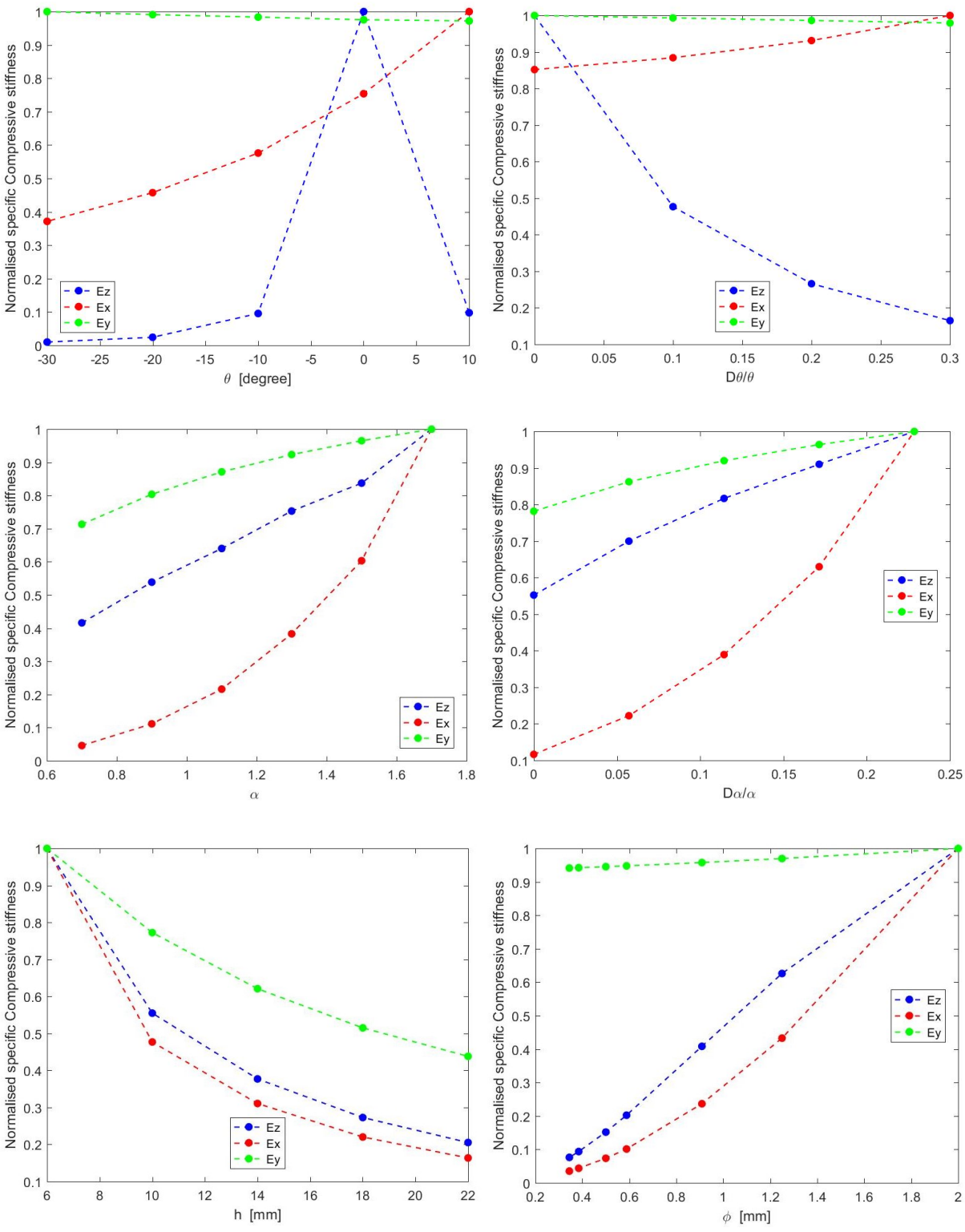

Figure 7.15: *Comparison graphs.*

The y direction is the stiffest one and the x direction is the softest one and, apart from the angle analyses, the x direction is the more influenced by the parameters. On the contrary, the y direction is the less influenced by the variables.
Considering equation (2.8) the z stiffness is twice higher than a classic cellular solid one.

7.2. Shear test

It is reminded that the shear tests have been run along all the three directions iteratively changing the value of the seven parameters mentioned in chapter 5.
All the results are displayed by trends which describe the relationship between the specific shear modulus and the changing parameter.
The designed lattice is not thought to present a high homogenized shear modulus, but in order to have a complete mechanical description of the frame capabilities it has been determined.
The first results shown are the ones on the x-y plane.

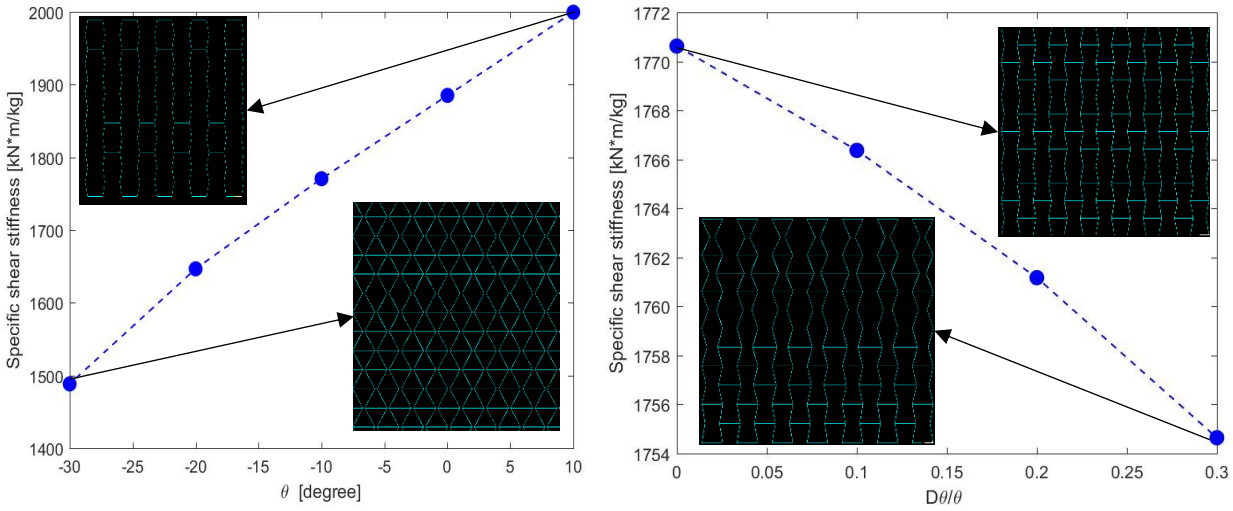

Figure 7.16: *Specific shear stiffness in function of the angle and the angle gradient.*

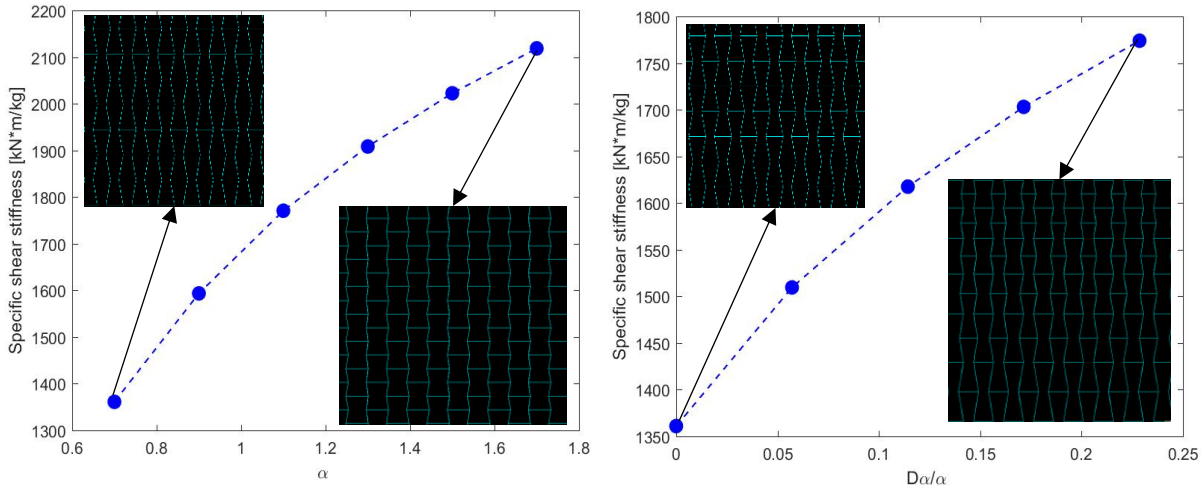

Figure 7.17: *Specific shear stiffness in function of the aspect ratio and the aspect ratio gradient.*

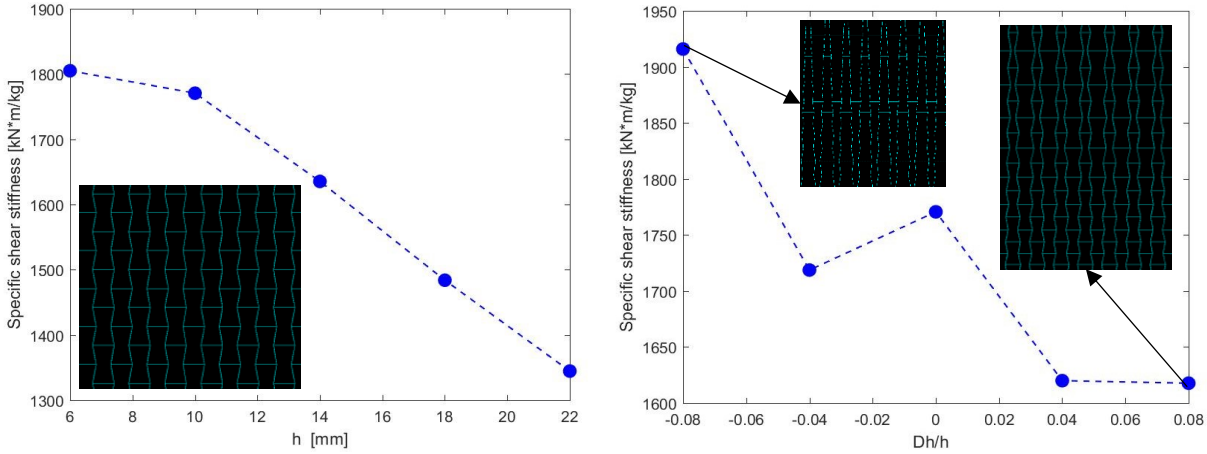

Figure 7.18: *Specific shear stiffness in function of the base edge and the base edge gradient.*

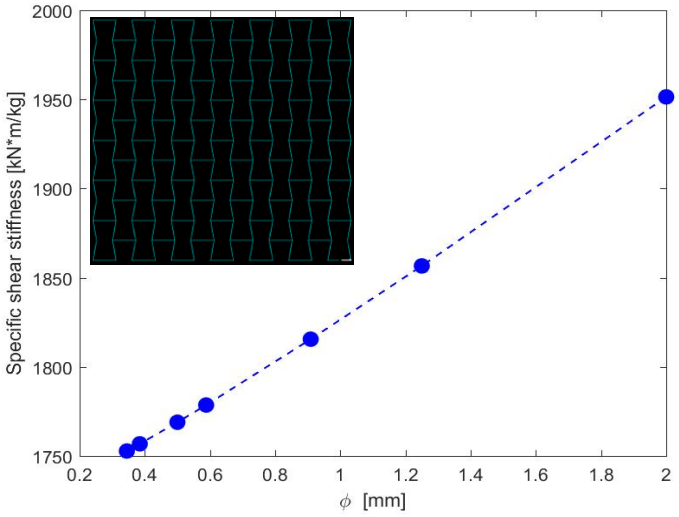

Figure 7.19: *Specific shear stiffness in function of the beam diameter.*

The trend of the specific shear stiffness in function of the base edge length is initially very influenced by the density which is strongly decreasing from the first value of "H" to the second, thus changing the slope of the shear stiffness which is always decreasing. Moreover, the trend on the right graph of figure 7.18 is fluctuating for the asymmetric changing of the density due to a discontinuous changing of the lattice when the base edge length changes.
All the gradients outputs are consistent with their referring graph.
It is interesting how meaningless is the influence of the diameter changing when compared to other parameters effect such as the aspect ratio: the influence of density has to be taken responsible for it.

The second results shown are the one referring to the shear modulus when loading the frame on the plane x-z.

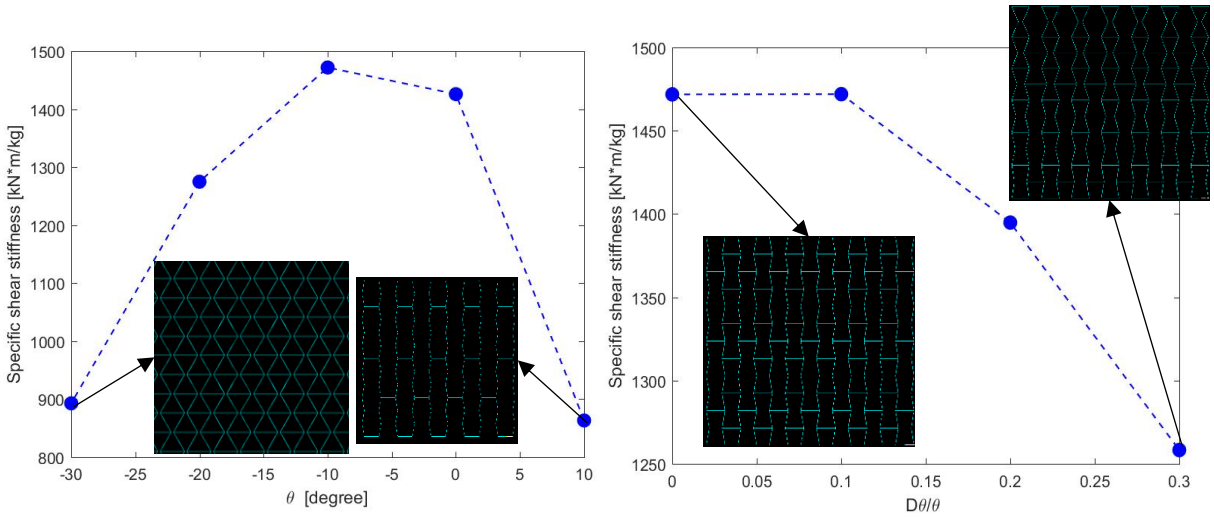

Figure 7.20: *Specific shear stiffness in function of the angle and the angle gradient.*

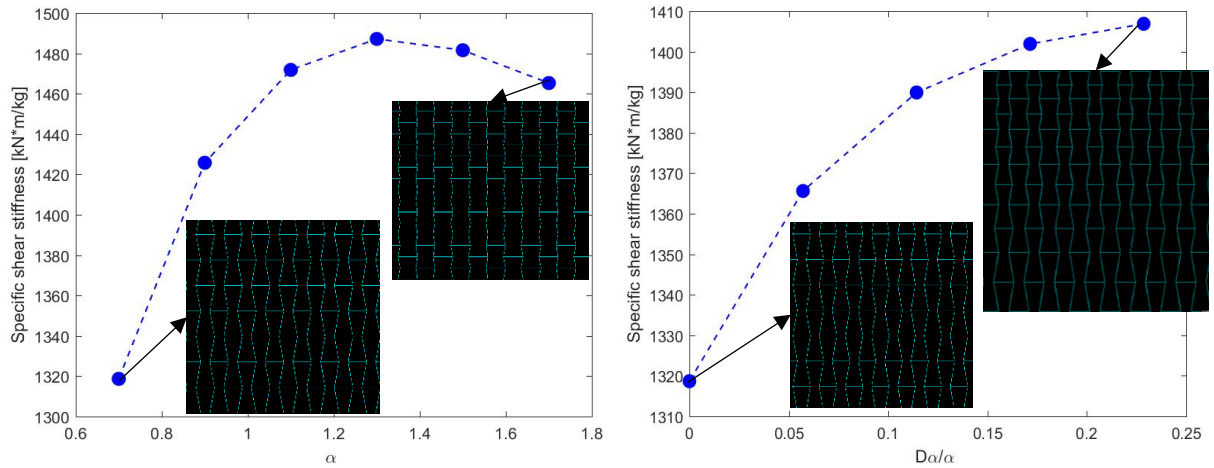

Figure 7.21: *Specific shear stiffness in function of the aspect ratio and the aspect ratio gradient.*

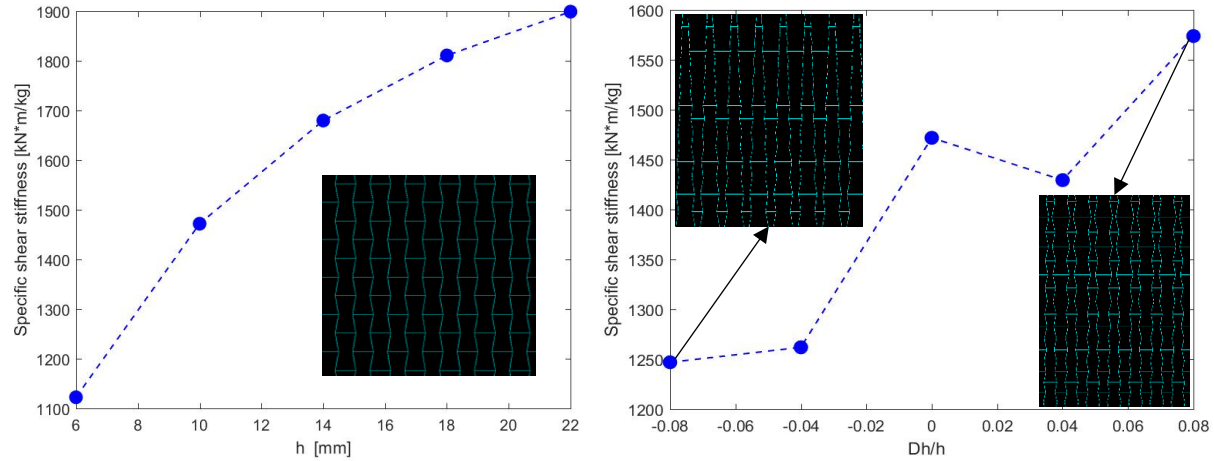

Figure 7.22: *Specific shear stiffness in function of the base edge and the base edge gradient.*

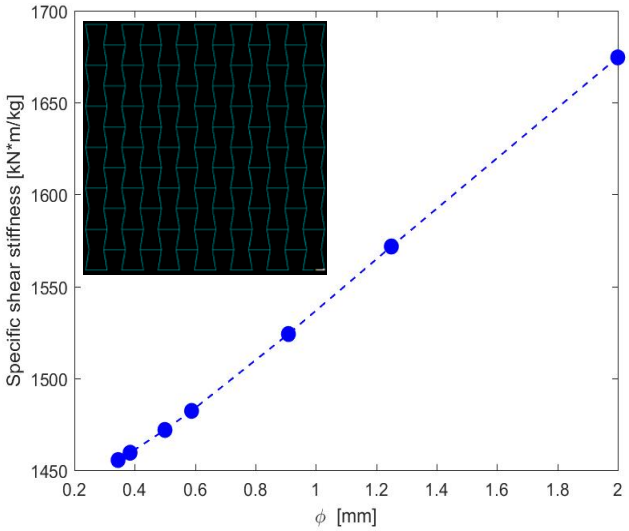

Figure 7.23: *Specific shear stiffness in function of the beam diameter.*

Also, for these results, the consistency between the results which are related to each other is easily checked. What is really surprising is the trend peak in the left graph of figure 7.20 which means that for auxetic structures with angles between -5° and -10° the specific shear stiffness is the highest possible. This could lead to interesting applications requiring a lightweight frame with relatively high shear stiffnesses.
The outputs in figure 7.21 show another specific shear modulus peak when dealing with aspect ratios between 1.2 and 1.4. However, this peak is mainly due to density trend which is increasing more than the shear modulus in the last analyses as shown in figure 7.24.

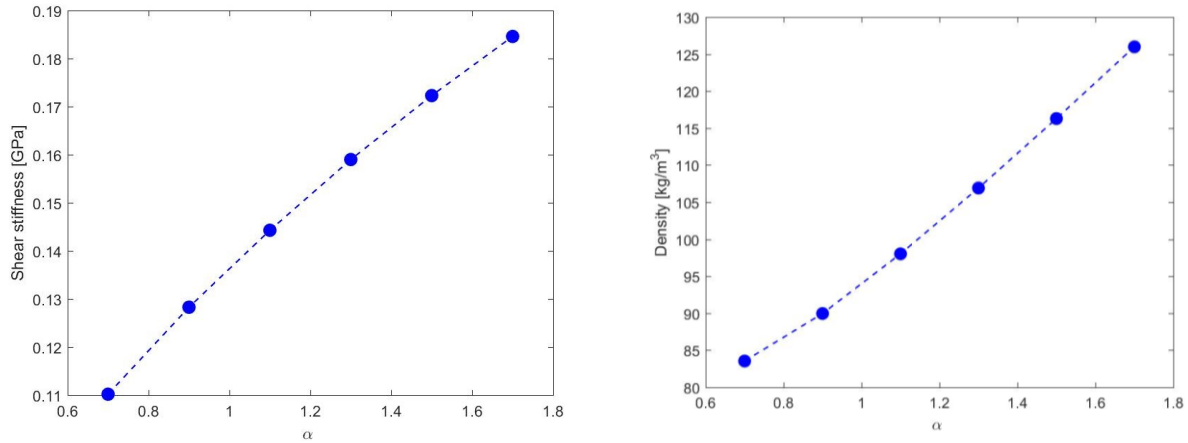

Figure 7.24: *Shear modulus and density in function of the aspect ratio.*

Furthermore, both the angle and the base edge length have a significative influence whereas the other two parameters are affecting results to a lesser extent.

The third set of results displayed below are referring to the specific shear modulus characterizing the lattice when it is loaded along the plane y-z.

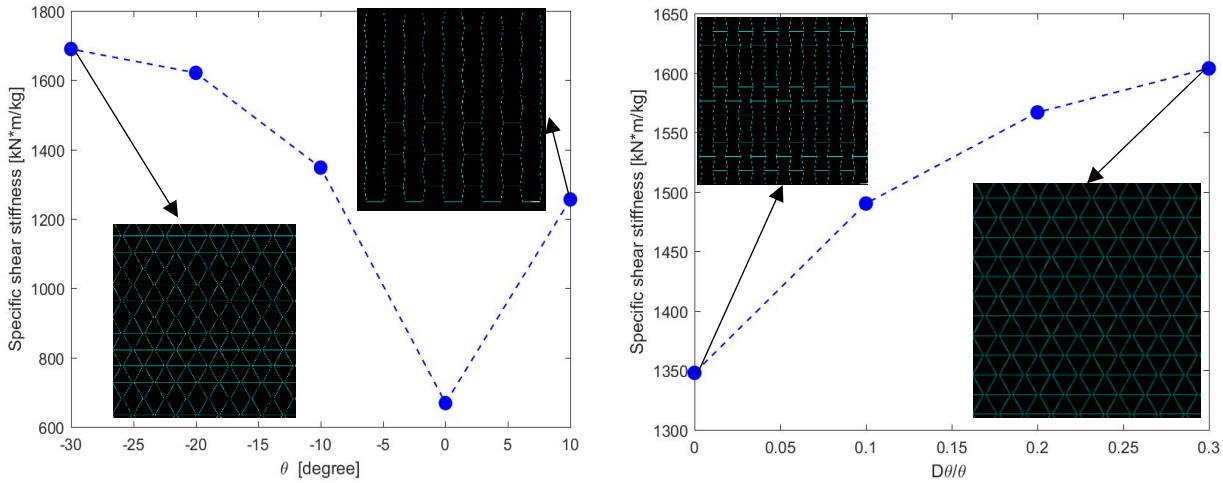

Figure 7.25: *Specific shear stiffness in function of the angle and the angle gradient.*

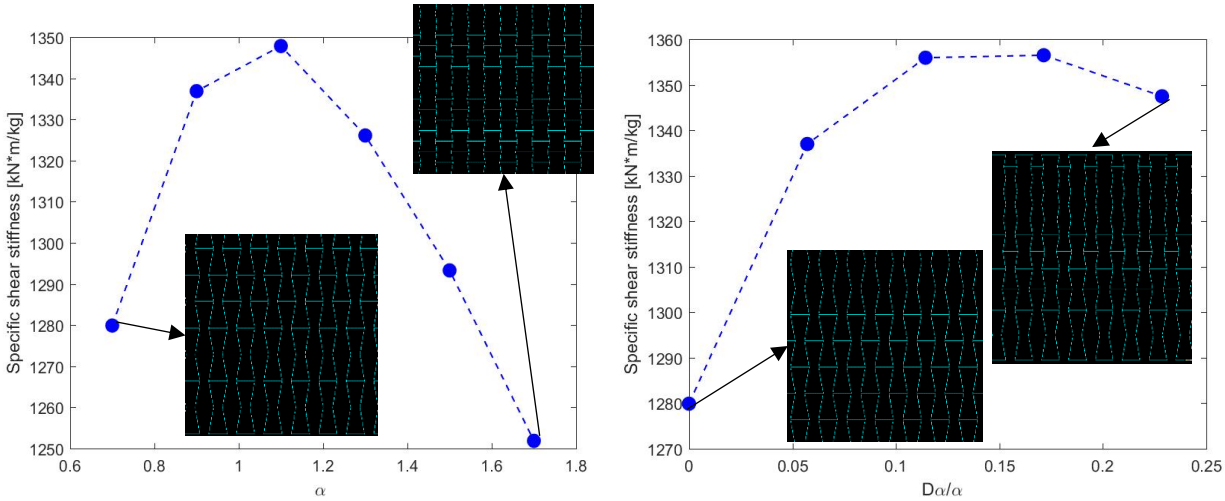

Figure 7.26: *Specific shear stiffness in function of the aspect ratio and the aspect ratio gradient.*

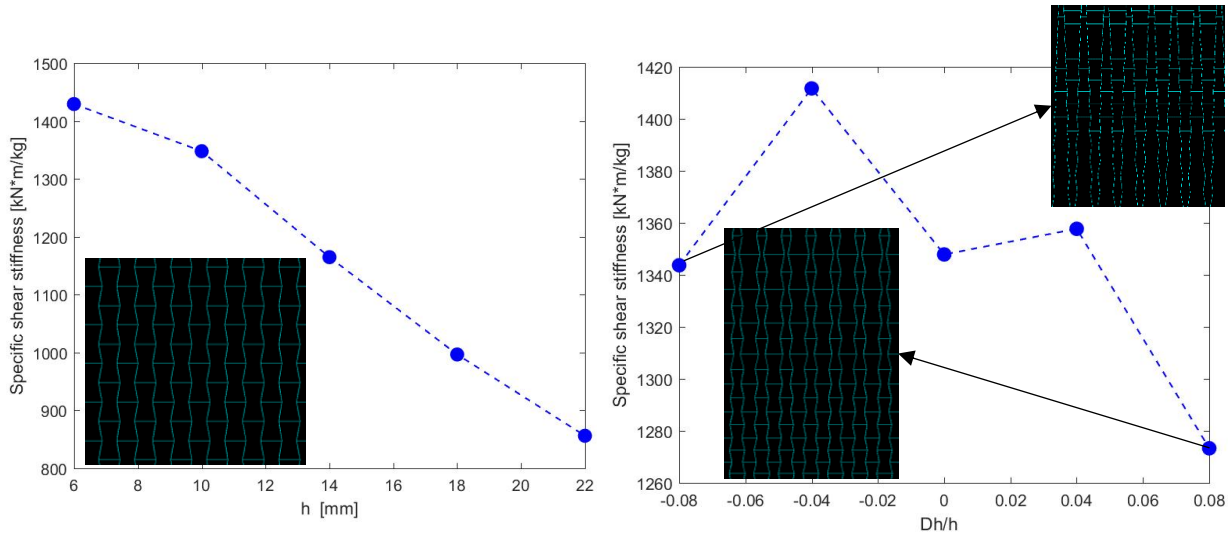

Figure 7.27: *Specific shear stiffness in function of the base edge and the base edge gradient.*

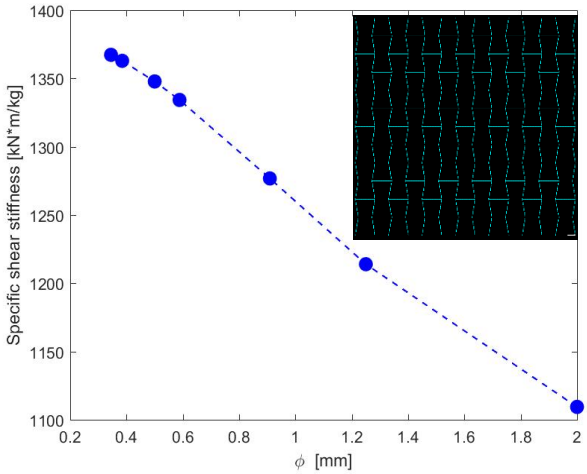

Figure 7.28: *Specific shear stiffness in function of the beam diameter.*

Likewise the previous two analyses, the consistency between the outputs is evident. Moreover, once again the angle and the side edge length are the more influencing variables. What is unnatural is the specific shear modulus trend in function of the beam diameter: increasing the latter, the former decreases. Looking at the figures below it is possible to understand that this result is a consequence of the poor diameter influence on the shear stiffness which is increasing as shown in figure 7.29.

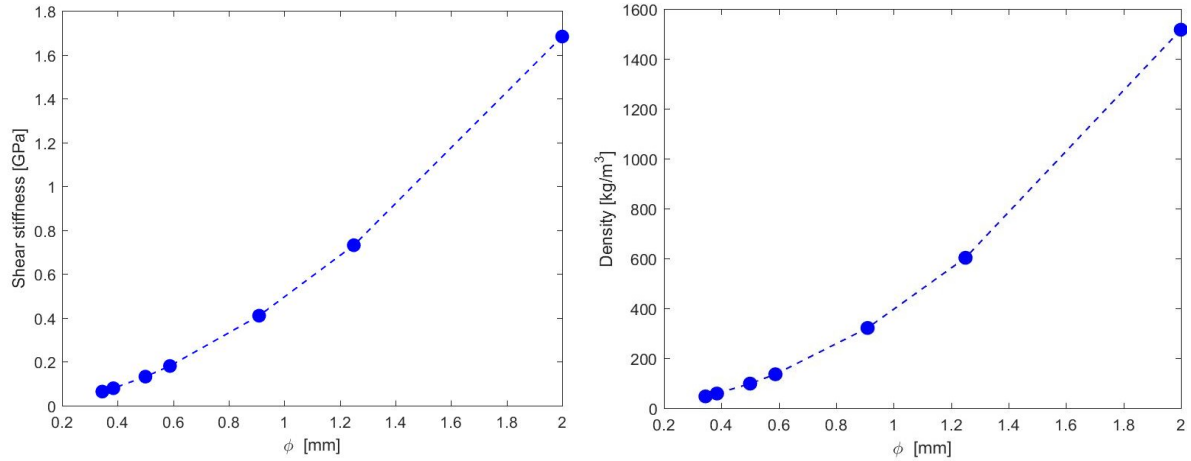

Figure 7.29: *Shear modulus and density in function of the beam diameter.*

However, the density has a steeper increase and thus the resulting specific shear modulus presents a decreasing trend.
In conclusion, in order to compare the trends of the three specific shear modulus and understand better the influences of the parameters, summary graphs are exposed in the next page. They show on the y axis the ratio between the stiffness and its maximum value for each case and on the x axis the value of the parameter whose effect is being analysed.

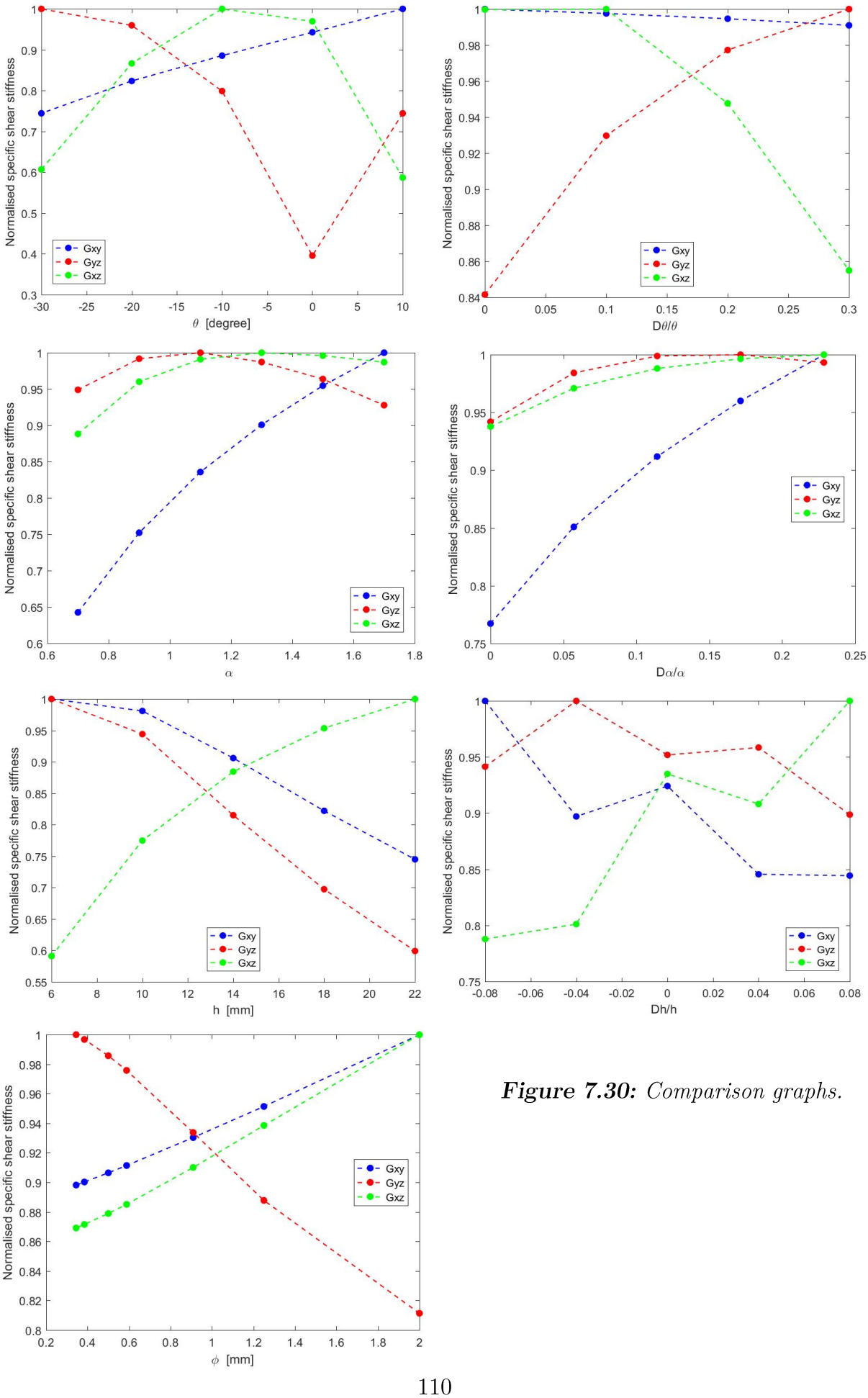

Figure 7.30: *Comparison graphs.*

Considering all the graphs in figure 7.30, it is possible to draw some conclusions.
Th influence of the beam diameter is small when measuring the specific shear stiffness and that is because the density is highly affected by the beam diameter while the shear stiffness goes with the second power of it as shown in equation (7.3).

$$\gamma = \chi \frac{T}{GA} \tag{7.3}$$

where "γ" is the shear strain, "T" is the shear force, "G" is the material shear modulus, "A" is the area of the cross-section and "χ" is the shear factor. The shear factor is dimensionless, so if the force is steady and the material is set, the deformation is inversely proportional to the second power of the diameter of the beam.
Furthermore, looking at the graph displaying the base edge length gradient results the fluctuation beforehand described is noticeable.
The most influencing parameters for the three cases are the angle and the base edge length.

7.3. Elastic energy absorption test

It is reminded that the elastic SEA tests have been run only along the z directions iteratively changing the value of the seven parameters mentioned in chapter 5.
All the results shown below are displayed by trends which describe the stress-strain curve and the relationship between the specific elastic SEA and the changing parameter.

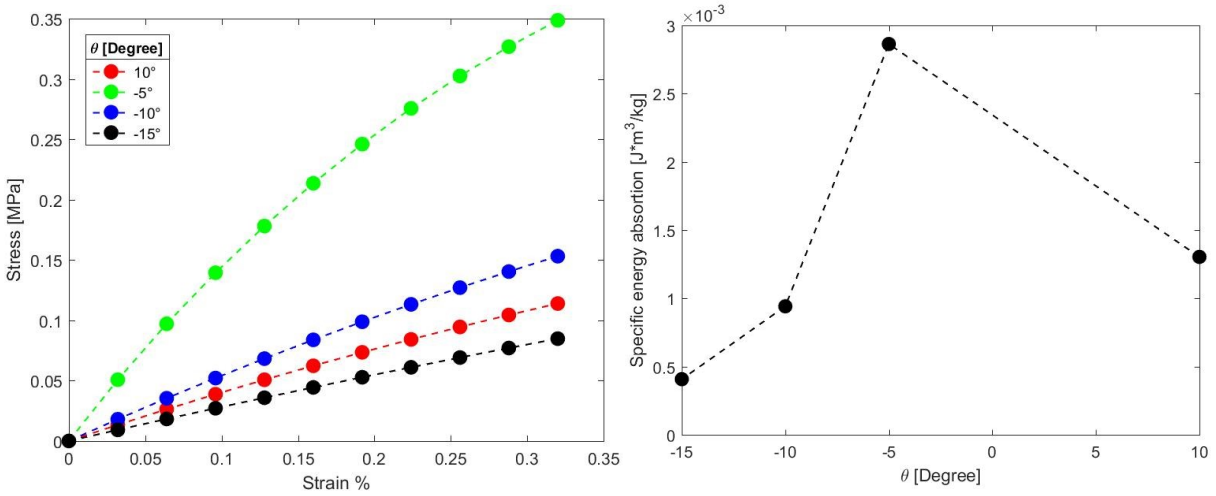

Figure 7.31: *Stress-strain relationship for different angles on the left and elastic SEA in function of the angle on the right.*

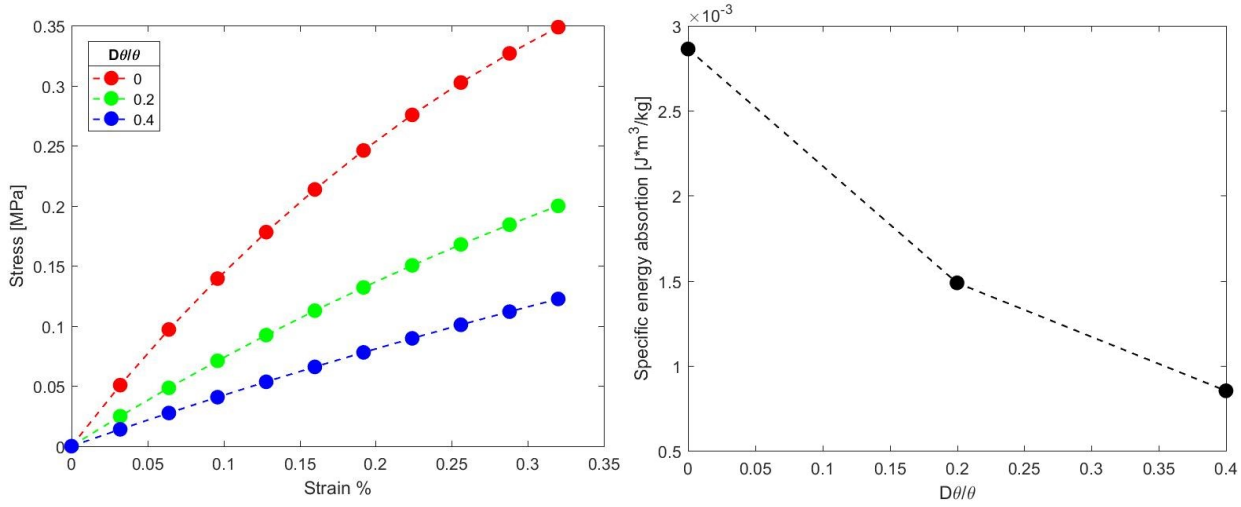

Figure 7.32: *Stress-strain relationship for different angle gradients on the left and elastic SEA in function of the angle gradients on the right.*

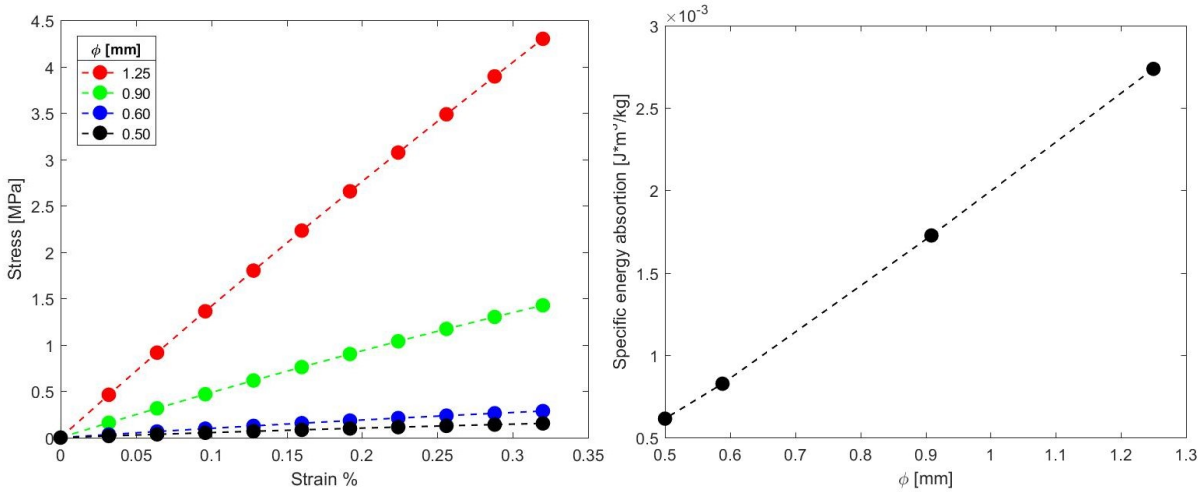

Figure 7.33: *Stress-strain relationship for different beam diameters on the left and elastic SEA in function of the beam diameter on the right.*

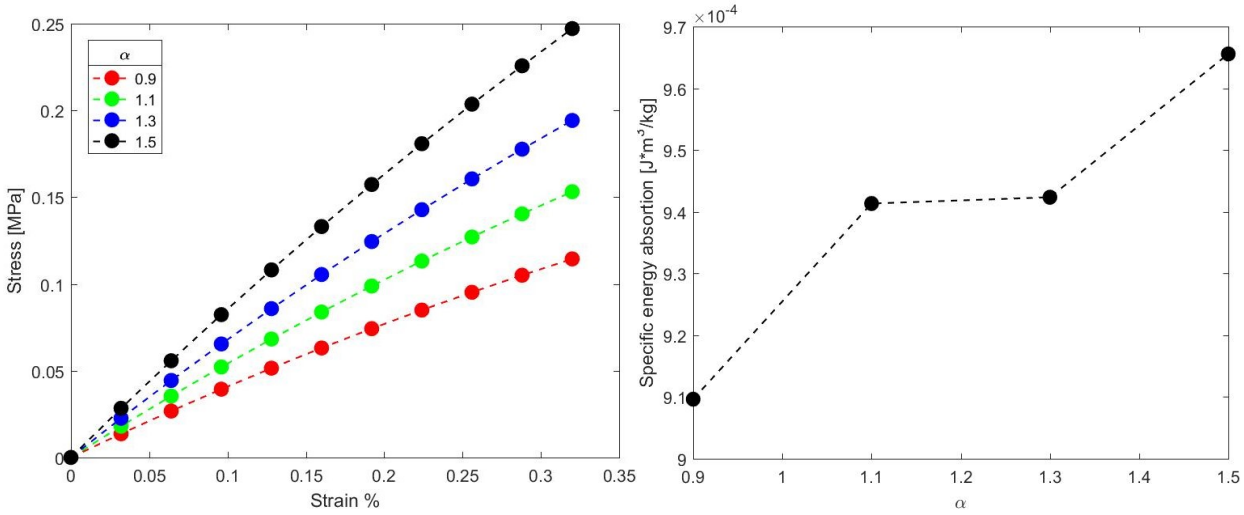

Figure 7.34: *Stress-strain relationship for different aspect ratios on the left and elastic SEA in function of the aspect ratio on the right.*

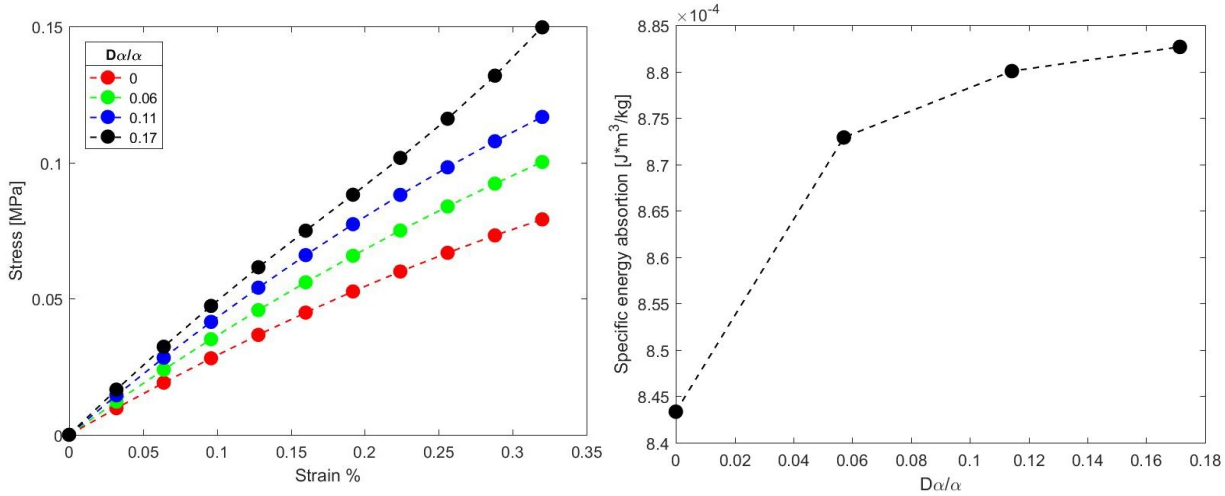

Figure 7.35: *Stress-strain relationship for different aspect ratio gradients on the left and elastic SEA in function of the aspect ratio gradient on the right.*

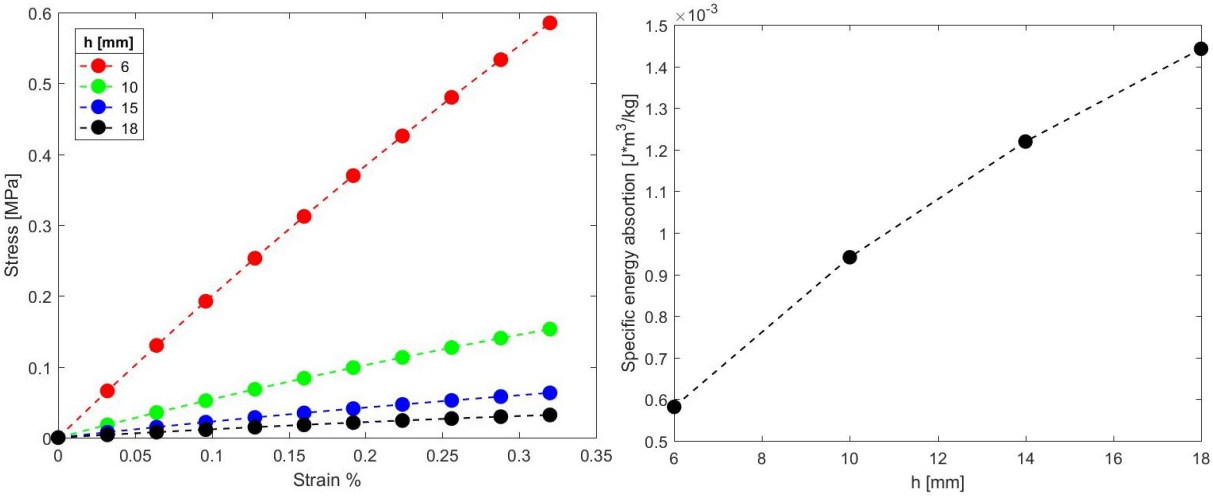

Figure 7.36: *Stress-strain relationship for different base edges on the left and elastic SEA in function of the base edge on the right.*

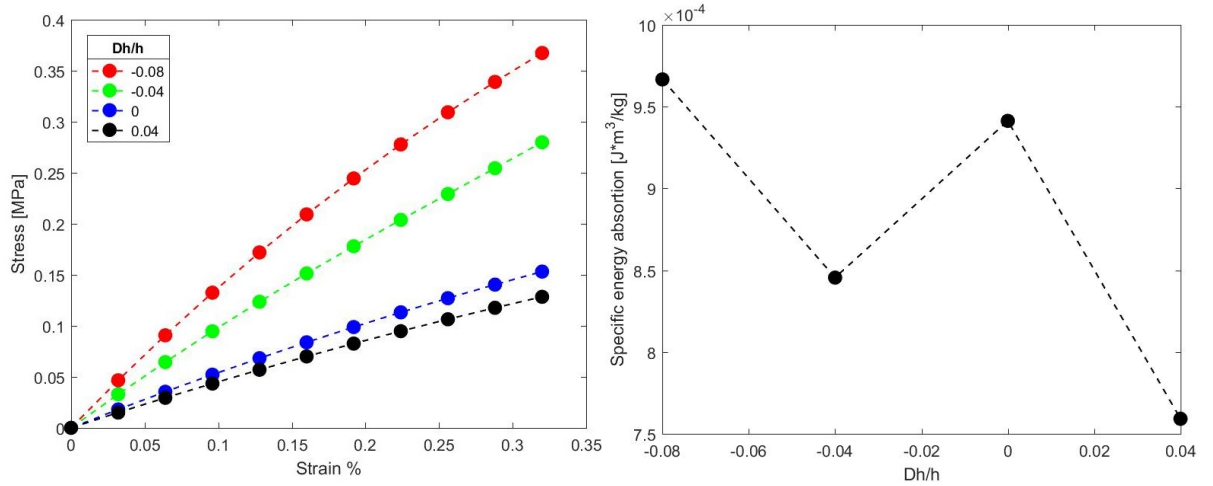

Figure 7.37: *Stress-strain relationship for different base edge gradients on the left and elastic SEA in function of the base edge gradient on the right.*

The majority of the specific elastic energy absorptions has been determined by integrating the compressive curve over 0 and 0.25% because for this strain value almost all the structures are approaching the yielding strength. However, for stiffer models such as when the beam diameter is increased, when the angle approaches zero and when the "H" is 6 mm, the stresses are higher for smaller strains and the integration threshold is 0.2%. Nonetheless, the SEA output is still noteworthy because sometimes the lattice can still absorb more energy even if it enters in the plastic regime earlier.

Thereby, when considering the results in order to give a final solution this concept will be taken into account because, on the one hand, a stiffer lattice could absorb more elastic energy in the elastic region of the curve, on the other hand, it shows stresses which overcome the yielding strength for lower strains risking an excessive reduction of the elastic regime. This could lead to the disadvantage of designing a lattice which consist

of very small elastic region and it is likely going to show plastic residual strains even during normal working conditions. Thus, too stiff lattices have not been considered and a trade-off has been accepted.
Furthermore, another important fact to point out is that when the structure exhibits an angle close to 0°, it begins to behave as a stretching-dominated frame thus being much more rigid but absorbing less plastic energy during the collapse. However, even if in this project the plastic energy absorption is not measured, the auxetic bending-dominated lattice studied has been designed this way because bending-dominated frames present higher plastic energy absorption due to their struts mobility. That is, they are suitable for generating a safety barrier to object impacts which is able to absorb the more energy possible. Consequently, the lattice cannot be stretching-dominated and for angles between -5° and 5° figure 7.31 must not be considered.
All in all, it can be stated that the structure is much more energy efficient when the angle approaches -5°, when the beam diameter, the base edge length and the aspect ratio are as high as possible. Nevertheless, it seems appropriate to specify that these results are deeply affected by the density trend. So, hereunder the volume SEA and the mass SAE are set out.

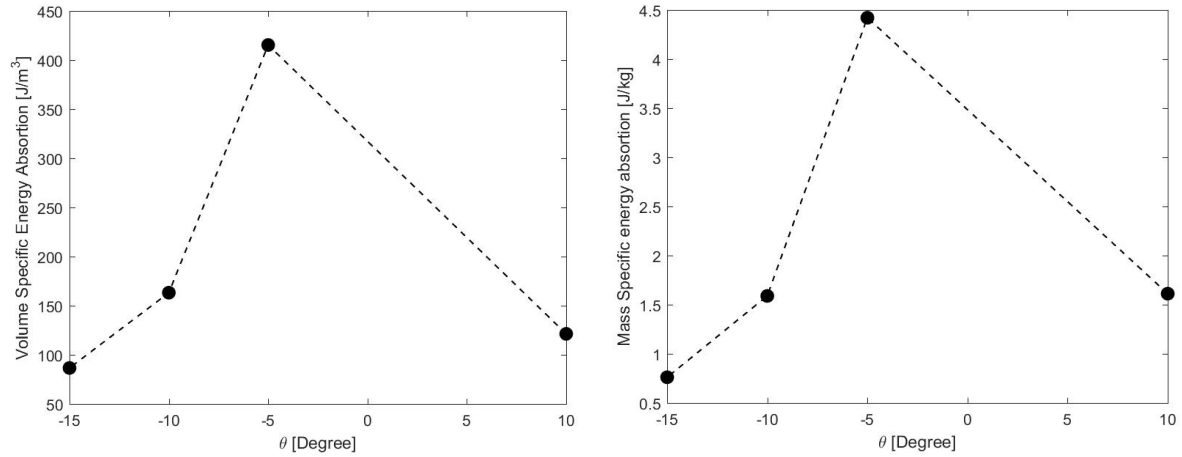

Figure 7.38: *Elastic volume and mass SEA in function of the angle.*

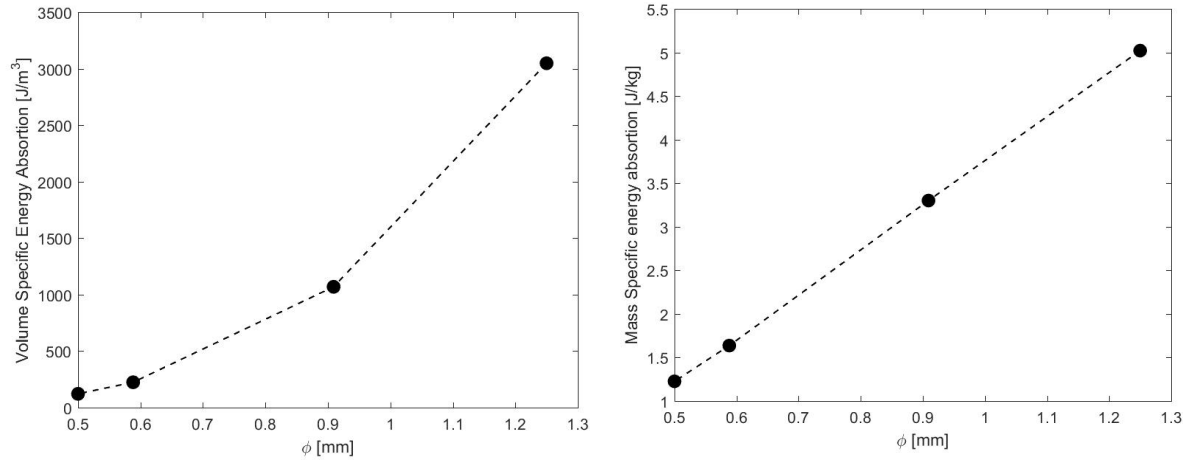

Figure 7.39: *Elastic volume and mass SEA in function of the beam diameter.*

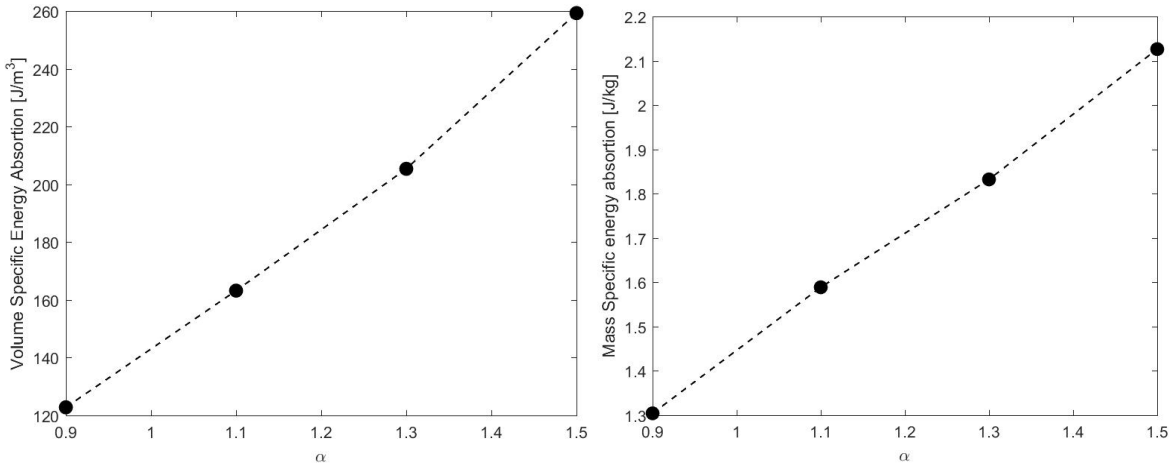

Figure 7.40: *Elastic volume and mass SEA in function of the aspect ratio.*

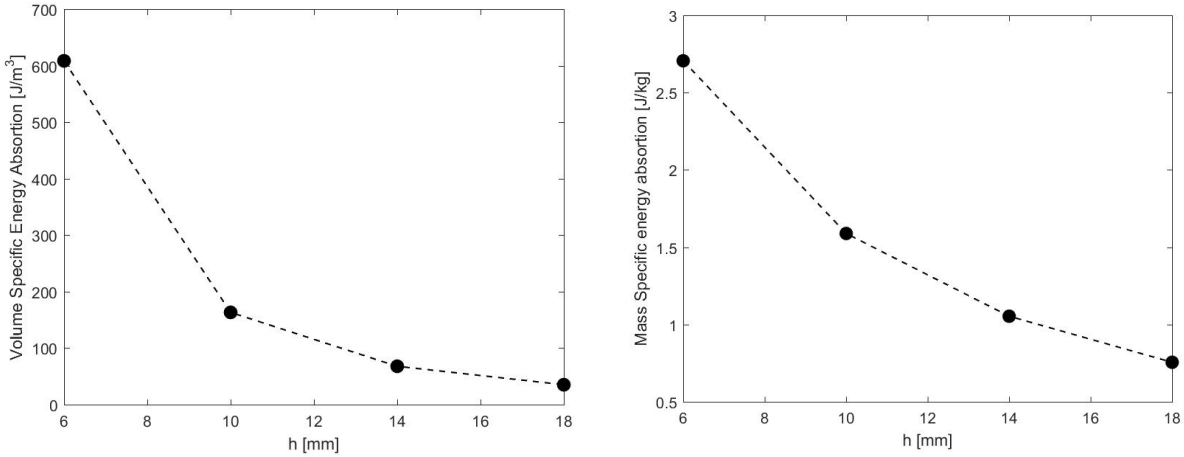

Figure 7.41: *Elastic volume and mass SEA in function of the base edge length.*

As it is highlighted by figure 7.41 in both graphs, the SEA is actually decreasing when the "H" is growing but this effect is completely reversed when taking into account density. In fact, "H" is variable which affects the density much more significantly than the energy absorption. All other graphs are consistent with the previous one.
Another relevant observation is that all the stress-strain curves showed are all consistent with the homogenized Young's modulus found in the compression tests.
Downstream from all these results, what is clear is that generally speaking having a high Young's modulus leads to high elastic energy absorption but in some cases, density can change the results when dealing with specific SEA. Plus, there is a stiffness threshold beyond which the elastic regime is reduced too much, and the elastic energy starts to decrease.
Since this last lattice mechanical property is very important for its application as a Rolls-Royce acoustic liner, it is necessary to compare the effects to each other in order to discover what are the "master" and "slave" variables. Therefore, in figure 7.42 and 7.43

comparison graphs are showed. The x axis indicates the percentage of parameter variation so as to get the relative influence of each geometric variable.

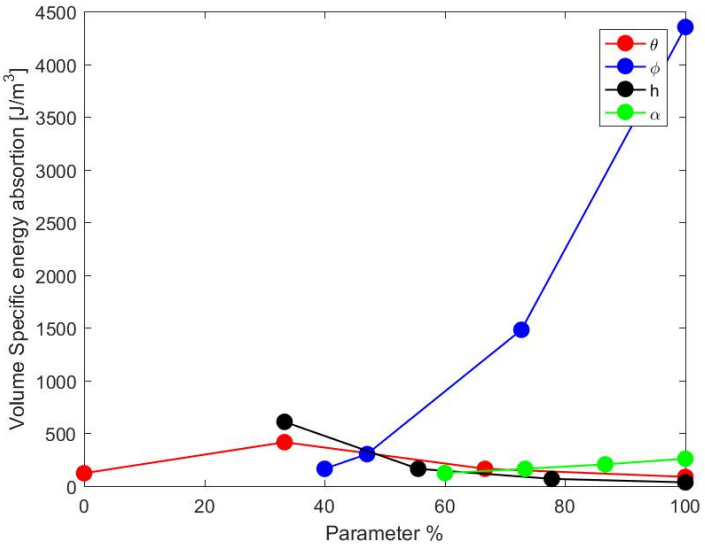

Figure 7.42: *Volume SEA comparison graph.*

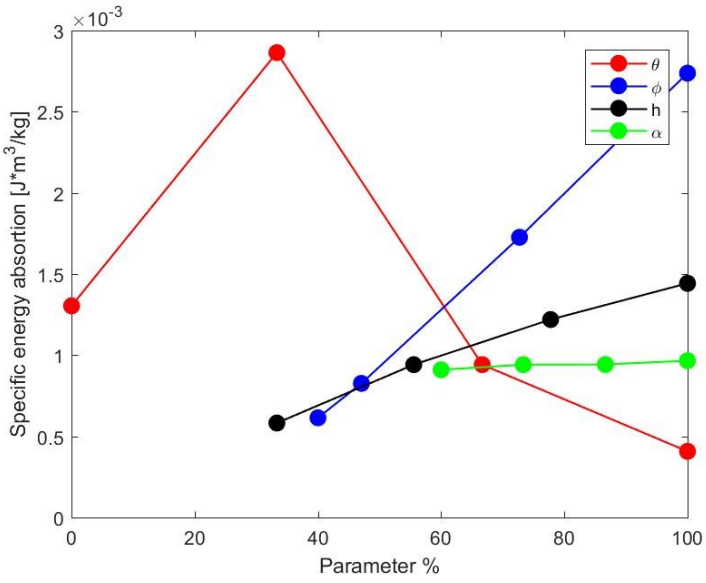

Figure 7.43: *Density SEA comparison graph.*

Observing the differences between these two graphs, it becomes clear how important is the density effect for the diameter and for the base edge length which are also the two most important factors to set for the final lattice design.

7.4. Substructuring investigation

From a modeling point of view the results are very interesting and they could really represent a starting point for deeper and more systematic investigations of the static condensation obtained by the substructuring.
It is reminded that three different way of modeling have been considered to emphasize substructuring advantages and disadvantages: classic approach, single-superelement approach and multiple-superelement approach.
Also, no physics observations and findings have to be drawn from the Young's modulus outputs, because the yielding strength is not taken into account. As matter of fact this results are only valid from modeling perspective.
Figure 7.44 shows the stress-strain relationship for the three cases.

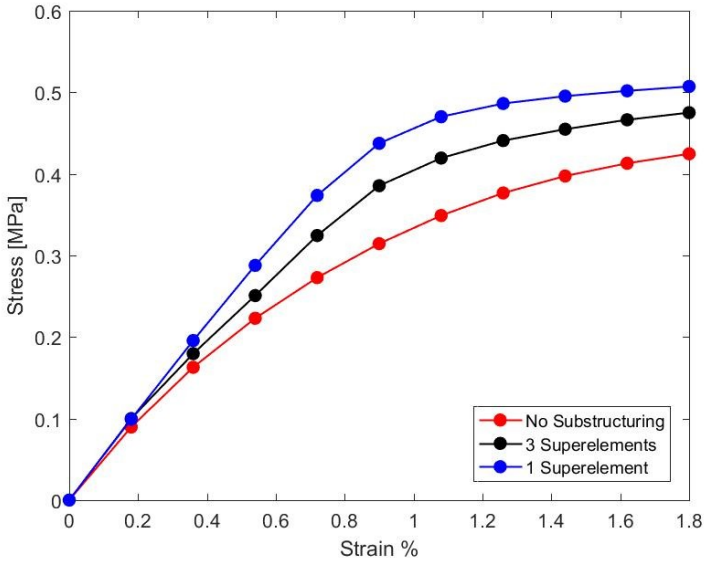

Figure 7.44: *Stress-strain curves.*

Unfortunately, Substructuring tend to increase the stiffness of the structure of the 23% on average. This is an expected result because the number of nodes is enormously decreased due to the single-superelement approach and thus the degree of freedom of the frame are reduced determining a stiffening effect.
However, the compressive curve trend is similar to the right one and using several smaller superelements could help approaching even more the "red" curve: with only three the stiffening effect is about 12%.
Therefore, these results show that, increasing the number of superelements, there is a saturation threshold beyond which the output will be the same of a classic modeling approach.
From the same analyses other factors have been investigated. Among them, time concerning results are considerably attractive as displayed in figure 7.45.

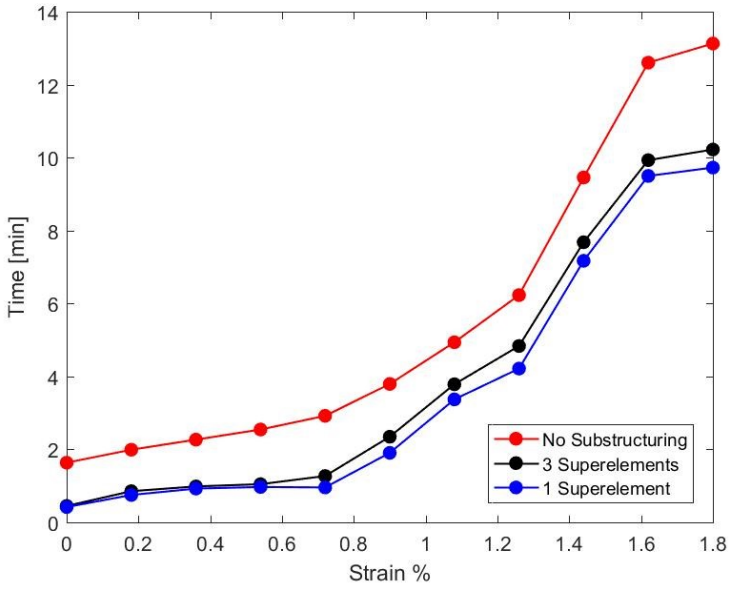

Figure 7.45: *Time-strain relationship.*

From a time point of view, it is noticeable that the presence of the single superlement can always reduce the solution time (up to 40% time reduction for high strains). In fact, time reduction due to substructuring is much more effective in the large deformations region when non-linear geometry is taken into account and equilibrium iterations are needed.

When using three superlements the analysis takes almost the same time required for a single superelement analysis but as already seen the accuracy is much higher. This is an extremely relevant finding which, if deepened, could bring to a surprising reduction of time associated with high simulation precision. Quantitatively speaking, for a 1.6% strain the reduction time for single-superlement approach is about 33% on a 13 minutes analysis whereas it is 30% for the multiple-superelement approach.

In figure 7.46 there is graph which could help explaining why the substructuring procedure significantly reduces the simulation time and the computational resources needed.

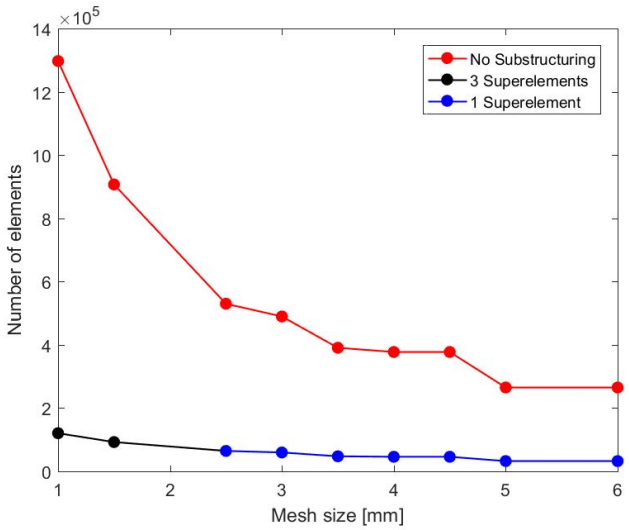

Figure 7.46: *Number of elements-mesh size relationship.*

Figure 7.46 is extremely relevant inasmuch as it points out that substructuring procedure provides a model which so much computationally lighter than the classic approach. In fact, it is possible to observe that changing the mesh size, and consequently the number of elements constituting the lattice, the number of effective elements used to run the simulation is almost unaltered. That is, the substructuring modeling approach is almost insensitive to the number of elements used and it increases a little bit just because of the upper row which is modeled with the classic approach. Therefore, the result is more computational cost-effective model.
Obviously, the difference in the number of elements between the single-superelement model and the multiple-superelement one is always equal to two elements and it is not recognizable.
Furthermore, another substantial observation has to be done: the single-superelement approach has a huge limiting disadvantage which is the impossibility to create the superelement matrix when the superelement is too big and complex. That is, it is not possible to crate endless superelement. The size threshold depends on the computer resources and so it may vary from computer to computer. Figure 7.46 displays a threshold for less than one hundred thousand elements which corresponds to a mesh size equals to 2.5 mm. Fortunately, this problem is completely overcome by the introduction of several smaller substructures as shown by the three-superelements modeling approach.
The concepts hitherto highlighted are shown also in the graphs below costituting figure 7.47.

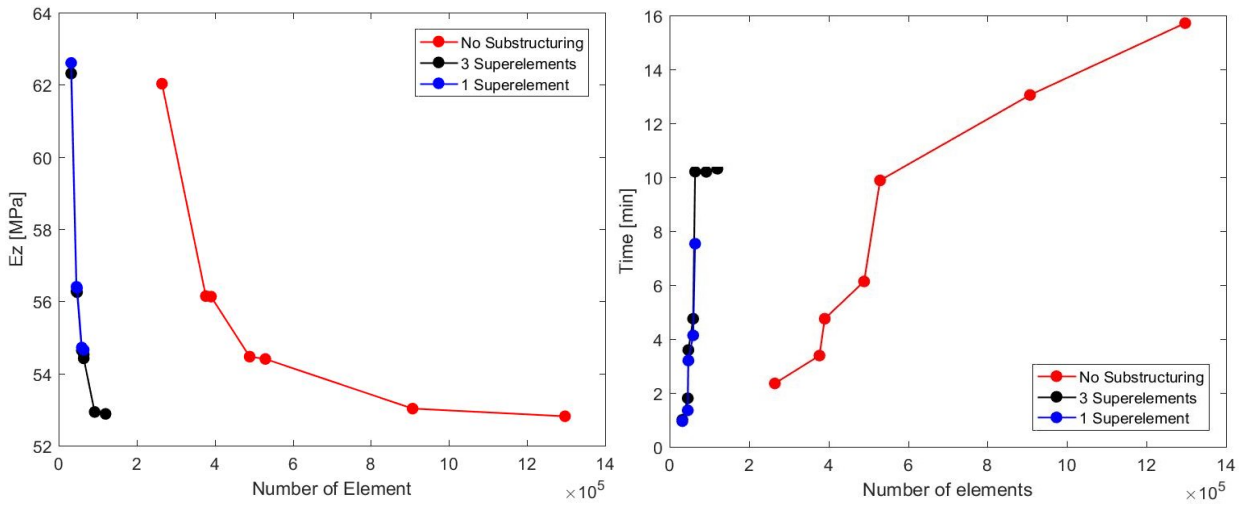

Figure 7.47: *Homogenized Young's Modulus-Number of elements relationship and Time-Number of elements relationship.*

In conclusion, it possible to state that:

- Substructuring tends to create a 23% stiffer model, but using appropriate number of superelements, which depends on the model, this issue is overcome;

- Substructuring allows the reduction of simulation time especially for large deformations and non-linear analyses and the time can be reduced up to the 35% of a classic approach simulation time;
- Substructuring is also an interesting solution from a computational resources point of view because it makes the model insensitive to the number of elements since they are all condensed into one bigger matrix. However, there is a maximum number of elements which can be condensed: this issue is overcome with multiple-superelements approach.

In the end, this approach is really appropriate for periodic structure like our lattice so it is an option that should always be taken into account. However, since this structure is completely new and there are no reference data in literature, accuracy has been preferred to speed when modeling the frame.

8.Proposed lattice

In connection with the results obtained and explained in the previous chapter, a final "optimised" structure has been proposed as a possible high-SEA in the elastic regime. It has to be underlined that the proposed frame is not exactly the best one because there has not been methodical optimization process.
In effect, the solution is also supposed to provide a high plastic energy absorption because, as already said, it is a bending-dominated auxetic lattice. However, this advantage has not been analysed so there is no evidence of it and should be experimentally proved.
The main Rolls-Royce requirements where high energy absorption, lightweight lattice and a structure height stretching from 30 mm to 35 mm. Also, since the acoustic liner is placed in a set volume, in order to avoid anomalous contacts between the lateral surfaces wherein the lattice is located and the lattice itself, an auxetic behaviour has been preferred. Furthermore, this last property has been mainly chosen because it usually shows considerable capabilities from an absorption energy point of view.
Moreover, other untold but natural requirement is that the frame must present sufficiently high elastic modulus and shear stiffness modulus.
All parameters influences considered, the final solution given is shown in figure 8.1.

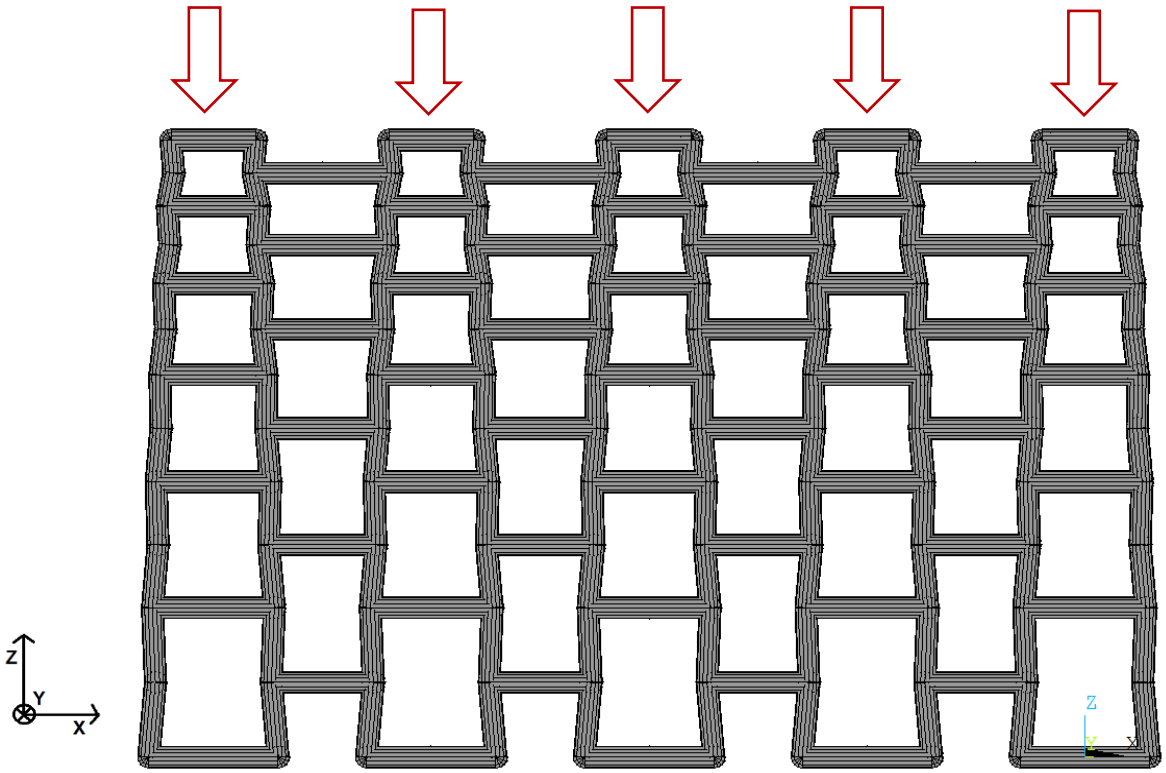

Figure 8.1: *x-z surface of the proposed high SEA lattice. Red arrows indicate the loading direction of the frame.*

A three-dimensional view is shown in figure 8.2.

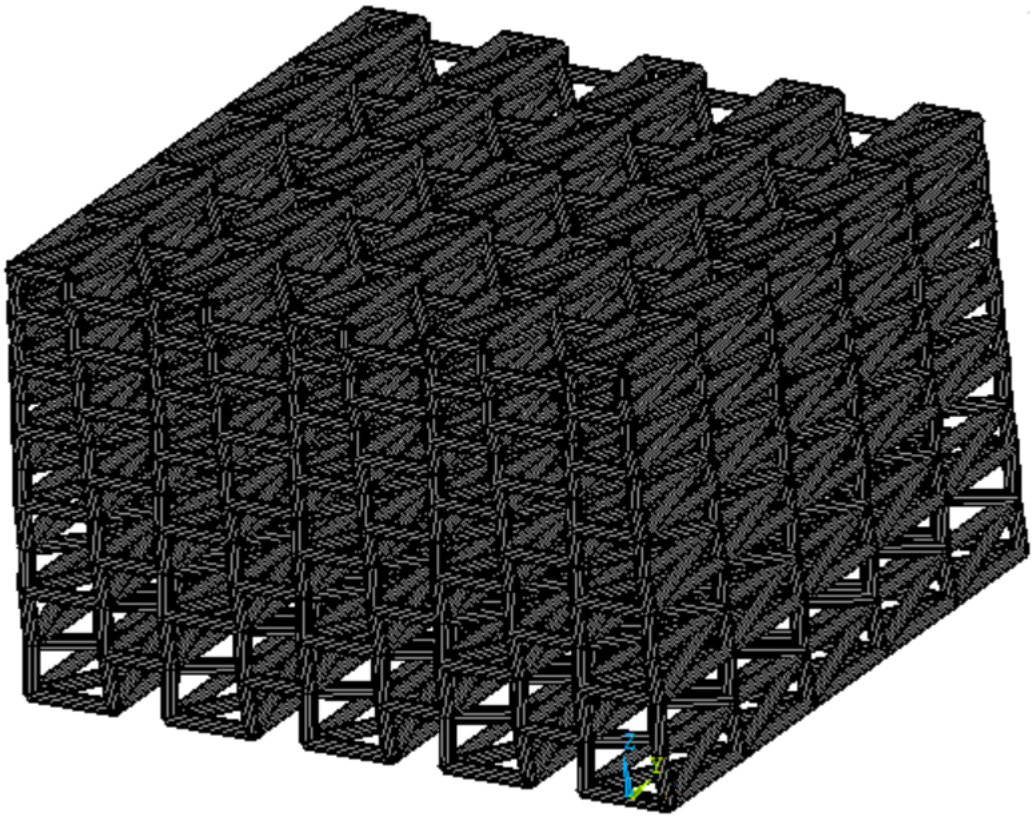

Figure 8.2: *Three-dimensional view of the proposed high SEA lattice.*

From the previous images, especially from figure 8.1, it is possible to check that the lattice consists of the following parameters:

- θ_1: -5°;
- H_1: 7 mm;
- α_1: 1.7;
- φ: 1.2 mm;
- CH: 10 mm;
- $D\theta/\theta_1$: 0.4;
- DH/H_1: -0.05;
- $D\alpha/\alpha_1$: 0.12;
- $Delay\_\theta$: 35%;
- NR: 6;
- NC: 5;

The angle, the diameter and the aspect ratio has been set at the respective values which showed the maximum specific energy absorption. On the contrary, the base edge length

chosen is relatively small for two reasons. The first one is because if "H" is bigger than that the lattice height requirements are not satisfied since the lattice becomes more than 40 mm height; the second motivation is because the real effect of increasing this factor is decreasing the energy absorption as said in paragraph 7.3. Thus, setting that value the only disadvantage is an augmented density which is fine if it is considered that the structure is already very lightweight.
Furthermore, gradients are introduced in order to increase the parameters influence on the SEA and to achieve the required lattice height.
Moreover, an angle gradient delay equal to 35% has been adopted so as to limit the angle growth along the z axis of the lattice, thus absorbing more energy. Therefore, the first two rows share the same angle value of -5°.
Moreover, since the frame is relatively stiff the yielding strength is overcome at a strain of 0.2% and thus the SEA has been calculated integrating over this range.
Figure 8.3 displays the stress-strain curve:

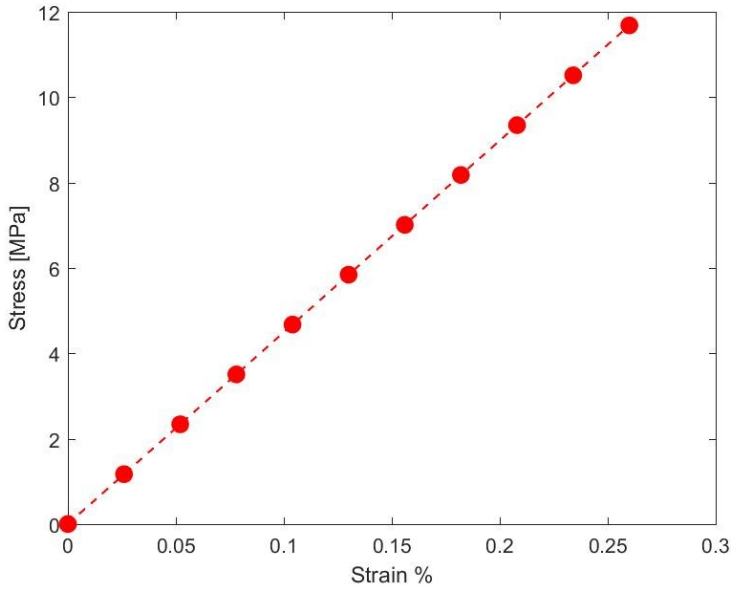

Figure 8.3: *Stress-strain curve for the proposed high SEA lattice.*

The compression, shear and SEA tests has been carried out also on this lattice and the outputs below have been derived:

E_z/ρ $[\frac{kN \cdot m}{kg}]$	E_y/ρ $[\frac{kN \cdot m}{kg}]$	E_x/ρ $[\frac{kN \cdot m}{kg}]$	G_{xy}/ρ $[\frac{kN \cdot m}{kg}]$	G_{yz}/ρ $[\frac{kN \cdot m}{kg}]$	G_{xz}/ρ $[\frac{kN \cdot m}{kg}]$	SEA $[\frac{J \cdot m^3}{kg}]$
2724	13960	76	3456	1320	1195	$4.5 \cdot 10^{-3}$

This lattice is meant to be manufactured via additive manufacturing because it is the only fabrication technique which is able to produce a so complex lattice in a reduced amount of time. No inner finishing is required because the roughness is not a problem for the functionality of the acoustic liner. The material is still stainless steel 316L thus it can be printed either with EBM or SLM machines. However, since Rolls-Royce uses EBM the specimen will be manufactured with this technique. Unfortunately, the geometrical complexity of the lattice doesn't allow to define a preferred building orientation on the platform machine and there is the need to use appropriate software such as "MAGICS" which could automatically define the best orientation in order to avoid supports and to ensure the DFAM rules.
From a fabricating time point of view, the best option is to orientate the lattice along the shortest dimension which is the z one. However, this observation is not so relevant since the production time is related only to a single specimen and not to a series production.

9.Conclusions

The main objective of this work has been designing and parametrically analysing a new forefront kind of lightweight 3D metamaterial which is completely tailorable to the costumer's needs. In fact, the metalattice defined has a massive design space which can allow the designer to change its morphology tuning its mechanical properties on the basis of the functionality required. Furthermore, a benchmark model has been set with auxetic behaviour and geometric variables gradients. On the one hand, having negative Poisson's Modulus, the solid can fulfil peculiar functionalities shrinking inward when compressed and, as shown by this thesis, it can absorb high deformation energy. On the other hand, a high level of gradients control along the loading direction of the lattice helps customizing its properties. Flatwise compression, shear and elastic energy absorption studies have been carried out with a homogenised equivalent material approach. Results has shown that each parameter has a different influence depending on the loading direction and on the type of test. In that regard, it has been noticed that the angle and the beam diameter are the most influencing geometric factors when speaking of the specific elastic energy absorption. As a matter of fact, the diameter is more effective on the compression and energy absorption analyses than on the shear ones. This latter mechanical property is considerably affected by the base edge length parameter because of its relevant influence on the density trend due to the size effect.
Consequently, downstream from these results a final high specific elastic energy absorption has been derived and proposed to Rolls-Royce as a valid replacement of the honeycomb material they are currently relying on.
Undoubtedly, the lattice designed fixes some functional problems such as the high moisture retention while providing an attractive alternative when considering the specific elastic energy absorption. However, the proposed solution still shows some disadvantages such as a mediocre elastic modulus and a low shear modulus if compared to other frames.
The other important aim of the project was to find out a modeling approach which could effectively reduce the computational complexity associated with this kind of periodic lattices which may be constituted by millions of beam elements. Moreover, the other major concern, from the modeling point of view, is the time-efficiency of the simulation. As stated throughout the whole thesis, numerical investigations can be very computationally expensive and time consuming, especially when geometrical non-linearities and contact elements are considered as required by the elastic energy absorption analysis. Thus, a remarkable solution has been sought in the "Substructuring" function provided by ANSYS. It has been proved that it can reduce the simulation time up to thirty percent of the one needed for a classic modeling approach, and that it dramatically reduces the number of elements solved in the solution environment thus minimizing the computer resources used. Unfortunately, there are two main disadvantages: a limited superelement matrix size which confines its maximum dimension

and almost a twenty percent stiffening effect. Results demonstrated that the former issue is completely overcome by relying on a multiple-superelements modeling approach, each of them smaller than the dimension threshold. On the contrary, the latter can only be reduced by increasing the number of superlements while decreasing their size.
In conclusion, it is possible to state that both initial purposes have been achieved and, since really appealing results have been obtained, both of them deserve to be further deepened.

Bibliography

[1] Helou M. and Kara S., 2018, Design, analysis and manufacturing of lattice structures: an overview. *International Journal of Computer Integrated Manufacturing*, School of Mechanical and Manufacturing Engineering, The University of New South Wales, Sydney, Australia.

[2] Bührig-Polaczek A., Fleck C., Speck T., Schuler P., Fischer S.F., Caliaro M. and Thielen M., 2016, Biomimetic cellular metals - using hierarchical structuring for energy absorption. *Bioinpiration & Biomimetics*, 11(4):045002, Germany.

[3] Thielen M., Speck T. and Seidel R., 2013, Viscoelasticity and compaction behaviour of the foam-like pomelo (citrus maxima) peel. *Journal of Material Science*, 48(9):3469-3478.

[4] Gibson L.J. and Ashby M.F., 1988, Cellular Solids: Structure and Properties, Cambridge University Press.

[5] Li Q.M., Magkiriadis I. and Harrigan J.J., 2006, Compressive Strain at the Onset of Densification of Cellular Solids. *Journal of cellular plastics,Volume 42*, School of Mechanical, Aerospace and Civil Engineering, The University of Manchester, Manchester, UK.

[6] Deshpande V.S., Ashby M.F. and Fleck N.A., 2001, Foam topology bending versus stretching dominated architectures. *Acta Materialia* 49 (2001)1035-1040, Cmbrifge University, Department of Engineering, Cambridge, UK.

[7] Ashby M.F., 2005, The properties of foams and lattices. *Philosophical transaction of the royal society*, University of Cambridge, Cambridge, UK.

[8] Pellegrino S. and Calladine C.R., 1986, *International Journal of Solids and Structures*.

[9] Kshertrimayum S.R., 2004, A brief intro to metamaterials. *IEEE potentials.*

[10] Lee J.H., Singer J.P. and Thomas E.L., 2012, Micro-/Nanostructured Mechanical Metamaterials. *Advanced Materials.*

[11] Zadpoor A., 2016, Mechanical Metamaterials. *Materials Horizons*, Department of Biomechanical Engineering, Delft University of Technology, Delft.

[12] Evans K.E.,1991, Tailoring the negative Poisson's ratio. Chem. Ind. 20, 654-657.

[13] Wan H., Ohtaki H., Kotosaka S., Hu G., 2004, A study of negative Poisson's ratios in auxetic honeycombs based on large deflection model. *European Journal of Mechanics A/Solids* 23, 95-106, Department of Mechanical Engineering, Saitama University, Saitama-kenn, Japan.

[14] Barchiesi E., Spagnuolo M. and Placidi L., 2017, Mechanical metamaterials: a state of the art. *Journals SAGE.*

[15] Hou Y., Tai Y.H., Lira C., Scarpa F., Yates J.R. and Gu B., 2013, The bending and failure of sandwich structures with auxetic gradient cellular cores. *Elsevier.*

[16] Lee S., Barthelat F., Hutchinson J.W. and Espinosa H.D., Dynamic failure of metallic pyramidal truss core materials – experiments and modelling. *International Journal of Plastics.*

[17] ANSYS Technology Guide.

[18] Salit V. and Weller T., On the feasibility of introducing auxetic behaviour into thin-walled structures. *Acta materialia, Elsevier.* Department of Aerospace engineering, Technion-Israel.

[19] ANSYS Advanced Analysis Techniques.

Annex

Hereunder, the most relevant scripts used are set out.

- ***MACRO "CELL"***

```
*CREATE,CELL
L1=ARG1/ARG2
*AFUN,DEG
TX=L1*COS(ARG3)
TZ=-L1*SIN(ARG3)
K,ARG6,ARG5,0,-ARG1/2
K,ARG7,ARG5,0,ARG1/2
K,ARG8,ARG5+TX,0,(ARG1/2)-TZ
K,ARG9,ARG5+2*TX,0,(ARG1+AR18)/2
K,AR10,ARG5+2*TX,0,-(ARG1+AR18)/2
K,AR11,ARG5+TX,0,-ARG1/2+TZ
K,AR12,ARG5,ARG4,-ARG1/2
K,AR13,ARG5,ARG4,ARG1/2
K,AR14,ARG5+TX,ARG4,(ARG1/2)-TZ
K,AR15,ARG5+2*TX,ARG4,(ARG1+AR18)/2
K,AR16,ARG5+2*TX,ARG4,-(ARG1+AR18)/2
K,AR17,ARG5+TX,ARG4,-ARG1/2+TZ
*DO,J,ARG6,AR10
L,J,J+1
*ENDDO
L,AR11,ARG6
*DO,J,AR12,AR16
L,J,J+1
*ENDDO
L,AR17,AR12
*DO,J,ARG6,AR11
L,J,J+6
*ENDDO
*DO,J,ARG7,ARG8
L,J,J+5
*ENDDO
L,AR17,ARG6
L,ARG8,AR15
L,AR10,AR17
L,ARG9,AR16
*END
```

➢ ***MACRO "BONDING"***

```
*CREATE,BONDING
*IF,ARG3,GT,1,THEN
      *IF,ARG2,GT,1,THEN
            *DO,C,1,(ARG2-1)                    !ARG2=columns number
                  *DO,R,1,(ARG3-1)              !ARG3=rows number
                        *DO,J,1,ARG1            !ARG1=nodes number
                        *IF,J,EQ,3+(12+8*(ARG2-1))*(R-1),THEN
                        L,J,J+15+8*(ARG2-1)
                        L,J,J+21+8*(ARG2-1)
                        *ELSEIF,J,EQ,13+8*(C-1)+(R-1)*(ARG2-2)*8+20*(R-1)
                        L,J,J+15+8*(ARG2-1)
                        L,J,J+19+8*(ARG2-1)
                        *ELSEIF,J,EQ,9+(C)*8+(R-1)*(ARG2-1)*8+12*(R-1)
                        L,J,J+15+8*(ARG2-1)
                        *ELSEIF,J,EQ,9+((ARG2-1)*8+12)*(R-1)
                        L,J,J+15+8*(ARG2-1)
                        *ELSEIF,ARG2,EQ,1,AND,J,EQ,9+12*(R-1)
                        L,J,J+15
                        *ENDIF
                        *ENDDO
                  *ENDDO
            *ENDDO
      *ELSEIF,ARG2,EQ,1
            *DO,R,1,(ARG3-1)
                  *DO,J,1,ARG1
                  *IF,J,EQ,3+12*(R-1),THEN
                  L,J,J+15
                  L,J,J+21
                  *ELSEIF,ARG2,EQ,1,AND,J,EQ,9+12*(R-1)
                  L,J,J+15
                  *ENDIF
                  *ENDDO
            *ENDDO
      *ENDIF
*ELSEIF,ARG3,EQ,1
*ENDIF
*END
```

➢ ***"MAIN SCRIPT (COMPRESSION)"***

```
FINISH
/CLEAR
/PREP7
H1=10                   !base edge length of the cell [mm]
ALPHA1=1.1              !ALPHA1=H1/L1 where L1 is the diagonal edge
THETA1=-10              !THETA1 in degree
CH=10                   !cell height along y [mm]
DT=0                    !theta gradient
DH=0                    !H gradient
DALPHA=0                !Alpha gradient
DI=1.2                  !beam diameter  [mm]
SIZE=4                  !mesh size [mm]
DELAY_H=0               !delay H gradient
DELAY_T=0               !delay theta gradient
DELAY_A=0               !delay alpha gradient
!!!!!!!!!!!!!!!!!!structure
*AFUN,DEG
NR=9                    !rows number
NC=8                    !columns number
NF=1                    !floors number
Q=(DELAY_H/100*NR)
W=(DELAY_T/100*NR)
E=(DELAY_A/100*NR)
*IF,Q,EQ,0,THEN
IQ=0
*ELSEIF,Q,NE,0
IQ=NINT(ABS(Q-0.5))
*ENDIF
*IF,E,EQ,0,THEN
IE=0
*ELSEIF,E,NE,0
IE=NINT(ABS(E-0.5))
*ENDIF
*IF,W,EQ,0,THEN
IW=0
*ELSEIF,W,NE,0
IW=NINT(ABS(W-0.5))
*ENDIF
*IF,DH,EQ,0,THEN
DBCL=H1+2*((H1/2)-(H1/ALPHA1)*SIN(-THETA1))          !dbcl
*ELSEIF,DH,GT,0
DBCL=H1+(NR-IQ)*DH+DI*4
*ELSEIF,DH,LT,0
```

```
DBCL=H1+DI*4
*ENDIF
!!!!element type
ET,1,BEAM188
SECTYPE,1,BEAM,CSOLID
SECDATA,DI/2,16,2
!!!!!material ( stainless steel 316L)
MP,EX,1,210000          !MPa
MP,DENS,1,0.0078        !density [g/mm^3]
MP,NUXY,1,0.3           !Poisson's modulus
MP,NUYZ,1,0.3
MP,NUXZ,1,0.3
!!!!!!!!!!!!!!geometry
!!!!!!!!!!!!!!!!first column
DIST=0
*DO,J,1,NR
*IF,E,GE,J,THEN
ALPHA=ALPHA1
*ELSEIF,E,LT,J
ALPHA=ALPHA1+DALPHA*(J-1-IE)
*ENDIF
*IF,W,GE,J,THEN
THETA=THETA1
*ELSEIF,W,LT,J
THETA=THETA1+(J-1-IW)*DT
*ENDIF
*IF,Q,GE,J,THEN
H=H1
KE1=1+(J-1)*(12)
KE2=2+(J-1)*(12)
KE3=3+(J-1)*(12)
KE4=4+(J-1)*(12)
KE5=5+(J-1)*(12)
KE6=6+(J-1)*(12)
KE7=7+(J-1)*(12)
KE8=8+(J-1)*(12)
KE9=9+(J-1)*(12)
KE10=10+(J-1)*(12)
KE11=11+(J-1)*(12)
KE12=12+(J-1)*(12)
*USE,CELL,H,ALPHA,THETA,CH,DIST,KE1,KE2,KE3,KE4,KE5,KE6,KE7,KE8,KE9,KE10,
KE11,KE12,0
*ELSEIF,Q,LT,J
H=H1+DH*(J-IQ-1)
KE1=1+(J-1)*(12)
```

```
KE2=2+(J-1)*(12)
KE3=3+(J-1)*(12)
KE4=4+(J-1)*(12)
KE5=5+(J-1)*(12)
KE6=6+(J-1)*(12)
KE7=7+(J-1)*(12)
KE8=8+(J-1)*(12)
KE9=9+(J-1)*(12)
KE10=10+(J-1)*(12)
KE11=11+(J-1)*(12)
KE12=12+(J-1)*(12)
*USE,CELL,H,ALPHA,THETA,CH,DIST,KE1,KE2,KE3,KE4,KE5,KE6,KE7,KE8,KE9,KE10,
KE11,KE12,DH
*ENDIF
DIST=DIST+(H/ALPHA)*2*COS(THETA)
*ENDDO
!!!!!!!!!!!!!!!!!!creating the repetition
LGEN,NC,ALL,,,0,0,DBCL
NUMMRG,ALL
NUMCMP,ALL
!!!!!!!!!!!!!!!!!!bonding the rows together
KSEL,ALL
*GET,A,KP,0,NUM,MAX
*USE,BONDING,A,NR,NC
!!!!!!!!!!!!!!!!!!creating the floors
LGEN,NF,ALL,,,0,CH,0
NUMMRG,ALL
NUMCMP,ALL
CSYS,5
LGEN,1,ALL,,,0,-90,0,,,1
CSYS,0
!!!!!!!!!!!!!!!!!!mesh
TYPE,1
REAL,1
LSEL,ALL
LESIZE,ALL,SIZE
LMESH,ALL
NSEL,ALL
*GET,X_MIN,NODE,0,MNLOC,X
*GET,X_MAX,NODE,0,MXLOC,X
*GET,Y_MIN,NODE,0,MNLOC,Y
*GET,Y_MAX,NODE,0,MXLOC,Y
*GET,Z_MIN,NODE,0,MNLOC,Z
*GET,Z_MAX,NODE,0,MXLOC,Z
```

```
NSEL,S,LOC,Z,0
CM,BOTTOM_N,NODE                    !bottom component
!!!!!!!!!!!!!!!constraints
CMSEL,S,BOTTOM_N,NODE
D,ALL,UX,0
D,ALL,UY,0
D,ALL,UZ,0
D,ALL,ROTZ,0
IRLF,-1             !* calculate the inertia properties (useful to determine the mass of the lattice)
!!!!!!!!!!!!!!!displacement
AA=-0.1
NSEL,S,LOC,Z,DIST
CM,NODE_TOP,NODE
*GET,N_LOAD,NODE,0,COUNT          !total number of nodes on the loading side
D,ALL,ROTZ,0.0
D,ALL,UZ,AA             ! given displacement [mm]
NSEL,ALL
FINISH
!!!!!!!!!!solution
/SOLU
ANTYPE,STATIC
SOLVE
*GET,MASS_T,ELEM,0,MTOT,X
FINISH
!!!!!!!!postprocessing
/POST1
ALLSEL,ALL
CMSEL,S,NODE_TOP,NODE
FSUM
*GET,N_FORCE,FSUM,0,ITEM,FZ
ALLSEL,ALL
*DIM,GEOM,,14
GEOM(1)=ALPHA1,THETA1,H1,CH,DI,DALPHA,DT,DH,DELAY_A,DELAY_T,DELAY_
H,NR,NC,NF
*DIM,RESULTS,,11
N_FAC=1
RESULTS(1)=X_MAX,X_MIN,Y_MAX,Y_MIN,Z_MAX,Z_MIN,MASS_T,N_FAC,N_LO
AD,N_FORCE
*CFOPEN,tlzd1,TXT
*VWRITE,AA
(3X,(E17.8,3X))
*CFCLOSE
*CFOPEN,tlzg1,TXT
*VWRITE,GEOM(1,1)
(3X,(E13.5))
```

```
*CFCLOSE
*CFOPEN,tlzr1,TXT
*VWRITE,RESULTS(1,1)
(3X,(E13.5))
*CFCLOSE
```

➢ ***"MAIN SCRIPT (SHEAR)"***

```
FINISH
/CLEAR
/PREP7
_H1=10                  !base edge length of the cell [mm]
_ALPHA1=1.1             !ALPHA1=H1/L1 where L1 is the diagonal edge
_THETA1=-10             !THETA1 in degree
_CH=10                  !cell height along y [mm]
_DT=0                   !theta gradient
_DH=0                   !H gradient
_DALPHA=0               !Alpha gradient
_DI=1.2                 !beam diameter  [mm]
_SIZE=4                 !mesh size [mm]
_DELAY_H=0              !delay H gradient
_DELAY_T=0              !delay theta gradient
_DELAY_A=0              !delay alpha gradient
!!!!!!!!!!!!!!!!!!structure
*AFUN,DEG
_NR=9                   !rows number
_NC=8                   !columns number
_NF=1                   !floors number
_Q=(_DELAY_H/100*_NR)
_W=(_DELAY_T/100*_NR)
_E=(_DELAY_A/100*_NR)
*IF,_Q,EQ,0,THEN
_IQ=0
*ELSEIF,_Q,NE,0
_IQ=NINT(ABS(_Q-0.5))
*ENDIF
*IF,_E,EQ,0,THEN
_IE=0
*ELSEIF,_E,NE,0
_IE=NINT(ABS(_E-0.5))
*ENDIF
*IF,_W,EQ,0,THEN
_IW=0
*ELSEIF,_W,NE,0
_IW=NINT(ABS(_W-0.5))
*ENDIF
*IF,_DH,EQ,0,THEN
_DBCL=_H1+2*((_H1/2)-(_H1/_ALPHA1)*SIN(-_THETA1))  !DISTANCE BETWEEN
THE CENTER LINE OF TWO CONSECUTIVE ROWS
*ELSEIF,_DH,GT,0
_DBCL=_H1+(_NR-_IQ)*_DH+_DI*4
```

```
*ELSEIF,_DH,LT,0
_DBCL=_H1+_DI*4
*ENDIF
!element type
ET,1,BEAM188
SECTYPE,1,BEAM,CSOLID
SECDATA,_DI/2,16,2
!material (Stainless steel 316L)
MP,EX,1,210000          !MPa
MP,DENS,1,0.0078        !Density [g/mm^3]
MP,NUXY,1,0.3           !Poisson's modulus
MP,NUYZ,1,0.3
MP,NUXZ,1,0.3
!!!!!!!!!!!!!!geometry
!!!!!!!!!!!!!!!creating the first column
*DIM,_VDIST,,_NR
*DIM,_VTHETA,,_NR
_DISTANCE=0
_T=1
*DO,J,1,_NR
*IF,_E,GE,J,THEN
_ALPHA=_ALPHA1
*ELSEIF,_E,LT,J
_ALPHA=_ALPHA1+_DALPHA*(J-1-_IE)
*ENDIF
*IF,_W,GE,J,THEN
_THETA=_THETA1
*ELSEIF,_W,LT,J
_THETA=_THETA1+(J-1-_IW)*_DT
*ENDIF
*IF,_Q,GE,J,THEN
_H=_H1
_KE1=1+(J-1)*(12)
_KE2=2+(J-1)*(12)
_KE3=3+(J-1)*(12)
_KE4=4+(J-1)*(12)
_KE5=5+(J-1)*(12)
_KE6=6+(J-1)*(12)
_KE7=7+(J-1)*(12)
_KE8=8+(J-1)*(12)
_KE9=9+(J-1)*(12)
_KE10=10+(J-1)*(12)
_KE11=11+(J-1)*(12)
_KE12=12+(J-1)*(12)
```

```
*USE,CELL,_H,_ALPHA,_THETA,_CH,_DISTANCE,_KE1,_KE2,_KE3,_KE4,_KE5,_K
E6,_KE7,_KE8,_KE9,_KE10,_KE11,_KE12,0
*ELSEIF,_Q,LT,J
_H=_H1+_DH*(J-_IQ-1)
_KE1=1+(J-1)*(12)
_KE2=2+(J-1)*(12)
_KE3=3+(J-1)*(12)
_KE4=4+(J-1)*(12)
_KE5=5+(J-1)*(12)
_KE6=6+(J-1)*(12)
_KE7=7+(J-1)*(12)
_KE8=8+(J-1)*(12)
_KE9=9+(J-1)*(12)
_KE10=10+(J-1)*(12)
_KE11=11+(J-1)*(12)
_KE12=12+(J-1)*(12)
*USE,CELL,_H,_ALPHA,_THETA,_CH,_DISTANCE,_KE1,_KE2,_KE3,_KE4,_KE5,_K
E6,_KE7,_KE8,_KE9,_KE10,_KE11,_KE12,_DH
*ENDIF
*VFILL,_VDIST(_T,1),DATA,(_H/_ALPHA)*2*COS(_THETA)
_DISTANCE=_DISTANCE+(_H/_ALPHA)*2*COS(_THETA)
*VFILL,_VTHETA(_T,1),DATA,_THETA
_T=_T+1
*ENDDO
!!!!!!!!!!!!!!!!!!creating the repetition
LGEN,_NC,ALL,,,0,0,_DBCL
NUMMRG,ALL
NUMCMP,ALL
!!!!!!!!!!!!!!!!!!bonding columns together
KSEL,ALL
*GET,_A,KP,0,NUM,MAX
*USE,BONDING,_A,_NR,_NC
!!!!!!!!!!!!!!!!!!creating floors
LGEN,_NF,ALL,,,0,_CH,0
NUMMRG,ALL
NUMCMP,ALL
CSYS,5
LGEN,1,ALL,,,0,-90,0,,,1
CSYS,0
!!!!!!!!!!!!!!!!!!mesh
TYPE,1
REAL,1
LSEL,ALL
LESIZE,ALL,_SIZE
LMESH,ALL
```

```
NSEL,ALL
*GET,_X_MIN,NODE,0,MNLOC,X
*GET,_X_MAX,NODE,0,MXLOC,X
*GET,_Y_MIN,NODE,0,MNLOC,Y
*GET,_Y_MAX,NODE,0,MXLOC,Y
*GET,_Z_MIN,NODE,0,MNLOC,Z
*GET,_Z_MAX,NODE,0,MXLOC,Z
!!!!!defining components including all lateral surfaces nodes
!!!!selecting the nodes to constrain and setting the component
_TNODESNUMBER=0
*DO,G,1,_NR                    !!!selecting the row
_THETA=_VTHETA(G,1)
_DIST=_VDIST(G,1)
*IF,G,EQ,1,THEN
_TOTDIST=0
*ENDIF
NALL
*IF,_THETA,EQ,0,THEN                    !!!!angle-based differentiation
NSEL,S,LOC,Z,_TOTDIST,_TOTDIST+_DIST
*GET,_XX,NODE,0,MNLOC,X
NSEL,R,LOC,X,_XX
*GET,_NODESNUMBER,NODE,0,COUNT              !!!counting the nodes
*DEL,_NN,,NOPR
*DIM,_NN,ARRAY,_NODESNUMBER
*VGET,_NN,NODE,,NLIST                          !!!!storing the nodes number
_TNODESNUMBER=_TNODESNUMBER+_NODESNUMBER
*ELSEIF,_THETA,LT,0
NSEL,S,LOC,Z,_TOTDIST
*GET,_XX,NODE,0,MNLOC,X
NSEL,R,LOC,X,_XX
*GET,_NODESNUMBER,NODE,0,COUNT
*DEL,_NN1,,NOPR
*DIM,_NN1,ARRAY,_NODESNUMBER
*VGET,_NN1,NODE,,NLIST
NALL
NSEL,S,LOC,Z,_TOTDIST+_DIST
*GET,_XX,NODE,0,MNLOC,X
NSEL,R,LOC,X,_XX
*GET,_NODESNUMBER,NODE,0,COUNT
*DEL,_NN2,,NOPR
*DIM,_NN2,ARRAY,_NODESNUMBER
*VGET,_NN2,NODE,,NLIST
_NODESNUMBER=2*_NODESNUMBER
_TNODESNUMBER=_TNODESNUMBER+_NODESNUMBER
*DEL,_NN,,NOPR
```

```
*DIM,_NN,ARRAY,_NODESNUMBER
*VFUN,_NN,COPY,_NN1
*VFUN,_NN(_NODESNUMBER/2+1),COPY,_NN2
*ELSE
NSEL,S,LOC,Z,_TOTDIST+_DIST/2
*GET,_XX,NODE,0,MNLOC,X
NSEL,R,LOC,X,_XX
*GET,_NODESNUMBER,NODE,0,COUNT              !!!counting the nodes
*DEL,_NN,,NOPR
*DIM,_NN,ARRAY,_NODESNUMBER
*VGET,_NN,NODE,,NLIST
_TNODESNUMBER=_TNODESNUMBER+_NODESNUMBER
*ENDIF
*DEL,_VETT,,NOPR
*DIM,_VETT,ARRAY,_TNODESNUMBER            !!!!!updating the 'VETT' array which
contains        !!!the selected nodes' number
*VFUN,_VETT(_TNODESNUMBER-_NODESNUMBER+1),COPY,_NN
*IF,G,GT,1,THEN
*VFUN,_VETT,COPY,_SM
*ENDIF
*DEL,_SM,,NOPR
*DIM,_SM,ARRAY,_TNODESNUMBER
*VFUN,_SM,COPY,_VETT
_TOTDIST=_DIST+_TOTDIST
*ENDDO
NALL
*DO,J,1,_TNODESNUMBER             !!!!!creating the component
_V=_VETT(J)
*IF,J,EQ,1,THEN
NSEL,S,NODE,,_V
*ELSE
NSEL,A,NODE,,_V
*ENDIF
*ENDDO
CM,_SIDE_NODES_CONS,NODE
ALLSEL,ALL
!!!!selecting the loaded nodes and setting the component!!!!!!
_TNODESNUMBER=0
*DO,G,1,_NR
_THETA=_VTHETA(G,1)
_DIST=_VDIST(G,1)
*IF,G,EQ,1,THEN
_TOTDIST=0
*ENDIF
NALL
```

```
*IF,_THETA,EQ,0,THEN
NSEL,S,LOC,Z,_TOTDIST,_TOTDIST+_DIST
*GET,_XXX,NODE,0,MXLOC,X
NSEL,R,LOC,X,_XXX
*GET,_NODESNUMBER,NODE,0,COUNT
*DEL,_NNN,,NOPR
*DIM,_NNN,ARRAY,_NODESNUMBER
*VGET,_NNN,NODE,,NLIST
_TNODESNUMBER=_TNODESNUMBER+_NODESNUMBER
*ELSEIF,_THETA,LT,0
NSEL,S,LOC,Z,_TOTDIST
*GET,_XXX,NODE,0,MXLOC,X
NSEL,R,LOC,X,_XXX
*GET,_NODESNUMBER,NODE,0,COUNT
*DEL,_NNN1,,NOPR
*DIM,_NNN1,ARRAY,_NODESNUMBER
*VGET,_NNN1,NODE,,NLIST
NALL
NSEL,S,LOC,Z,_TOTDIST+_DIST
*GET,_XXX,NODE,0,MXLOC,X
NSEL,R,LOC,X,_XXX
*GET,_NODESNUMBER,NODE,0,COUNT
*DEL,_NNN2,,NOPR
*DIM,_NNN2,ARRAY,_NODESNUMBER
*VGET,_NNN2,NODE,,NLIST
_NODESNUMBER=2*_NODESNUMBER
_TNODESNUMBER=_TNODESNUMBER+_NODESNUMBER
*DEL,_NNN,,NOPR
*DIM,_NNN,ARRAY,_NODESNUMBER
*VFUN,_NNN,COPY,_NNN1
*VFUN,_NNN(_NODESNUMBER/2+1),COPY,_NNN2
*ELSE
NSEL,S,LOC,Z,_TOTDIST+_DIST/2
*GET,_XXX,NODE,0,MXLOC,X
NSEL,R,LOC,X,_XXX
*GET,_NODESNUMBER,NODE,0,COUNT
*DEL,_NNN,,NOPR
*DIM,_NNN,ARRAY,_NODESNUMBER
*VGET,_NNN,NODE,,NLIST
_TNODESNUMBER=_TNODESNUMBER+_NODESNUMBER
*ENDIF
*DEL,_VET,,NOPR
*DIM,_VET,ARRAY,_TNODESNUMBER
*VFUN,_VET(_TNODESNUMBER-_NODESNUMBER+1),COPY,_NNN
*IF,G,GT,1,THEN
```

```
*VFUN,_VET,COPY,_SMT
*ENDIF
*DEL,_SMT,,NOPR
*DIM,_SMT,ARRAY,_TNODESNUMBER
*VFUN,_SMT,COPY,_VET
_TOTDIST=_DIST+_TOTDIST
*ENDDO
NALL
*DO,J,1,_TNODESNUMBER
_H=_VET(J)
*IF,J,EQ,1,THEN
NSEL,S,NODE,,_H
*ELSE
NSEL,A,NODE,,_H
*ENDIF
*ENDDO
CM,_SIDE_NODES_DISP,NODE
ALLSEL,ALL
!!!!!constraints
NALL
NSEL,S,LOC,Y,0
D,ALL,UY,0
D,ALL,UZ,0          !!!!!!these constraints are needed otherwise the lattice is ipostatic
D,ALL,ROTX,0
D,ALL,ROTY,0
NALL
CMSEL,S,_SIDE_NODES_CONS,NODE
D,ALL,UX,0
D,ALL,UZ,0
D,ALL,ROTX,0
D,ALL,ROTY,0
NALL
IRLF,-1             !* calculate the inertia properties (useful to determine the mass of the lattice)
!!!!!!!!!!!!!!!displacement
_A=-1
_B=1
NSEL,S,LOC,Y,_CH*_NF
D,ALL,UY,_A           ! given displacement [mm]
NSEL,ALL
CMSEL,S,_SIDE_NODES_DISP,NODE
D,ALL,UX,_B
NALL
FINISH
!!!!!!!!!!solution
/SOLU
```

```
ANTYPE,STATIC
SOLVE
*GET,_MASS_T,ELEM,0,MTOT,X
FINISH
!postprocessing
/POST1
ALLSEL,ALL
CMSEL,S,_SIDE_NODES_CONS,NODE
*GET,_NODESNUMBERX,NODE,0,COUNT
*DIM,_VNFORCEX,ARRAY,_NODESNUMBERX
*DIM,_GGGX,ARRAY,_NODESNUMBERX
*VGET,_GGGX,NODE,,NLIST
*DO,J,1,_NODESNUMBERX
NALL
CMSEL,S,_SIDE_NODES_CONS,NODE
*GET,_N_FORCE_X,NODE,_GGGX(J,1),RF,FX
_VNFORCEX(J,1)=_N_FORCE_X
*ENDDO
*VSCFUN,_FTOTX,SUM,_VNFORCEX
ALLSEL,ALL
NSEL,S,LOC,Y,0
*GET,_NODESNUMBERY,NODE,0,COUNT
*DIM,_VNFORCEY,ARRAY,_NODESNUMBERY
*DIM,_GGGY,ARRAY,_NODESNUMBERY
*VGET,_GGGY,NODE,,NLIST
*DO,J,1,_NODESNUMBERY
NALL
NSEL,S,LOC,Y,0
*GET,_N_FORCE_Y,NODE,_GGGY(J,1),RF,FY
_VNFORCEY(J,1)=_N_FORCE_Y
*ENDDO
*VSCFUN,_FTOTY,SUM,_VNFORCEY
!ALLSEL,ALL
!CMSEL,S,SIDE_NODES_CONS,NODE
!FSUM                                    !!!with FSUM number sign is always positive
!*GET,N_FORCE_X,FSUM,0,ITEM,FX
!ALLSEL,ALL
!NSEL,S,LOC,Y,0
!*GET,N_FORCE_Y,NODE,,RF,FY
!FSUM
!*GET,N_FORCE_Y,FSUM,0,ITEM,FY
!ALLSEL,ALL
*DIM,_GEOM,,14
_GEOM(1)=_ALPHA1,_THETA1,_H1,_CH,_DI,_DALPHA,_DT,_DH,_DELAY_A,_DE
LAY_T,_DELAY_H,_NR,_NC,_NF
```

```
*DIM,_RESULTS,,9
_RESULTS(1)=_X_MAX,_X_MIN,_Y_MAX,_Y_MIN,_Z_MAX,_Z_MIN,_MASS_T,_
FTOTX,_FTOTY
*DIM,_AA,,2
_AA(1)=_A,_B
*CFOPEN,'tlzd1',TXT
*VWRITE,_AA(1,1)
(3X,(E17.8))
*CFCLOSE
*CFOPEN,'tlszg1',TXT
*VWRITE,_GEOM(1,1)
(3X,(E13.5))
*CFCLOSE
*CFOPEN,'tlzr1',TXT
*VWRITE,_RESULTS(1,1)
(3X,(E13.5))
*CFCLOSE
```

➢ ***"MAIN SCRIPT (SEA)"***

```
FINISH
/CLEAR
/PREP7
H1=10                   !base edge length of the cell [mm]
ALPHA1=1.1              !ALPHA1=H1/L1 where L1 is the diagonal edge
THETA1=-10              !THETA1 in degree
CH=10                   !cell height along y [mm]
DT=0                    !theta gradient
DH=0                    !H gradient
DALPHA=0                !Alpha gradient
DI=1.2                  !beam diameter  [mm]
SIZE=4                  !mesh size [mm]
DELAY_H=0               !delay H gradient
DELAY_T=0               !delay theta gradient
DELAY_A=0               !delay alpha gradient
!!!!!!!!!!!!!!!!!!structure
*AFUN,DEG
NR=9                    !rows number
NC=8                    !columns number
NF=5                    !floors number
Q=(DELAY_H/100*NR)
W=(DELAY_T/100*NR)
E=(DELAY_A/100*NR)
*IF,Q,EQ,0,THEN
IQ=0
*ELSEIF,Q,NE,0
IQ=NINT(ABS(Q-0.5))
*ENDIF
*IF,E,EQ,0,THEN
IE=0
*ELSEIF,E,NE,0
IE=NINT(ABS(E-0.5))
*ENDIF
*IF,W,EQ,0,THEN
IW=0
*ELSEIF,W,NE,0
IW=NINT(ABS(W-0.5))
*ENDIF
*IF,DH,EQ,0,THEN
DBCL=H1+2*((H1/2)-(H1/ALPHA1)*SIN(-THETA1))        !dbcl
*ELSEIF,DH,GT,0
DBCL=H1+(NR-IQ)*DH+DI*4
*ELSEIF,DH,LT,0
```

```
DBCL=H1+DI*4
*ENDIF
!elements type
ET,1,BEAM188
SECTYPE,1,BEAM,CSOLID
SECDATA,DI/2,16,2
ET,2,SOLID186
ET,3,SHELL181
SECTYPE,2,SHELL
SECDATA,DI/2
!material (stainless steel 316L)
MP,EX,1,210000                          !MPa
MP,DENS,1,0.0078                        !Density [g/mm^3]
MP,NUXY,1,0.3                           !Poisson's modulus
MP,NUYZ,1,0.3
MP,NUXZ,1,0.3
MP,EX,2,210*(10**10)                    !MPa
MP,NUXY,2,0.3                           !Poisson's modulus
MP,NUYZ,2,0.3
MP,NUXZ,2,0.3

!geometry
!!!!!!!!!!!!!!!creating the first column
DIST=0
*DO,J,1,NR
*IF,E,GE,J,THEN
ALPHA=ALPHA1
*ELSEIF,E,LT,J
ALPHA=ALPHA1+DALPHA*(J-1-IE)
*ENDIF
*IF,W,GE,J,THEN
THETA=THETA1
*ELSEIF,W,LT,J
THETA=THETA1+(J-1-IW)*DT
*ENDIF
*IF,Q,GE,J,THEN
H=H1
KE1=1+(J-1)*(12)
KE2=2+(J-1)*(12)
KE3=3+(J-1)*(12)
KE4=4+(J-1)*(12)
KE5=5+(J-1)*(12)
KE6=6+(J-1)*(12)
KE7=7+(J-1)*(12)
KE8=8+(J-1)*(12)
```

```
KE9=9+(J-1)*(12)
KE10=10+(J-1)*(12)
KE11=11+(J-1)*(12)
KE12=12+(J-1)*(12)
*USE,CELL,H,ALPHA,THETA,CH,DIST,KE1,KE2,KE3,KE4,KE5,KE6,KE7,KE8,KE9,KE10,
KE11,KE12,0
*ELSEIF,Q,LT,J
H=H1+DH*(J-IQ-1)
KE1=1+(J-1)*(12)
KE2=2+(J-1)*(12)
KE3=3+(J-1)*(12)
KE4=4+(J-1)*(12)
KE5=5+(J-1)*(12)
KE6=6+(J-1)*(12)
KE7=7+(J-1)*(12)
KE8=8+(J-1)*(12)
KE9=9+(J-1)*(12)
KE10=10+(J-1)*(12)
KE11=11+(J-1)*(12)
KE12=12+(J-1)*(12)

*USE,CELL,H,ALPHA,THETA,CH,DIST,KE1,KE2,KE3,KE4,KE5,KE6,KE7,KE8,KE9,KE10,
KE11,KE12,DH
*ENDIF
DIST=DIST+(H/ALPHA)*2*COS(THETA)
*ENDDO
!!!!!storing the length of the diagonal line
*GET,N,LINE,0,NUM,MAXD
*GET,ND,LINE,N,LENG
!!!!!!!!!!!!!!!!!!creating the repetition
LGEN,NC,ALL,,,0,0,DBCL
NUMMRG,ALL
NUMCMP,ALL
!!!!!!!!!!!!!!!!!!bonding the column together
KSEL,ALL
*GET,A,KP,0,NUM,MAX
*USE,BONDING,A,NR,NC
!!!!!!!!!!!!!!!!!!creating the floors
LGEN,NF,ALL,,,0,CH,0
NUMMRG,ALL
NUMCMP,ALL
CSYS,5
LGEN,1,ALL,,,0,-90,0,,,1
CSYS,0
!!!!!!!creating the top areas for the contact
```

```
ALLSEL
LSEL,S,LOC,Z,DIST
LDELE,ALL,,,1
ALLSEL
*USE,SUPPORT,NR,NC,NF
!!!!!!!!!!!!!!!!!!Mesh of the beams and surfaces
ALLSEL
LESIZE,ALL,SIZE
TYPE,3
MAT,1
SECNUM,2
AMESH,ALL
ALLSEL
LSEL,ALL
TYPE,1
MAT,1
SECNUM,1
LMESH,ALL
NUMCMP,ALL
ALLSEL
NSEL,ALL
*GET,X_MIN,NODE,0,MNLOC,X
*GET,X_MAX,NODE,0,MXLOC,X
*GET,Y_MIN,NODE,0,MNLOC,Y
*GET,Y_MAX,NODE,0,MXLOC,Y
*GET,Z_MIN,NODE,0,MNLOC,Z
*GET,Z_MAX,NODE,0,MXLOC,Z
NSEL,S,LOC,Z,0
CM,BOTTOM_N,NODE                    !bottom component
!!!!!!!!!!!!!!!!constraints
CMSEL,S,BOTTOM_N,NODE
D,ALL,UX,0
D,ALL,UY,0
D,ALL,UZ,0
D,ALL,ROTZ,0
D,ALL,ROTX,0
D,ALL,ROTY,0
ALLSEL,ALL
IRLF,-1             !* calculate the inertia properties (useful to determine the mass of the lattice)
!!!!!!!!!!!!!!!creating the upper platform (Kp indexed counter clockwise)!!!!!!!
KSEL,ALL
*GET,M,KP,0,NUM,MAXD    !!!finding the last keypoint number
MXX=ND*(COS(ASIN(CH/ND)))/2          !!!calculating the last H of the column
K,M+1,MXX+10,-5,DIST+5
K,M+5,MXX+10,-5,DIST+10
```

```
K,M+2,MXX+10,CH*NF+5,DIST+5
K,M+6,MXX+10,CH*NF+5,DIST+10
K,M+3,-MXX-(NC-1)*DBCL-10,CH*NF+5,DIST+5
K,M+7,-MXX-(NC-1)*DBCL-10,CH*NF+5,DIST+10
K,M+4,-MXX-(NC-1)*DBCL-10,-5,DIST+5
K,M+8,-MXX-(NC-1)*DBCL-10,-5,DIST+10
V,M+1,M+2,M+3,M+4,M+5,M+6,M+7,M+8
!!!!! mesh of the volume!!!!!!!!!
ALLSEL
VSEL,ALL
ESIZE,8
TYPE,2
MAT,2
VMESH,ALL
ALLSEL,ALL
!!!!!!!!!!!!!!!displacement!!!!!!!!!!!!
NSEL,S,LOC,Z,DIST+10
AA=-6
D,ALL,UZ,AA     !15 mm displacement
D,ALL,UX,0
D,ALL,UY,0
D,ALL,ROTX,0
D,ALL,ROTY,0
D,ALL,ROTZ,0
ESEL,ALL
NALL
!!!!!!contact!!!
ALLSEL
R,1
ET,4,TARGE170
NSEL,S,LOC,Z,DIST+10
TYPE,4
REAL,2
ESURF
NALL
ET,5,CONTA174
NSEL,S,LOC,Z,DIST
TYPE,5
REAL,2
ESURF,,TOP
ALLSEL
FINISH
!!!!!!solution!!!!!!!!!!!!!!!!!!
/SOLU
NLGEOM,ON
```

```
ANTYPE,STATIC
*GET,TWALLBEFORE,ACTIVE,,TIME,WALL        !saves the wall time before solution
SOLVE
*GET,TWALLAFTER,ACTIVE,,TIME,WALL         !saves the wall time after solution
SOLUTION_TIME=(TWALLAFTER-TWALLBEFORE)
*GET,MASS_T,ELEM,0,MTOT,Z
FINISH
/POST1
ALLSEL,ALL
NSEL,S,LOC,Z,0
FSUM
*GET,N_FORCE,FSUM,0,ITEM,FZ
ALLSEL,ALL
*DIM,GEOM,,14
GEOM(1)=ALPHA1,THETA1,H1,CH,DI,DALPHA,DT,DH,DELAY_A,DELAY_T,DELAY_
H,NR,NC,NF
*DIM,RESULTS,,11
N_FAC=1
N_LOAD=1
F_CR1=N_FORCE
RESULTS(1)=X_MAX,X_MIN,Y_MAX,Y_MIN,Z_MAX,Z_MIN,MASS_T,N_FAC,N_LO
AD,N_FORCE,F_CR1
*CFOPEN,'thetalysubs_disp1',TXT
*VWRITE,AA
(3X,(E17.8,3X))
*CFCLOSE
*CFOPEN,'thetalygeometry1',TXT
*VWRITE,GEOM(1,1)
(3X,(E13.5))
*CFCLOSE
*CFOPEN,'thetalyresult1',TXT
*VWRITE,RESULTS(1,1)
(3X,(E13.5))
*CFCLOSE
```